LEVEL III 6

Earthquake Characteristics and Earthquake-Explosion Discrimination

~~Semi Annual~~ FINAL Technical Report No. 8

(18) AFOSR

(19) TR-79-0451

(6)

Sponsored by
Advanced Research Projects Agency (DOD)
ARPA Order No. 3291

(9) Rept. no. 8 (Fiscal)
1 May - 31 Oct 78

Superseded AD-A067368 (incomplete) ymc

(11) 1979

(12) 34

(15) AFOSR-75-2775

ARPA Order-3291
Program Code 7F10
Name of Grantee: University of Colorado
Effective Date of Grant: 1 November 1974
Grant Expiration Date: 31 October 1978
Amount of Grant: $328,016
Grant Number: AFOSR-75-2775
Principal Investigator: Charles Archambeau (303-492-8028)
Program Manager: William J. Best
Title of Work: (6) Earthquake Characteristics and Earthquake-Explosion Discrimination

(10)

Semi-Annual Technical Report No. 8

Charles B. Archambeau, V.F. Cormier, C. Kisslinger, G. Lundquist, J. Stevens, K. Wyss

AD A067887

Table of Contents

I. Technical Report Summary.

During this report period, from May through October, 1978, we concentrated on four areas of study, in particular: (1) The development of asymptotic and modal wave propagation methods for the description of seismic wave propagation effects in the near regional and teleseismic distance ranges; (2) The study of the frequency dependence of earth's anelasticity as a function of depth and geologic province; (3) The development of theoretical relaxation source representations for seismic sources in non-homogeneously prestressed media and inversion procedures for such sources and; (4) The development of advanced methods for seismic (vector field) signal detection and analysis. The major results of this work are: (1) We have developed and applied full-wave asymptotic methods, which employ the Langer approximation in the frequency domain, and in a systematic comparative study with the Cagniard method have demonstrated that there is general agreement in the predictions of both methods when they can be compared. However, in some distance ranges, observable differences occur, notably in the regional distance range from 10°-20°. In these cases convergence of results from the two methods only occur when multiple reflections, within finely layered zones in regions of large velocity gradient, are included in the Cagniard method. Other observable differences occur when anelasticity is included, particularly if a frequency dependent intrinsic Q factor is considered, since the Cagniard approach cannot directly treat anelasticity except in an approximate, incomplete fashion. On the other hand, the frequency domain full-wave theory incorporates anelasticity directly and all the effects of a frequency dependent intrinsic Q parameter can be computed. We have also applied the full wave theory to the synthesis of complete seismograms in the near field distance range and developed the analytical relations required to compute synthetics. This theoretical development has also been extended to provide a basis for the computation of synthetics at the source anti-pole. In both cases we have computed seismograms based on the theoretical results. Comparisons, between mode superposition methods on the one hand and observations on the other, indicate that the method is both accurate and fast computationally. (2) We have developed a mode superposition approach, which has been descriptively termed the "Locked Mode Approximation Method", for the generation of complete synthetic seismograms (P-SV and SH). The method is applicable in both the near and regional distance ranges, using a layered half space as the model, and can easily be extended to a spherical earth for teleseismic studies. The method is approximate in the sense that a high velocity layer at depth is introduced to trap the modes so that P and S waves can be synthesized. The method has been completely formulated, with general source representations included, and has been tested computationally for accuracy (relative to an exact result without the artificial high velocity layer) and speed of computation. Complete P-SV seismograms, for explosion sources for example, over the distance range from 50 to 500 km and the frequency range from 0 to 2 Hz have been generated for a layered crust-upper mantle model, with all the P wave reflected and refracted arrivals obtained conforming in arrival time with ray theory predictions and similarly for the SV body phases. Initial comparisons with asymptotic wave theory results and known analytic solution show good agreement in wave form and amplitude as well. This modal superposition method, in addition to giving complete results in the distance and frequency range of interest, with stable results having been obtained up to 25 Hz, is capable of incorporating complex medium moduli (or complex velocities), so that anelastic effects may be directly treated. In addition, it is ideally suited to source studies since the modes need only be computed once for a particular earth model and these results can be combined with source representations, corresponding to

any source hypocentral depth and source type, to obtain theoretical seismograms at all distances and azimuths, for a variety of source configurations, by means of a very simple and fast mode excitation computation. (3) A frequency dependent "absorption band model" for the intrinsic Q (quality factor or dissipation function) in the earth has been introduced into the theoretical wave propagation methods. Based on comparative studies of predictions using this anelastic model with observations, we have concluded that such a frequency dependence is appropriate for the earth's upper mantle in particular, and that the variation of the intrinsic Q and its frequency dependence is such that the resulting teleseismic mean dissipation function, Q_m (the Q function averaged over the ray path) is such that a high Q_m "window" exists at relatively high frequencies (in the range from 1.5 to about 4.5 Hz, with the peak at about 3 Hz). This result has important implications for source property and magnitude studies (m_b) and event detection work, as well as conquences with respect to the earth's thermal and mechanical properties. (4) The creation of a spherical cavity in a prestressed medium has been used in the past as a model for the tectonic release effects from explosions as the fundamental generating solution for relaxation models of earthquakes. An exact solution is given for the seismic radiation from the sudden creation of a spherical surface in an arbitrarily prestressed medium. The radiation for the case of pure shear is worked out in detail and compared with previous solutions to show how previous solutions approximate the exact solution. The most important results consist of the spectra and waveforms computed for inhomogeneous stress fields. It is found that failure in an inhomogeneous prestress environment results in a radiation pattern which is not pure quadrupole in nature. The inhomogeneous case also can lead to a low frequency far field spectral peak with the magnitude of the peak varying as a function of the angular coordinates. (5) An elastodynamic source of radiation is most generally and compactly expressed in terms of a Green's function integral equation and this representation serves as a convenient analytical form in the generation of an inversion scheme designed to provide estimates of source properties from observed radiation. A principal difficulty with this approach is specification of a sufficiently general Green's function in an appropriate analytical form. In this regard we have derived suitable layered space Green's functions expressed as eigenfunction expansions in the frequency domain. These functions are then used in the integral solutions for a relaxation source representation of the radiation field from an earthquake. The resulting field is shown to have an analytical structure which allows field variations to be expressed in integral relations similar to those for the field itself. These results serve as the basis for the systematic inversion of observed earthquake radiation field data for source properties and, in particular, we show how spatially variable tectonic stress changes due to failure can be estimated. (6) Narrow-band filtering can be used to generate well-defined magnitude data from seismic time series; these magnitudes being measures of energy arriving at particular group arrival times. Sets of variable frequency magnitudes have been computed for both observed and synthetic seismograms, where the latter results have been used to provide a theoretical framework for the interpretation of the observed data. These magnitude data can be associated with particular phases (P, S, or surface waves) and used in a manner similar to the ordinary m_b and M_s data. In particular, the data can be used to discriminate between underground explosions and earthquakes and to provide estimates of the tectonic stress changes produced by earthquakes as well as failure zone dimensions. The use of very high-frequency magnitudes along with relatively low-frequency magnitudes is however, a more powerful and sensitive means of identifying explosions than is the ordinary m_b versus M_s criteria, as is shown by a comparative study of a large group of seismic events. Further, the inference of tectonic stress levels using this approach provides estimates of the stress changes produced near the point of failure initiation, and this information is probably more pertinent to the description and understanding of an earthquake failure process than is the gross average stress drop estimates obtained by most other methods.

II. Applications of Full Wave Asymptotic Theory to the Prediction of Elastodynamic Source Fields in the Near, Regional and Teleseismic Distance Ranges

A. P Wave Interactions with Upper Mantle Structure: Full Wave-Cagniard Comparisons - Vernon F. Cormier

INTRODUCTION

Waveform modeling at distances less than 40 degrees can predict the large effects that both rapid velocity variation and anelasticity have on the waveforms of seismic body waves. Because the effects of non-planar layers, lateral heterogeneity, and the frequency dependence of the radiation pattern of the source all become more difficult to predict as the wavelength of seismic radiation decreases; waveform modeling has generally been more successful at longer periods of seismic radiation (100-10 sec.) than shorter periods (5- .1 sec). Earth models derived from the study of body waves of long period are nonetheless valuable in providing simple starting models for the study of short period data valuable to the seismic discrimination problem.

One such long period model, T7, for P wave velocity in western North America has been given recently by Burdick and Helmberger (1978). In extending the full wave theory summarized in previous technical reports (Cormier, 1978, 1977) to practical earth models for P waves, we have begun by examining the theory's waveform predictions for the T7 model (Figs. 2a-e) compared to the predictions given by the Cagniard-de Hoop method of synthesis used by Burdick and Helmberger. In completing this comparison we hope to (1) resolve whether the assumption of primary ray multiples in the Cagniard-deHoop method, which has been shown to be a problem for body waves

interacting with a strong velocity discontinuity such as the core-mantle boundary (Cormier and Ruff, 1978), is inadequate near weak velocity discontinuities postulated for the earth's mantle and to demonstrate the applicability and efficiency of the full wave theory to regions of complicated ray interactions.

METHOD OF SYNTHESIS INCLUDING AN EARTHQUAKE SOURCE

A synthetic seismogram of a body wave at teleseismic (farfield) distances commonly is described by the convolution of several time domain operators:

$$G(t,\Delta) = I(t)* S(t,\Delta)* C(t,\Delta)* A(t,\Delta)* M(t,\Delta) \qquad (1)$$

(e.g., Burdick and Helmberger, 1978), where the function I is the seismograph response to an impulse in displacement; S the time behavior of the source and often for shallow focus earthquakes the free surface and crustal interactions near the source; C the impulse of response of the crust under the receiver station, A a time domain operator describing the effects of anelasticity, and M the impulse of response of the earth model below the crust. It is important to note that each convolution operation except that of the instrument function represents an approximation valid only in the far field and only when a sufficiently small cone of take-off angles of seismic rays can describe the model response M. A frequency domain method of seismogram synthesis may avoid all of these approximation by including the effects of source, receiver crust and attenuation in the integrand of an integral [Γ] over horizontal wave number or ray parameter

p having the form:

$$u(\Delta_o,t) = \frac{1}{\pi}\int_o^\infty \omega^{1/2}\ \mathrm{Re}\left[\int_\Gamma f\ e^{i\omega J_{dp}e^{-i\omega t}}\right]d\omega \qquad (2)$$

The simplest approximation that can be avoided in such a full wave theory is that of the time domain attenuation operator A. We may incorporate attenuation via a complex velocity profile, as in Cormier and Richards (1976), using the Q model SL8 (Anderson and Hart, 1976) but neglecting the dispersive effect of linear attenuation. (We will later include tests of the dispersive effects on long period waveforms as we have already done for short period waveforms as reported by Lundquist.)

It would be quite simple to incorporate a finite number of free surface and receiver crust interactions in the composition of the response function f and phase function $\hat{J}$ of eq. 2. We shall later use this procedure as a check against the results obtained from separation of functions S and C from the ray parameter integrand. Initially, the effects of the source time function, free surface interactions and receiver crust, however, have been separately modeled and convolved in the time domain.

Model studies generally do not require the physical rigor of source theories that seek to obtain precise estimates of such properties as stress drop, moment, or source multiplicity. A sufficient theory can reproduce the waveform of a body wave bottoming in a structurally smooth region such as the lower mantle. Thus a simple box car time function (e.g., Mikomo, 1969) can adequately model the body phases of deep-focus earthquakes. A trapezoidal time function combined with the effects of a double-couple

radiation pattern and near receiver reflected and converted phases can usually model the source function of body waves in the pass band of the long period instruments of the WWSSN and SRO seismic networks (Helmberger, 1974). Such a procedure has been used by Hermann (1975) to invert long period P waveforms for focal depth and focal mechanism. Following Helmberger and Burdick (1978), we employed this procedure to model the source function of the Oroville, Borrego, and Truckee earthquakes using the source paramaters reported by Burdick (1977). When the directivity effects of source finiteness must be modeled (long period S waves for example), a separate source function S may still be defined using a simple propagating line dislocation source model, as in Langston (1978).

Using the approach outlined above to incorporate an earthquake source and the uniformly asymptotic theory, using contours Γ to evaluate the ray parameter integral in eq. 2 as described in Richards (1973, 1976) and Cormier and Richards (1977), we synthesized seismograms of the P wave for the Oroville, Borrego, and Truckee earthquakes in earth model T7 ($T-\Delta$ curve shown in Fig. 1) of Burdick and Helmberger (1978). The results and comparison with the Cagniard synthesis of Burdick and Helmberger are discussed in the next section and summarized in Fig. 2a-e for the Oroville earthquake.

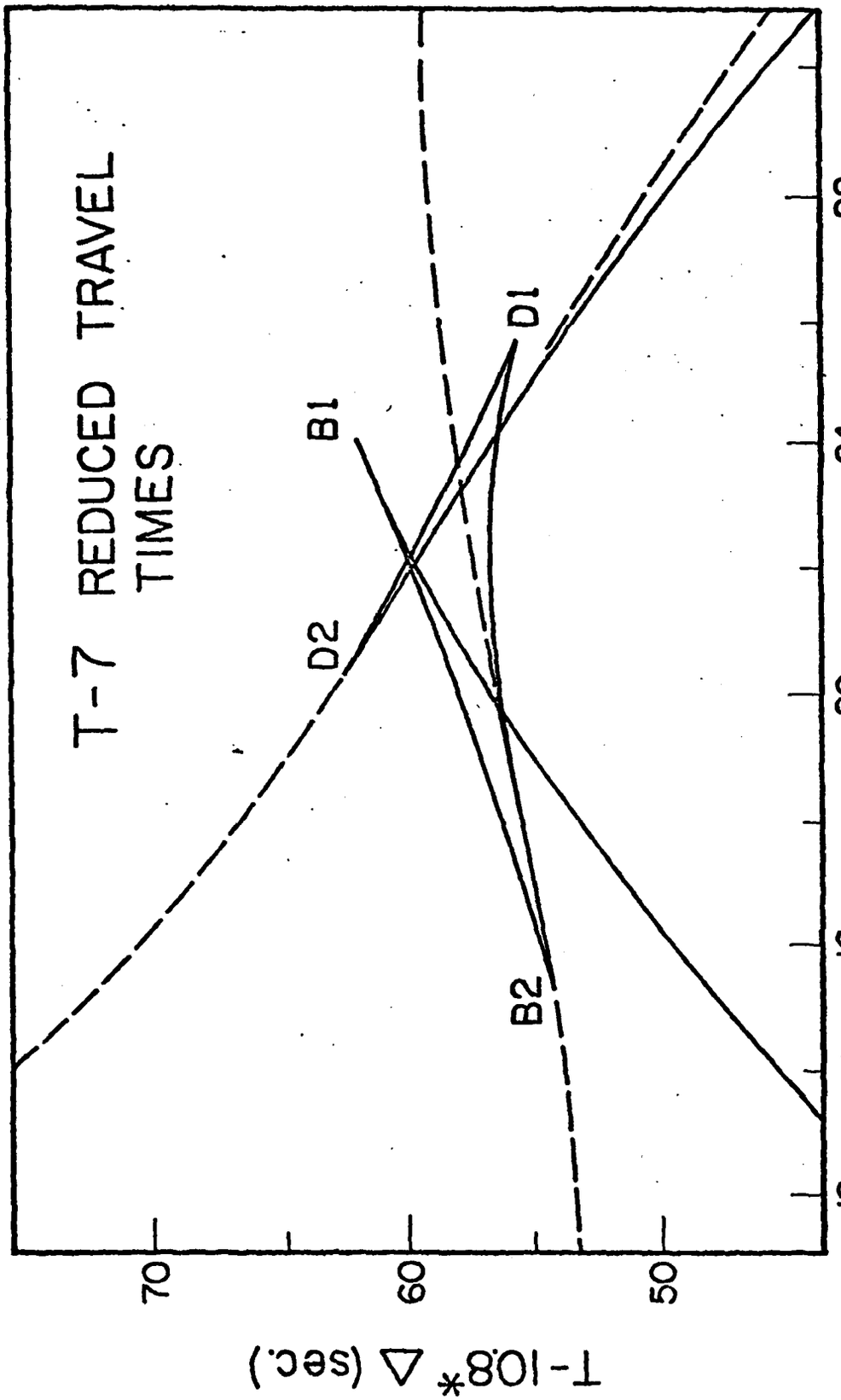

Figure 1. Reduced travel time curve for earth model T7, weaker amplitude arrivals dashed.

FEATURES OF SYNTHETIC SEISMOGRAMS 10-30°

10-20°

Synthetic seismograms for this distance range are shown in Figures (2a-b). The phase of largest amplitude represents a ray bottoming above the 400 km discontinuity. This phase also forms the apparent first arrival. An infinite set of rays interacting with the high velocity lid above the low velocity zone of T7 arrives earlier than the phase of maximum amplitude. Although this study included the lid interactions, their amplitudes are too small to be visible in the period range for which the model response was calculated (64-2 sec). Undoubtedly, in this period range seismic energy can efficiently tunnel out of the 30 km thick lid of T7 and propagate deeper in the mantle.

The two smaller arrivals following the large apparent first arrival are partial reflections from the 400 km and 670 km discontinuities. Note that their amplitude increases slowly and continuously as distance approaches the T-Δ cusps B2 and D2 for critical incidence on the 400 and 670 discontinuities. After convolution with a source function and an instrument response it becomes difficult to identify these partial reflections in the predicted waveform. The later positive peak of smaller amplitude in the observed waveform at station SES may be associated with a 400 km discontinuity.

Note that the Cagniard predicted waveforms have a smoother secondary peak for the source-convolved records than those predicted by the full wave method. This apparent difference may either be due to (1) the different procedure by which anelasticity was included; to (2) the fact that the Cagniard waveforms are constructed from the interference of only primary rays in a stack of homogenous layers; or to (3) the fact that the seismograms

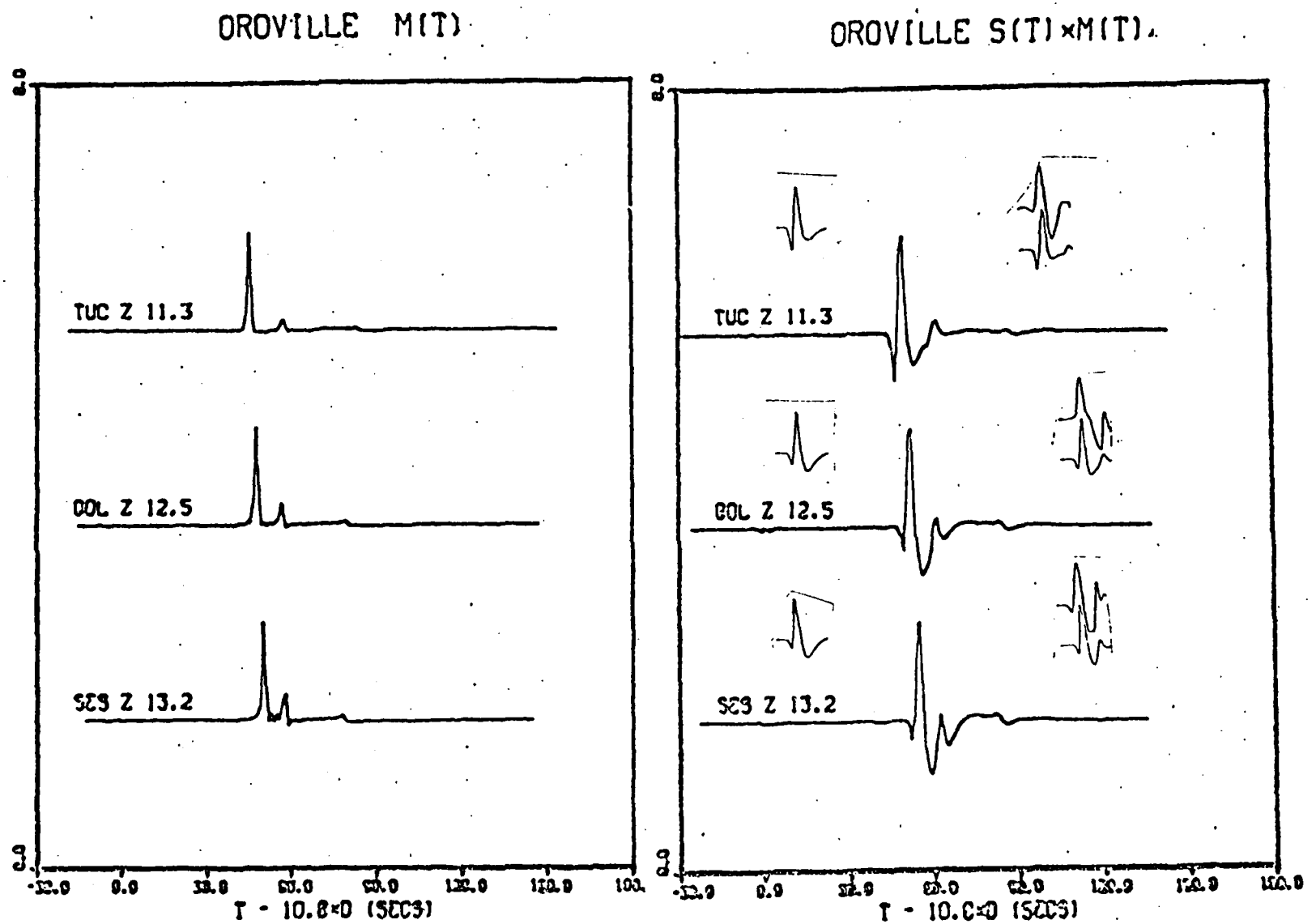

Figure 2a. Left column: synthetic impulse response including the effects of non-dispersive anelasticity calculated using full wave theory. Right column: source-instrument convolved seismogram using the source parameters given by Burdick (1977). Source function shown to upper left of each trace, data (top) and Cagniard synthesized pulse (bottom) shown to upper right of each trace.

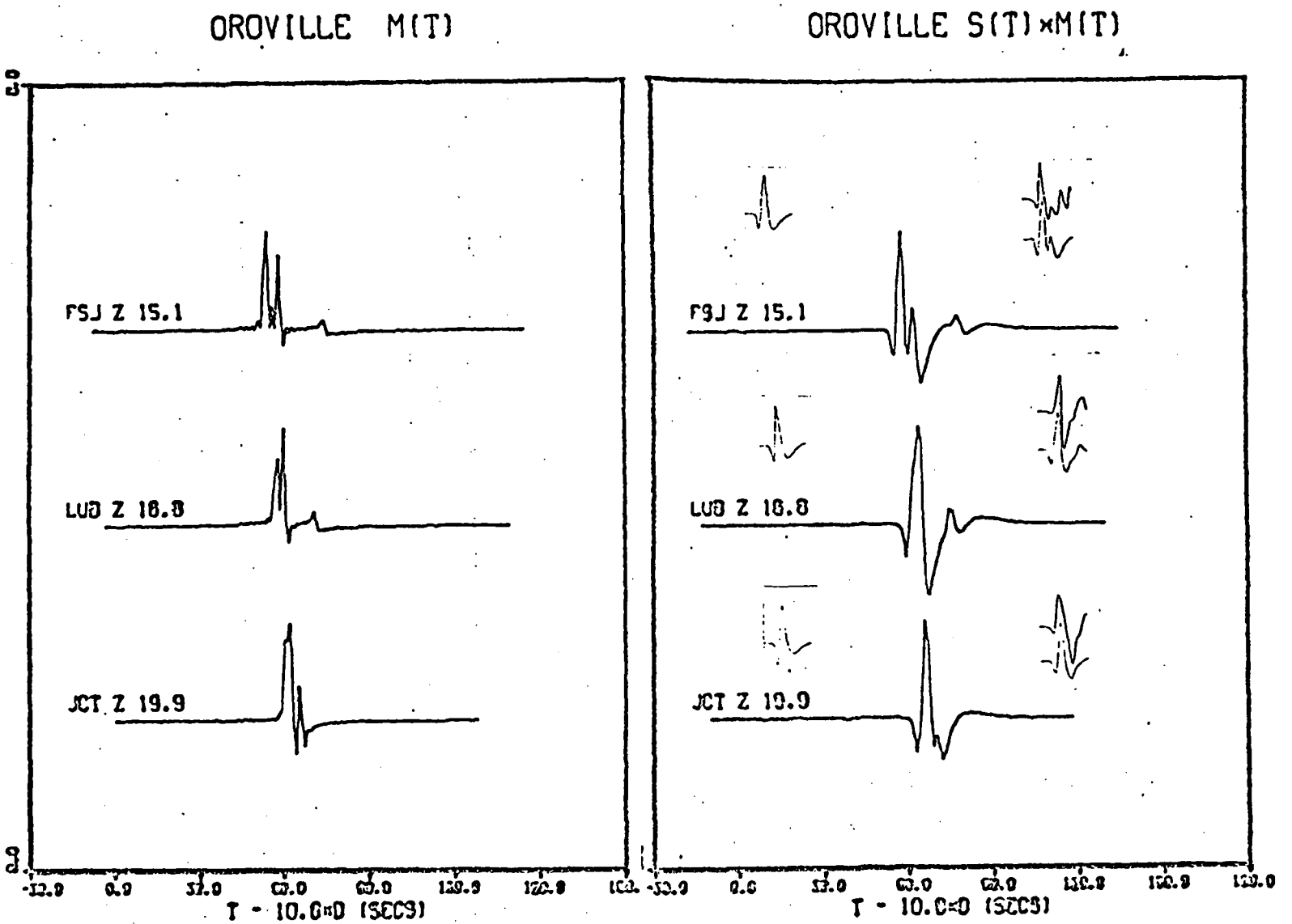

Figure 2b. Left column: synthetic impulse response including the effects of non-dispersive anelasticity calculated using full wave theory. Right column: source-instrument convolved seismogram using the source parameters given by Burdick (1977). Source function shown to upper left of each trace, data (top) and Cagniard synthesized pulse (bottom) shown to upper right of each trace.

are plotted in differing scales. If (1) can be demonstrated to effect the partial reflection predictions, then the full wave results are to be preferred because the different anelastic structure sampled by different rays are propertly included. The Cagniard results, in contrast, applied an average time domain operator to describe the effects of anelasticity for all of the rays composing the seismogram. However, in view of the fact that Burdick and Helmberger (1978) tested the assumption of the average Q operator against that of a Q operator applied to individual rays in thin layers and found insignificant difference in predicted waveforms, then (2) or (3) may be a more likely explanation for the differences in the results for partial reflections near the cusps of critical incidence.

If (3) can be eliminated, it can be determined whether the primary multiple assumption in Cagniard synthesis remains accurate near critical T-Δ cusps. The response near a critical cusp has been shown to be the effect of an infinite set of rays (Cormier and Richards, 1977) that can be included in a full wave theory. Moreover it has been demonstrated that higher order multiples in a stack of thin homogeneous layers must be included in Cagniard seismogram synthesis for rays interacting with a boundary having a strong velocity jump (Cormier and Ruff, 1978). Thus (2) appears to be a likely possibility.

20-25° (Figs. 2c-d)

In this distance range phases due to two interfering T-Δ triplications interfere to form a rather simple waveform after convolution with the source function. The most overwhelming feature of both the synthetics and the data in this distance range is an increase in amplitude. This

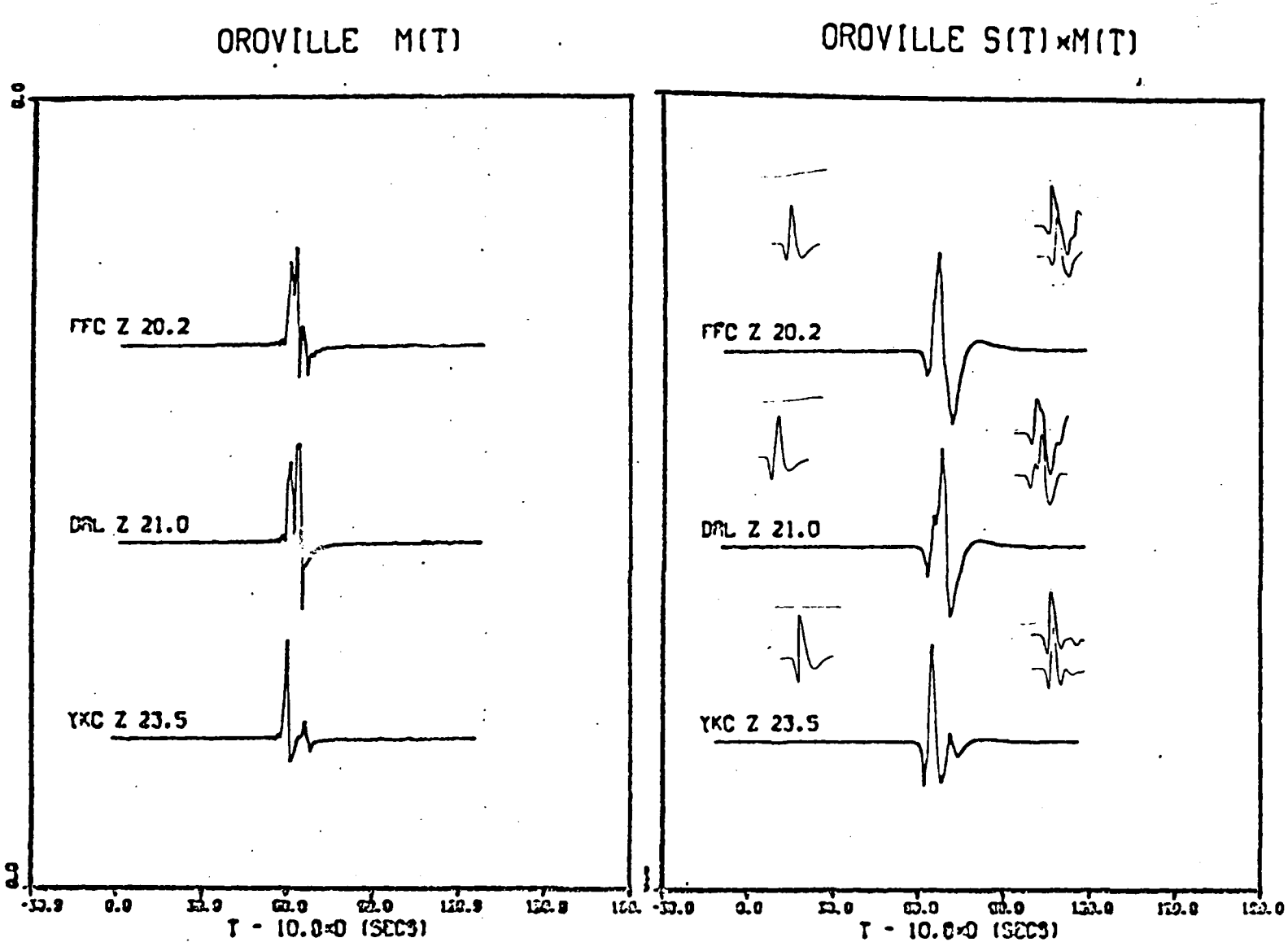

Figure 2c. Left column: synthetic impulse response including the effects of non-dispersive anelasticity calculated using full wave theory. Right column: source-instrument convolved seismogram using the source parameters given by Burdick (1977). Source function shown to upper left of each trace, data (top) and Cagniard synthesized pulse (bottom) shown to upper right of each trace.

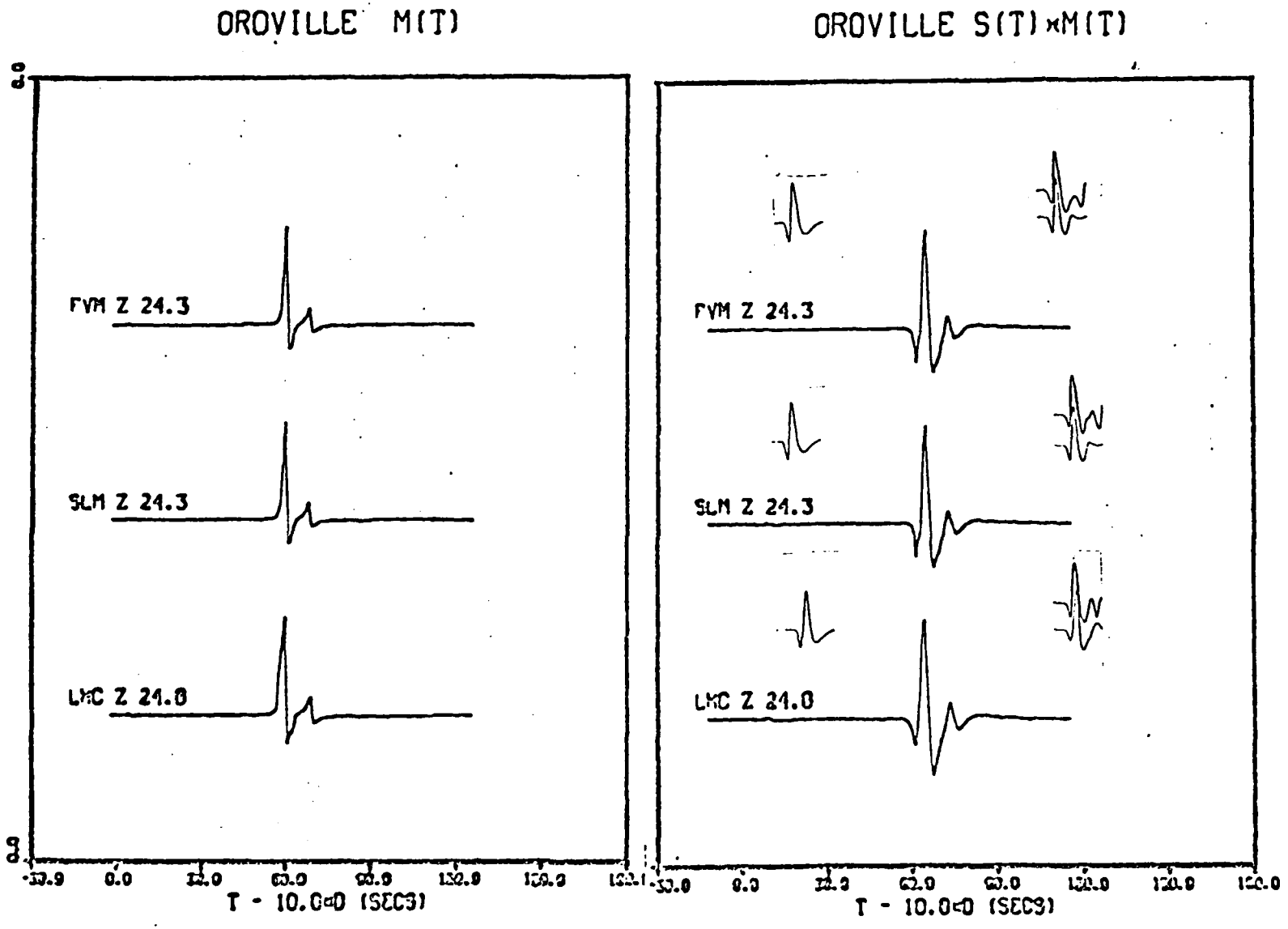

Figure 2d. Left column: synthetic impulse response including the effects of non-dispersive anelasticity calculated using full wave theory. Right column: source-instrument convolved seismogram using the source parameters given by Burdick (1977). Source function shown to upper left of each trace, data (top) and Cagniard synthesized pulse (bottom) shown to upper right of each trace.

amplitude increase near 20° represents Gutenberg's "20° discontinuity" that he attributed to a rapid but smooth velocity increase between 500 and 700 km depth. Discrimination between a smooth velocity profile in these depth ranges and a velocity profile having one or more discontinuous velocity increases really cannot be achieved by long period siesmic data near 20°. Fine scale features of the long period waveform at distances less than 20° and greater than 25° may provide the resolution required, but the effects of both source and crustal structure must be known so that they can be convincingly eliminated as the explanation of the small scale waveform features.

25-30° Fig. 2e

In this distance range several ray interactions with the 400 and 670 km discontinuities begin to separate from the waveform containing the ray that bottoms below the 670 discontinuity. These interactions in order of increasing travel time are (1) the interference head wave along the underside of the 670 discontinuity, (2) a diffracted wave along the top side of the 670 discontinuity from the D1 cusp, (3) an interference head wave along the underside of the 400 km discontinuity, and (4) a diffracted wave along the top side of the 400 km discontinuity from the B1 cusp. Agreement between the full wave predicted and the Cagniard predicted waveforms is good for the first 10-15 seconds. Agreement between the methods for the later portion of the waveforms must be checked by obtaining plots of the Cagniard results at the same scale. Differences between the methods in this portion of the waveform will again bear upon the accuracy of the primary multiple assumption used in standard application of Cagniard

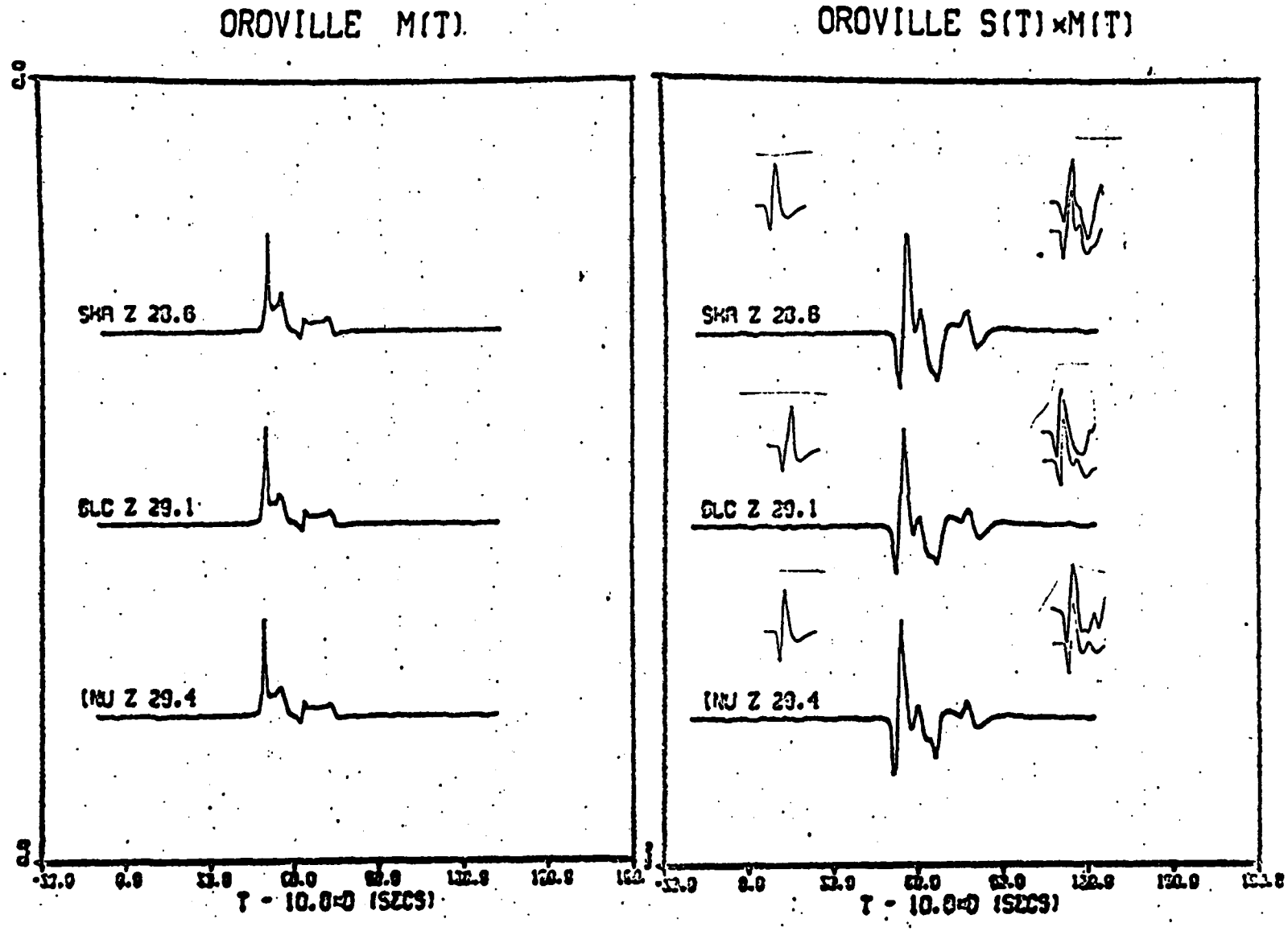

Figure 2e. Left column: synthetic impulse response including the effects of non-dispersive anelasticity calculated using full wave theory. Right column: source-instrument convolved seismogram using the source parameters given by Burdick (1977). Source function shown to upper left of each trace, data (top) and Cagniard synthesized pulse (bottom) shown to upper right of each trace.

synthesis. Stations SHA and INU exhibit the strongest indication of earth structure influencing waveform. The inflection in the negative slope of the large pulse at SHA and the secondary peak at INU, arriving after the large pulse, may be the combined effect of the four phases interacting with the 400 and 670 discontinuities in T7. At all distances it can be observed that the full wave and Cagniard synthetic waveforms agree with each other better than either agree with the data.

SUMMARY

Good agreement has been obtained bewteen Cagniard and fullwave synthesized waveforms of P waves interacting with a model of the earth's upper mantle that satisfies travel times and approximately accounts for the long-period waveforms observed at 10-30°. There are minor differences in the waveforms that will not affect the interpretations that Burdick and Helmberger (1978) used in deriving the T7 earth model for western North America. These differences, however, should be resolved by careful comparison of synthetic waveforms at the same scale in order that the breakdown in the primary ray assumption of Cagniard synthesis can be defined.

Future work will also be directed toward applying full wave synthesis to determine upper mantle structure beneath central Asia. Several source time functions appropriate for long period WWSSN stations have been derived by Herrmann and Hewitt (1975) for earthquakes in the Tien Shan region for which we have obtained seismograms from the Soviet seismographic station network (ESSN). The seismograms obtained from Tien Shan earthquakes at the Soviet network are in an ideal distance range for study of upper mantle structure (10-40°)

and a preliminary survey of the available records from the SK broadband instruments indicates that several of the Soviet stations may supplement data available from the WWSSN network for the Tien Shan earthquakes. In the course of this study we will wish to ascertain whether the sharp mantle discontinuities suggested by the study of Burdick and Helmberger (1978) of western North America and the study of King and Calcagnile (1976) of Europe are also a required structural feature of the upper mantle beneath central Asia.

References

Anderson, D. L., and R. S. Hart, 1976. An earth model based on free oscillations and body waves, J. Geophys. Res., 81, 1461-1475.

Burdick, L. J., 1977. Broad band seismic studies of body waves, Ph.D. Thesis, Calif. Inst. of Technol., Pasadena.

Burdick, L.J., and Helmberger, D.V., 1978. The upper mantle P velocity structure of the western United States, J. Geophys. Res., 83, 1699-1712.

Cormier, V.F., and Richards, P.G., 1976. Comments on 'The damping of core waves' by Anthony Qamar and Alfredo Eisenberg, J. Geophys. Res., 81, 3066-3068.

Cormier, V. F., and Richards, P.G., 1977. Full wave theory applied to a discontinuous velocity increase: the inner core boundary, J. Geophys., 43, 3-31.

Cormier, V. F., 1977. Synthesis of Long Period Body Waves in an Anelastic Earth, Semi-Annual Technical Report, No. 6, ARPA Order 3291, CIRES, Univ. of Colorado, Boulder.

Cormier, V. F., and Ruff, L., 1978. A comparison of full wave and Cagniard synthesis of P waves interactional with the earth's core, Semi-Annual Technical Report, No. 7, ARPA Order 3291, CIRES, Univ. of Colorado, Boulder.

Helmberger, D.V., 1974. Generalized ray theory for shear dislocation, Bull. Seismol. Soc. Amer., 64, 45-64.

King, D.W., and Calcagnile, G., 1976. P wave velocities in the upper mantle beneath Fennoscandia and western Russia, Geophys. J. Roy. Astron. Soc., 46, 407-432.

Hermann, R. B., and Hewitt, T., 1975. Source characteristics from long period P wave observations, Semi-Annual Technical Report, No. 2, ARPA Order 1827, CIRES, Univ. of Colorado, Boulder.

Hermann, R.B., 1975. Focal depth determination from the signal character of long period P waves, Semi-Annual Technical Report, No. 2, ARPA Order 1827, CIRES, Univ. of Colorado, Boulder.

Langston, C.A., 1978. The February 9, 1971 San Fernando Earthquake: A study of finiteness in teleseismic body waves, Bull. Seismol. Soc. Am., 68, 1-30.

Mikomo, T., 1969. Long-period P waveforms and the source mechanism of intermediate earthquakes, J. Phys. Earth, 17, 169-313.

Richards, P.G., 1973. Calculation of body waves for caustics and tunnelling in core phases. Geophys. J. Roy. Astron. Soc., 35, 243-264.

Richards, P.G., 1976. On the adequacy of plane-wave reflection-transmission coefficients in the analysis of seismic body waves, Bull. Seism. Soc. Am., 66, 707-718.

B. Asymptotic Wave Theory Applied to the Synthesis of Complete Seismograms in the Near Field - Vernon F. Cormier

INTRODUCTION

The mode sum seismograms described by Harvey in another section of this report (Section IV) will provide an important constraint on near and regional field descriptions of explosions and earthquakes. The method of synthesizing these seismograms has relied on a description of the earth model with planar homogeneous layers. Because we will be interested in modeling the seismograms observed primarily on short period seismograph systems, the ability of asymptotic solutions for the radial or depth eigenfunctions to approximate the solutions for inhomogeneous layers in the limit of sufficiently high frequency deserves investigation. Such solutions of the type recently obtained by Woodhouse (1978) will allow a much simpler description of complicated earth models with a small number of inhomogeneous layers and with negligible additional computational cost for the layer eigenfunctions. (Specifically, many fewer multiplications will be required in a simpler description of the earth model.) The well-known beahvior of the uniformly asymptotic solutions (Airy functions) to the depth eigenfunctions of an inhomogeneous layer may simplify any search scheme for frequency-wavenumber poles required to generate a mode sum seismogram (Garmany, personal communication). Such a procedure may prove to be a necessity for an earth model having regions of strong velocity and density gradient. In the following discussion a procedure is outlined for application of such an asymptotic wave theory to the P-SV propagation problem. Simple examples are given for the SH problem.

THEORY

By applying the vector representation theorem for a sphere, the seismic displacement vector $\underline{u}$ may be written as

$$\underline{u} = \int_{-\infty}^{\infty} d\omega e^{i\omega t} \sum_{\ell=0}^{\infty} \sum_{m=-\ell}^{\ell} \left(U\underline{P}_\ell^m + V\underline{B}_\ell^m + W\underline{C}_\ell^m \right) \tag{1}$$

where $\underline{P}_\ell^m$, $\underline{B}_\ell^m$, $\underline{C}_\ell^m$ are the vector spherical harmonics defined by

$$\underline{P}_\ell^m = \hat{\underline{r}} Y_\ell^m(\theta,\phi), \quad \underline{B}_\ell^m = \underline{\nabla}_1 Y_\ell^m(\theta,\phi),$$

$$\underline{C}^m = -\hat{\underline{r}} \times \underline{\nabla}_1 Y^m(\theta,\phi); \quad (\underline{\nabla}_1 = \hat{\theta}\partial_\theta + \operatorname{cosec} \hat{\phi}\partial_\theta)$$

(Morse and Feshbach, 1953). $\hat{\underline{r}}$, $\hat{\underline{\theta}}$, and $\hat{\underline{\phi}}$ are unit vectors in the spherical coordinate directions r, θ, ϕ. The radial eigenfunctions U, V, and W satisfy vector-matrix equations of the form

$$\partial_r \underline{f}^T = \omega(\underline{\underline{A}}_o^T + \omega^{-1}\underline{\underline{A}}_1^t + \omega^{-R}\underline{\underline{A}}_2^T)\underline{f}^T \tag{2}$$

for SH type body waves and toroidal free oscillations, and

$$\partial_r \underline{f}^S = \omega(\underline{\underline{A}}_o^S + \omega^{-1}\underline{\underline{A}}_1^S + \omega^{-2}\underline{\underline{A}}_2^S)\underline{f}^S \tag{3}$$

for P-SV type body waves and spheroidal free oscillations, when gravitational effects can be ignored at high frequencies (Woodhouse, 1978). The stress-

displacement vectors $\underline{f}^T$, $\underline{f}^S$ are defined in terms of the radial eigenfunctions as:

$$\underline{f}^T = \begin{bmatrix} W \\ \omega^{-1} T \end{bmatrix}, \quad \underline{f}^S = \begin{bmatrix} U \\ \omega\, V \\ p \\ \omega^{-1} P \\ p\, S \end{bmatrix}; \quad \text{where } p = [\ell(\ell+1)]^{1/2}/\omega$$

In the limit of infinite frequency ω, p may be identified as a seismic ray parameter or horizontal slowness.

A matrix $\underline{F}$ satisfying either eq. (2) or (3) in the column vectors $\underline{f}^T$, $\underline{f}^S$ is defined as a fundamental matrix (Gilbert and Backus, (1966)or matricant (Gantmacher, 1959). As shown by Gilbert and Backus (1966) the fundamental matrices of these equations allow a convenient and notationally compact method of satisfying the boundary conditions at layers of an earth model having discontinuities in elastic moduli and/or density. The stress-displacement vector $\underline{f}$ at a radius a is related to that at a radius r_n through a propagator matrix $\underline{P}$ constructed from the fundamental matrix for each layer:

$$\underline{f}(a) = \underline{P}(a, r_n)\, \underline{f}(r_n),$$

where $$\underline{P}(a, r_n) = \underline{F}(a)\, \underline{F}^{-1}(r_1) \cdots \underline{F}(r_{n-1})\, \underline{F}^{-1}(r_n)$$

The general solution to eq. (2) or (3) for the displacement-stress vector $\underline{f}$, including the effects of a source vector term $\underline{S}$, can be written as

$$\underline{f}(a) = \underline{\underline{P}}(a,r_o)\ \underline{f}(r_o) + \int_{r_o}^{a} \underline{\underline{P}}(a,\xi)\underline{S}(\xi)\,d\xi \qquad (4)$$

where r_o is some reference radius at which a starting solution $\underline{f}(r_o)$ is defined (Wasow, 1965). As an example of the application of the solution above, consider the stress-displacement vector for SH type body waves:

$$\begin{bmatrix} W(a) \\ \omega^{-1}T(a) \end{bmatrix} = \left[\underline{\underline{P}}(a,r_o)\right] \begin{bmatrix} W(r_o) \\ \omega^{-1}T(r_o) \end{bmatrix} + \int_{r_o}^{a} \underline{\underline{P}}(a,\xi)\underline{S}(\xi)\,d\xi$$

We will define a source vector $\underline{S}$ of the form

$$\underline{S} = \begin{bmatrix} 0 \\ -F\delta(r-r_S)/r^2 \end{bmatrix}$$

(A generalized source can be included by expanding its representation as a vector of force density in vector spherical harmonics and incorporating the appropriate coefficients for $\underline{P}_\ell^m$, $\underline{B}_\ell^m$, $\underline{C}_\ell^m$ in the definition of $\underline{S}$.)
We next assume that the radial eigenfunction W will be observed at the earth's surface (r=a). Thus the vanishing of shear stress at the r=a requires

$$\begin{aligned} W(a) = {} & [P_{22}(a,r_o)\ P_{11}(a,r_o) - P_{12}(a,r_o)\ P_{21}(a,r_o)]\ W(r_o) \\ & + [P_{12}(a,r_o)\ P_{22}(a,r_s) - P_{22}(a,r_o)\ P_{12}(a,r_s)]\ Kr_s^2/P_{22}(a,r_o) \end{aligned} \qquad (5)$$

At this stage the solution form given by eq. (5) is independent of any representation of the earth model, e.g., planar homogeneous layers, spherical inhomogeneous layers, etc. We will now assume that the earth model is specified by spherical inhomogeneous layers and apply Woodhouse's (1978) asymptotic solution to the propagator matrix for such layers, namely

$$\underline{\underline{P}}(r_2,r_1) = \underline{\underline{E}}(r_2)\ \underline{\underline{E}}^{-1}(r_1)$$

$$= r_2^{-1}\ \underline{\underline{R}}(r_2)\left[\underline{\underline{I}} + \omega^{-1} r_2\ \underline{\underline{T}}^{(1)}(r_2)\right] \underline{\underline{\phi}}(r_2)\underline{\underline{G}}(r_2) \qquad (6)$$

$$\cdot\ \underline{\underline{G}}^{-1}(r_1)\underline{\underline{\phi}}^{-1}(r_1)\left[\underline{\underline{I}} - \omega^{-1}\ \underline{\underline{T}}^{(1)}(r_1)\right] \underline{\underline{R}}^{-1}(r_1) r_1$$

where for SH type body waves

$$\underline{\underline{R}} = \begin{bmatrix} 0 & \mu^{-1/2} \\ \mu^{-1/2} & 0 \end{bmatrix} \qquad (7a)$$

$$\underline{\underline{\phi}} = \begin{bmatrix} |\partial_r \phi|^{1/2} & 0 \\ 0 & -\mathrm{sgn}(\partial,\phi)\,|\partial_r \phi|^{-1/2} \end{bmatrix} \qquad (7b)$$

$$\underline{\underline{G}} = \pi^{1/2} \begin{bmatrix} \omega^{-1/6}\, Ai'(-\omega^{2/3}\phi) & \omega^{-1/6}\, Bi'(-\omega^{2/3}\phi) \\ \omega^{1/6}\, Ai(-\omega^{2/3}\phi) & \omega^{1/6}\, Bi(-\omega^{2/3}\phi) \end{bmatrix} \qquad (7c)$$

$$\phi = -\left|\operatorname{sgn}\left(\frac{p^2}{r^2} - \frac{1}{\beta^2}\right)\right| 3/2 \int_{r_p}^{r} \left|\frac{p^2}{r^2} - \frac{1}{\beta^2}\right|^{1/2} dr \Bigg|^{2/3} \qquad (7d)$$

The matrix $\underline{\underline{T}}$ describes coupling of up and downgoing waves, which is important when the second order radial derivative of velocity is large. (r_p is the turning point radius, that radius at which $p^2/r^2 = 1/\beta^2$. A limitation of the Airy function solutions (Ai and Bi) is that they must be applied to an inhomogeneous layer in which only <u>one</u> turning point is present, so a low velocity zone must be described by more than one layer.)

The solution form is the same for planar inhomogeneous layers with $p^2/r^2 \to k^2$ in the above formulae. (Thus little is gained by applying an earth flattening transformation before specifying the velocity variation in the inhomogeneous layers.)

We note also that the matrix solution G may contain any linear independent set of Airy functions. The set $\mathrm{Ai}(-\omega^{2/3}\phi)$, $\mathrm{Ai}(-e^{+2\pi i/3}\omega^{2/3}\phi)$ can also be used to define the matrix G, and is preferred when the analogy is made to the radial eigenfunctions, that is the spherical Bessel function j_n and spherical Hankel function $h_n^{(1)}$. This choice of the linear independent pair of Airy functions: (1) readily allows the identification of seismic rays in the final solution form for displacement; (2) moves ray parameter poles off the real ray parameter axis facilitating the evaluation of the sum over ℓ, in eq. (1), by Watson transformation and numerical integration and (3) generates sets of poles, the residues of which can be associated with Rayleigh type surface waves, interference head waves, and Stoneley type boundary waves (e.g., Uberall, 1975). Woodhouse's choice of the independent

solutions Ai and Bi, on the other hand, is most useful in a mode summation approach to the evaluation of eq. (1), because, in an earth model without anelasticity, poles in the ω plane will then be on the real ω axis.

By substituting the results for the asymptotic propagator matrix (eq. 6 and 7a-d) in the solution form given by eq. (5), it can be noted that the problems of choosing a reference radius r_o and defining a starting solution $W(r_o)$ resolve themselves automatically. We may assume a solution form of $W(r_o) \sim Ai(-\omega^{2/3}\phi)$, allowing only an exponentially decaying solution at a radius r_o far below that of any turning point radius r_p. The r_p domain corresponds to a domain in ray parameter needed to evaluate eq. (1) at a particular distance. Thus we may imagine r_o to be very deep, and set $W(r_o) = 0$. Equivalently, it can be shown that the entire expression in brackets multiplying $W(r_o)$ in eq. (5) approaches zero for r_o chosen sufficiently deep. Setting $Ai(-\omega^{2/3}\phi)\big|_{r_o} = 0$ or $W(r_o) = 0$ and applying the Wronskian relation:

$$Ai\big|_a \; Bi'\big|_a - Ai'\big|_a \; Bi\big|_a = \text{const.} \tag{8}$$

it can be shown for an earth model described by a continuously inhomogeneous sphere, that:

$$W(a) = C r_s^{-2} \omega^{1/3} \left|\partial_r \phi\right|^{-1} \operatorname{sgn}(\partial_r \phi) \left[Ai(-\omega^{2/3}\phi)\big|_{r_s}\right] \Big/ \left[Ai'(-\omega^{2/3}\phi)\big|_a\right] \tag{9}$$

where r_s is the radius of the source and C is a constant.

A feature that this solution must possess is a "ray-mode duality" (Pekeris, 1948); that is, all possible seismic rays for SH waves in a spherical earth must be contained in the solution. To see that this is indeed so, we can asymptotically expand the functions A_i and A_i' by using the first term in asymptotic expansion of these functions for large argument $|-\omega^{2/3}\phi|$. Thus

$$\left[Ai(-\omega^{2/3}\phi)\Big|_{r_s}\right] \Big/ \left[Ai'(-\omega^{2/3}\phi)\Big|_{a}\right]$$

$$\sim \frac{\left[e^{-i\pi/4}\, e^{+i\omega J_1} + e^{+i\pi/4}\, e^{-i\omega J_1}\right]}{\omega Q\left[e^{+i\pi/4}\, e^{+i\omega J_2} + e^{-i\pi/4}\, e^{-i\omega J_2}\right]} \tag{10}$$

where:

$$Q = \left(\frac{1}{\beta^2} - \frac{p^2}{r^2}\right)^{1/2}$$

$$J_1 = \int_{r_p}^{r_s} Q\,dr$$

$$J_2 = \int_{r_p}^{a} Q\,dr.$$

Now by performing a binomial expansion of the denominator of expression on the right side of eq. (10), it can be shown that a resultant sum of phasors corresponds to the accumulated $T(p)-\Delta(p)$ phase of the rays: sS + S + sSS + SS + ..., including the effects of a π phase change upon free surface reflection and a $\pi/2$ relative phase shift between those rays having an even and odd number of turning points.

SUMMARY

In the theoretical section above it has been shown how the asymptotic propagator theory developed by Woodhouse (1978) may be applied to the synthesis of a complete seismogram containing all possible ray interactions and surface waves. The example given was that for SH type body waves in an unlayered (continuous) inhomogeneous earth. Application of the theory to P-SV type waves in general earth models will follow the outline of procedures outlined above. In future applications we wish to determine whether a mode summation scheme or a ray parameter integral scheme is more efficient for the evaluation of eq. (1) and the synthesis of seismograms in the distance range from 0 to 200 km from the source. In applications to practical earth models, we see no reason to include more than five inhomogeneous layers to describe the velocity variation in the crust and upper mantle having a low velocity zone. The argument of the Airy functions required in the propagator matrix evaluations can be rapidly calculated when the earth model is described in each inhomogeneous layer by the function:

$$\ln(r) = P(\eta) \qquad (11)$$

where P represents a polynomial in the parameter $\eta = \frac{r}{v(r)}$ (Richards, Garmany, personal communications). Furthermore, anelasticity can be incorporated by allowing the polynomial coefficients in the above formula to be complex.

References

Gantmacher, F. R., 1959. The Theory of Matrices: 2 vols., Chelsea, New York, translated from the Russian by K.A. Hirsch.

Gilbert, F. and Backus, G.E., 1966. Propagator matrices in elastic wave and vibration problems. Geophysics, 31, 326-332.

Morse, P. M. and Feshbach, H., 1953. Methods of Theoretical Physics, McGraw-Hill.

Pekeris, C. L., 1948, Theory of propagation of explosive sound in shallow water, in Propagation of Sound in the Ocean, Geol. Soc. Am. Memoir 27.

Uberall, H., 1975. Surface waves in acoustics, in Physical Acoustics, vol. 10, edited by W.P. Mason and R. N. Thruston, Academic Press, New York, 1-60.

Wasow, W., 1965. Asymptotic Expansions for Ordinary Differential Equations, vol. 14, Pure and Applied Mathematics, Interscience Publishers, John Wiley, New York.

Woodhouse, J. H., 1978. Asymptotic results for elastodynamic propagator matrices in plane-stratitied and spherically stratified earth models, Geophys. J. Roy Astron. Soc., 54, 263-280.

C. The Horizontal Wave Function in Antipodal and Near Source Representations of Seismic Displacement

Vernon F. Cormier

(Submitted to the Geophysical Journal of the Royal Astronomical Society)

ABSTRACT

Representations for seismic displacement are given for the antipodal and source regions on a sphere. Representations on a flattened sphere are found by transforming relevant spherical formulae. Asymptotic forms of the horizontal wavefunction in these representations are examined for their domains of validity. These domains are expressed as functions in frequency, ray parameter, and angular distance from the source or its antipode. The first two terms of the uniform asymptotic expression for the Legendre function by Szego remain valid for arbitrarily small values of radian distance (Δ) and radial order number (ωp). The first term in the asymptotic separation of the Legendre function $P_n(\cos \Delta)$, or the Bessel function $J_o(kx)$, into traveling wave components becomes accurate to within 0.1% at $|\omega p \Delta|$ or $|kx|$ equal to 10.

INTRODUCTION

Calculation of seismic displacement from an asymptotic wave theory often requires the inversion of an integral transform in space. In a layered half space this step involves the evaluation of the Sommerfeld integral (e.g., Ewing et al., 1959) or in a sphere the evaluation of an integral over the horizontal wavenumber derived from either a Watson or Poisson transform of a partial wave series (e.g., Scholte, 1956). The integrand in the wavenumber integral in both planar and spherical coordinates contains as a factor a horizontal wavefunction that represents the solution to the horizontally separated part of a Helmholtz equation for potential. Replacement of the horizontal wavefunction in the integrand by an asymptotic representation simplifies the evaluation of the wavenumber integral. Care, however, must be taken that the asynptotic representation chosen is valid in the desired domain of frequency, wavenumber, and distance. This research note specifies rules as functions of frequency, wavenumber, and epicentral distance for choosing one or another asymptotic representation of the horizontal wavefunction. These rules allow appropriate asymptotic representations for the horizontal wavefunctions to be chosen for seismogram synthesis in both the source and antipodal regions.

DISPLACEMENT REPRESENTATIONS

Consider the Fourier-transformed displacement potential χ observed on a homogeneous sphere of radius r due to an explosive point source at $r_s < r$ and radian distnace Δ. χ may be expended in terms of spherical Hankel functions $h^{(1)}$ and $h^{(2)}$,

$$(1) \qquad \chi(r,\omega,\Delta) = S \sum_{n=0}^{\infty} (n + 1/2)\, h_n^{(1)}(\kappa r)\left[h_n^{(1)}(\kappa r_s) + h_n^{(2)}(\kappa r_s)\right] P_n(\cos \Delta) \quad ,$$

where $\kappa = \omega/v$ and S incorporates constants for source normalization and strength. S can be generalized to be a function $S(\omega,\phi,p)$ of frequency ω, azimuth ϕ, and ray parameter p to describe the far field radiation pattern and spectrum of any multipole point source (Minster, 1973).

The step required to generalize eq. (1) to an inhomogeneous sphere basically consists in substituting generalized vertical wavefunctions $g^{(1)}$ and $g^{(2)}$ for $h^{(1)}$ and $h^{(2)}$. Asymptotic wave theory takes $g^{(1)}$ and $g^{(2)}$ as asymptotic solutions to the radial part of the Helmholtz equation satisfied by χ in an inhomogeneous sphere. Asymptotic expensions for $g^{(1)}$ and $g^{(2)}$ have been discussed by Langer (1949), Olver (1956), and Richards (1976). In the application of asymptotic wave theory it is also convenient to convert by either a Watson or Poisson transform the discrete sum over radial order number to an integral over continuous radial order number γ or, as in Richards (1973), to an integral over ray parameter p, where

$$n = \nu - 1/2 = \omega p - 1/2 \quad .$$

The angle of emergence e can then be defined in terms of ray parameter p and $S(\omega,\phi,e)$ incorporated in the ray parameter integrand.

The Watson and Poisson transforms are equivalent. The Poisson transform, however, can be more readily interpreted in terms of traveling waves on a sphere and its contour along the real p axis simplifies the

discussion of any contour deformation required to efficiently solve a particular wave propagation problem. Thus we introduce two possible Poisson transforms of eq. (1)

$$\text{(2a)} \qquad \chi(r,\omega,\Delta) = \frac{\omega^2}{2} \sum_{m=-\infty}^{\infty} (-)^{m+1/2} \int_0^{\infty} pS(\omega,\phi,p)\, M(r,\omega,p) \cdot P_n(\cos\Delta) \exp(2i\, m\pi\omega p)\, dp$$

$$\text{(2b)} \qquad \chi(r,\omega,\Delta) = \frac{\omega^2}{2} \sum_{m=-\infty}^{\infty} (-)^{m} \int_0^{\infty} pS(\omega,\phi,p)\, M(r,\omega,p) \cdot P_n(\cos\Delta') \exp[i(2m+1)\pi\omega p]\, dp$$

where $\Delta' = \pi - \Delta$, $M(r,\omega,p) = g^{(1)}_{\omega p-1/2}(r_s)\,[g^{(1)}_{\omega p-1/2}(r) + g^{(2)}_{\omega p-1/2}(r)]$.

In a sphere having one or more discontinuities, M can be taken to be the product of generalized reflection-transmission coefficients representing one term in a ray expansion (Scholte, 1956; Richards, 1973). More generally M can be taken as a reflectivity function for a stack of layers having spherical boundaries (Frazer, 1977) analogous to the reflectivity function Fuchs and Muller (1968) defined for planar layers.

Equation (2a) follows from applying the Poisson transform,

$$\sum_{n=0}^{\infty} f(n) = \frac{1}{2} \sum_{m=-\infty}^{\infty} (-)^m \int_0^{\infty} f(\nu) \exp(2im\pi\nu)\, d\nu$$

directly to eq. (1). Eq. (2b) follows by substituting the identity $P_n(-\cos\Delta) = (-)^n P_n(\cos\Delta)$ in eq. (1) and then applying the Poisson transform (Nussenzweig, 1969).

The terms in $m \neq 0$ in eqs. (2a-2b) can be interpreted as traveling waves making m circuits about the earth's center. For example $m = 1$ at the distance for which the seismic phase PK4KP has a caustic surface (420°). In most applications to seismic body waves $m = 0$.

For Δ measured from the source $(0 \leq \Delta < \pi)$ and $m \neq 0$ eq. (2a) properly describes the seismic radiation directly above the source. Eq. (2a) is also correct for $m = 0$, provided the source can be adequately represented by its far field term at $\Delta = 0$ for frequency ω. For Δ' measured from the antipode $(0 \leq \Delta' < \pi)$ evaluation of eq. (2b) will properly describe the antipodal focusing of seismic radiation, examples of which have recently been given by Rial (1978). Far from either the source or antipode, the Legendre function in either eq. (2a) or eq. (2b) can be asymptotically expanded into traveling wavefunctions $Q^{(1)}$ and $Q^{(2)}$. The next section will consider the domain of validity of this expansion and more general asymptotic expansions of P_n.

PRACTICAL EVALUATION OF THE HORIZONTAL WAVEFUNCTION

The defining formula

The Legendre function $P_n(\cos\Delta)$ can be defined in terms of an infinite series,

$$(3) \qquad P_n(\cos\Delta) = \sum_{s=0}^{\infty} \frac{(\omega p+1/2)_s (\omega p-1/2)_s \left(\frac{1-\cos\Delta}{2}\right)^s}{\Gamma(s+1)s!}$$

where $(a)_0 = 1$ and

$$(a)_s = a(a+1)(a+2)\ldots(a+s-1) \quad .$$

A truncated formula (3) may always be calculated but rapidly becomes both inefficient and imprecise as the individual terms in the series become large. In a computer having a 60 bit word length the precision becomes worse than 1% when

$$(1-\cos\Delta)\cdot(\omega p)^2 > 2 \quad ,$$

which can be used as a practical criterion for abandoning the use of eq. (3) for calculating $P_n(\cos\Delta)$.

Szego's uniformly asymptotic formula

We next examine Szego's (1934) uniform asymptotic expression for $P_n(\cos\Delta)$, generally valid for large $|\omega p|$ and uniform in the sense that it remains continuously accurate as $\cos\Delta \to 0$. The complete asymptotic expression is

$$P_n(\cos\Delta) = \left(\frac{\Delta}{\sin\Delta}\right)^{1/2} \left[J_0(\omega p\theta) \sum_{s=0}^{p} \frac{A_s(-\Delta^2)}{(\omega p)^{2s}} \right.$$

$$\left. - \frac{\Delta}{\omega p} J_1(\omega p\Delta) \sum_{s=0}^{p-1} \frac{B_s(-\Delta^2)}{(\omega p)^{2s}} + R_p \right] \quad ,$$

where truncation of terms of order less than $(\omega p)^{-2p}$ leaves a remainder Rp .

The first two terms in this series are given by

$$(4) \qquad P_n(\cos\Delta) \approx \left(\frac{\Delta}{\sin\Delta}\right)^{1/2}\left[J_0(\omega p\Delta) + (\cos\Delta - 1/\Delta)\,\frac{J_1(\omega p\Delta)}{8\omega p}\right]$$

The term in J_1 can be included simply in most Bessel function calculation schemes. In practice, however, values of ωp are usually such that the J_1 term is small at both large and small Δ .

The traveling wavefunctions $Q_n^{(1)}$ $Q_n^{(2)}$

To derive an expression for P_n in terms of traveling wavefunction $Q_n^{(1)}$ and $Q_n^{(2)}$, we first separate J_0 and J_1 in eq. (4) into Hankel functions:

$$J_0(\omega p\Delta) = \frac{1}{2}\left[H_0^{(1)}(\omega p\Delta) + H_0^{(2)}(\omega p\Delta)\right]$$

$$J_1(\omega p\Delta) = \frac{1}{2}\left[H_1^{(1)}(\omega p\Delta) + H_1^{(2)}(\omega p\Delta)\right]$$

The functions $Q^{(1)}$ and $Q^{(2)}$ may then be defined by substituting asymptotic expressions for $H^{(1)}$ and $H^{(2)}$ valid for $|\omega p\Delta| \gg 1$ and separating the terms in $H_{0,1}^{(1)}$ and $H_{0,1}^{(2)}$. Thus

$$(5a) \qquad P_n(\cos\Delta) \approx Q_n^{(1)} + Q_n^{(2)} \quad ,$$

where for retention of only the first term of the asymptotic expansion of $H^{(1)}_{0,1}$,

$$(5b) \qquad Q^{(1)}_{n} = \sqrt{\frac{1}{2\omega p \pi \sin \Delta}}\, e^{\mp i\omega p\Delta \pm i\,\pi/4}$$

$$(5c) \qquad P_n \approx \sqrt{\frac{2}{\omega p \sin \Delta}}\, \cos(\omega p\Delta - \pi/4)$$

An apparently more general definition of the functions $Q^{(1)}_{(2)}$ by asymptotic series in $H^{(1)}_{0}{}_{(2)}(\omega p\Delta)$ and $H^{(1)}_{1}{}_{(2)}(\omega p\Delta)$ can be obtained as in Gilbert (1976). These series, however, offer little advantage over the simpler formula (5) when $\Delta \to 0$ because the functions $H^{(1)}_{0,1}{}_{(2)}$ have a logarithmic singularity for zero argument. Equivalently stated, a fully uniform expansion of the horizontal wavefunction as $\Delta \to 0$ does not permit its separation into functions representing waves traveling opposite directions.

Comparison of formulae for $P_n(\cos \Delta)$

Figure 1 compares the formulae (3), (4), and (5c) for $P_n(\cos \Delta)$ for a range of real p and a sequence of distances Δ . From Figure 1 it is apparent that the first two terms of the Szego asymptotic eq. (4) approximates $P_n(\cos \Delta)$ well everywhere in the chosen domains of $\omega p\Delta$. This may appear surprising when it is noted that the terms in the asymptotic series by Szego contain factors in negative powers of ωp that apparently diverge as $\omega p \to 0$. Instead the second term, for example, can be shown to be regular as $\omega p \to 0$ because the coefficient $B_1 \sim 1/\omega p$ while $J_1 \sim \omega p$.

The point in $\omega p\Delta$ space at which the asymptotic representation

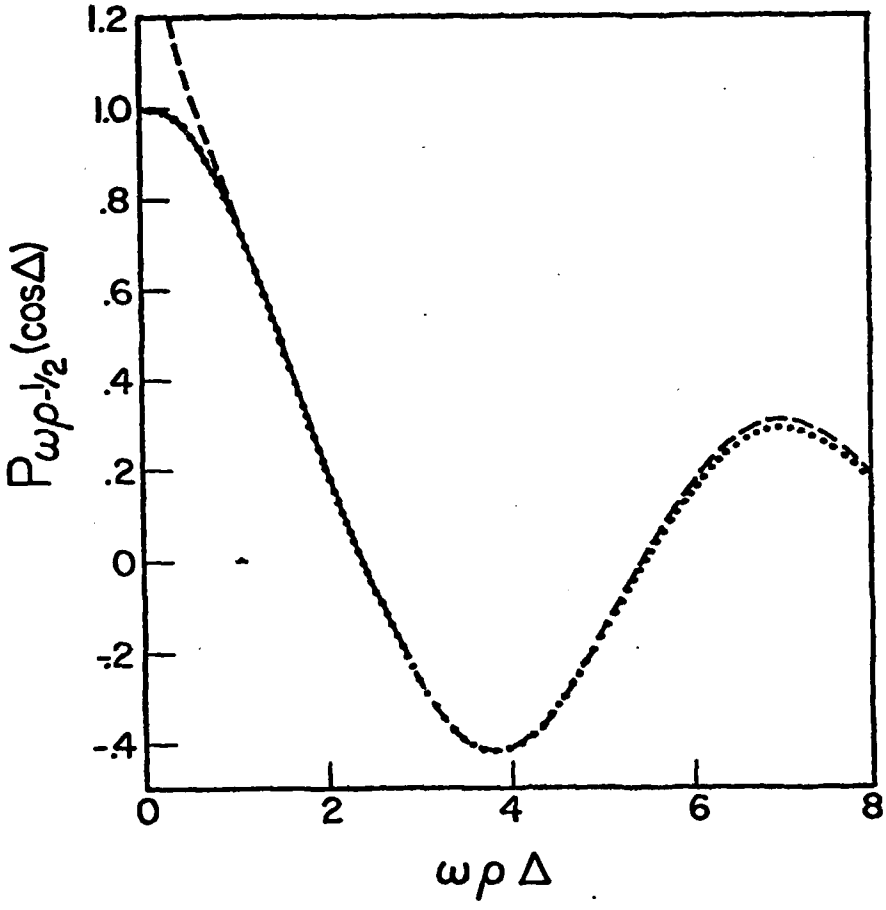

Figure 1. Behavior of asymptotic approximations to the Legendre function $P_n(\cos\Delta)$ as a function of the non-dimensional product $\omega p\Delta$. The defining formula eq. (3) is shown by the solid line ——— , the first two terms of the Szego asymptotic formula eq. (4) by the dotted line · · · · , and the asymptotic form given by eq. (5c) by the dashed line _ _ _ _ .

given by eq. (5c) begins to approximate the Szego formulae (4) within 0.1% occurs at $|\omega p\Delta| = 10$. Thus the separation of $Q^{(1)}$ and $Q^{(2)}$ as defined by eq. (5b) becomes accurate to within this error only if $|\omega p\Delta| > 10$. If $Q^{(1)}$ and $Q^{(2)}$ are defined in terms of the Hankel functions $H^{(1)}_{0,1}$ as in Gilbert (1976), then one must be careful when $|\omega p\Delta|$ is much smaller to sum the contribution to displacement calculated from the $Q^{(1)}$ and $Q^{(2)}$ traveling waves in order to cancel the logarithmic singularity in $H^{(1)}_{0,1}$.

Representations far from the source or antipode

Far from the antipode or source ($|\omega p\Delta| > 10$) , any term m in the displacement representations (2a-2b) can be written as

$$(6) \qquad \chi_m(r,\omega,\Delta) = (-1)^{m+1/2} \frac{\omega^2}{2} \int_0^\infty \text{pSM } Q^{(2)}(\cos\Delta) e^{i2m\pi\omega p}\, dp \ ,$$

for Δ measured as the shortest great circle distance between source and receiver. When the distance is measured from the antipode, the expression becomes either

$$(7a) \qquad \chi_m = (-1)^m \frac{\omega^2}{2} \int_0^\infty \text{pSM } Q^{(1)}(\cos\Delta') e^{i[(2m\pi+1)\omega p}\, dp$$

for zero or even numbers of anitpodal passages, or

$$(7b) \qquad \chi_m = (-1)^{m+1/2} \frac{\omega^2}{2} \int_0^\infty \text{pSM } Q^{(2)}(\cos\Delta') e^{i[(2m\pi+1)\omega p}\, dp$$

for odd numbers of antipodal passages.

The above expressions can be compactly stated for Δ measured from source to receiver and including any antipodal passages or circuits about the earth's center as

$$(8) \qquad \chi_m(r,\omega,\Delta) = \sqrt{\frac{\omega^3}{8\pi|\sin\Delta|}}\; e^{i\pi/2[[\Delta/\pi]]} \int_0^\infty p^{1/2} S_M\, e^{i(\omega p\Delta-\pi/4)}\, dp \quad ,$$

where $[[\, x \,]]$ is the greatest integer $\leq x$.

As noted by Wait (1960) and Brune (1961), each antipodal passage shifts the phase of a traveling wave by $\pi/2$. Intrinsically the phase shift is as much the consequence of spherical geometry as it is of the properties of any asymptotic expansions of spherical wavefunctions.

FLAT EARTH REPRESENTATIONS

By recognizing the earth flattening transformation to be simply a variable change, flat earth representations for displacement potential valid in the source and antipodal regions can be derived from eqs. (2a) and (2b).

Given the relation of horizontal distance as measured on the surface of a sphere of radius R to distance x measured on a flat surface

$$(9) \qquad R\Delta = x \quad ,$$

and the flattening transformation of velocity from Muller (1971) ,

$$v_f = \frac{R}{r} v_s \quad ;$$

then it follows that

$$\frac{\omega r \sin(i)\ \Delta}{V_s} = \frac{\omega \sin(i)\ x}{V_f}$$

or

$$\omega p \Delta = kx \tag{10}$$

Substituting (9) and (10) above into eq. (4) gives a flattened form of Szego's asymptotic P as either

$$P_n(\cos\ ) \quad \left[\frac{x/R}{\sin(x/R)}\right]^{1/2} \left\{ J_0(kx) + \left[\frac{x}{R}\ \cot\left(\frac{x}{R}\right) - 1\right] \frac{J_1(kx)}{8kx} \right\} \tag{11}$$

Eq. (2a-2b) become

$$\chi(z,\omega,x) = \frac{\omega}{2}\left[\frac{x/R}{\sin(x/R)}\right]^{1/2} \sum_{m=-\infty}^{\infty} (-)^{m+1/2}$$

$$\int_0^{\infty} k\, S(\omega,\phi,k)\, M(z,\omega,k)\, J_0(kx)\, \exp(2im\pi Rk)dk \quad , \tag{12}$$

for x measured from the source, or

$$\chi(z,\omega,x) = \frac{\omega}{2}\left[\frac{x/R}{\sin(x/R)}\right]^{1/2} \sum_{m=-\infty}^{\infty} (-)^{m}$$

$$\int_0^{\infty} k\, S(\omega,\phi,k)\, M(z,\omega,k)\, J_0(kx)\, \exp[i(2m+1)\pi Rk]dk \quad , \tag{13}$$

for x measured from the antipode. The J_1 term has been dropped for the reasons previously mentioned. Far from the source or antipode we have eq. (8) in the flattened form:

$$(14) \qquad \chi(z,\omega,x) = \sqrt{\frac{\omega R}{8\pi|\sin(x/R)|}}\; e^{i\pi/2[[\,x/R\pi\,]]} \int_0^\infty k^{1/2}{}_{SM}\, e^{ikx-i\pi/4}\, dk$$

The flattened representations above have been obtained by variable mapping rather than by any limiting process on radius R. These expressions ought then to be valid in the domain of (r,Δ) equivalent to that of (z,x).

The function M in either spherical or flattened coordinates is a function of velocities, densities, layer thicknesses, and cosines η, where

$$\eta_s = \left(1 - \frac{p^2 v_s^2}{r^2}\right)^{1/2} = \eta_f = \left(1 - \frac{k^2 v_f^2}{\omega^2}\right)^{1/2}$$

Waves bottoming at and near the earth's center

The vertical slownesses in both the spherical and flattened cases remain regular as $r \to 0$ and $z \to -\infty$ because whenever such evaluations are required p and $k \to 0$. Any other functions of velocity in the flattened M can be expressed as velocity ratios that remain finite as $z \to -\infty$. Any numerical difficulties in dividing zero by zero in the M calculation are minimized by the fact that k or p is a factor in the integrand. The limiting value of the integrand at zero p or k must therefore be zero. Thus the earth flattening transformation, as used in

the evaluation of integral representations of displacement, would remain valid even for body waves bottoming at the earth's center. The k integral must, of course, be evaluated along a path sufficiently close to the origin; the proper form of the horizontal wavefunction in the displacement representation must be chosen; and any approximation of the velocity profile by homogeneous layers must be sufficiently accurate in the frequency domain of interest.

From the appearance of k or p as a factor in the integrand, it can also be concluded that it should never be necessary to deform the p or k integration path into the left half of the p or k plane. The integration path may be simply terminated at the origin whenever there are pole, saddle, or branch cut contributions in its neighborhood.

CONCLUSIONS

Integral representations in the far field for the potentials of seismic displacement have been obtained in both the antipodal and source regions. Flattened representations follow from simple variable mappings of the spherical formulae. The asymptotic separation of the horizontal wavefunction into traveling wave components does not become valid unless $|\omega p \Delta|$ or $|kx|$ are sufficiently large.

Acknowledgments. The author benefitted from many discussions with Jose Rial and constructive suggestions by Paul G. Richards. This research was supported by the Air Force Office of Scientific Research under grant AFOSR-75-2775.

REFERENCES

Brune, J. N., Nafe, J. E. and Alsop, L. E. 1961. The polar phase shift of surface waves on a sphere, Bull. Seism. Soc. Am., 51, 247-257.

Ewing, W. M., Jardetzky, W. S. and Press, F. 1957. Elastic Waves in a Layered Medium, McGraw-Hill Book Company Inc., New York.

Frazer, L. N. 1977. Use of the sperical layer matrix in inhomogeneous media, Geophys. J. Roy. astr. Soc., 50, 743-749.

Fuchs, Von K. 1968. Das Reflexions und Transmissions vermögen eines geschichteten Mediums mit beliebeger Tiefen-Verteilung der elastischen Moduln und der Dichte für schragen Einfall ebener Wellen, Zeit. Geophys., 34, 387-413.

Gilbert, F. 1976. The representation of seismic displacements in terms of traveling waves, Geophys. J. Roy. astr. Soc., 44, 275-280.

Langer, R. E. 1949. The asymptotic solutions of ordinary linear differential equations of the second order, with special reference to a turning point, Trans. Amer. Math. Soc., 37, 397-416.

Minster, J. B. 1974. Elastodynamics of failure in a continuum. Ph.D. thesis, California Institute of Technology, Geophysics.

Muller, G. 1971. Approximate treatment of elastic body waves in media with spherical symmetry, Geophys. J. Roy. astr. Soc., 21, 261-283.

Nussenzweig, H. M. 1969. High-frequency scattering by a transparent sphere. I. Direct reflection and transmission, J. Math. Phys., 10, 82-125.

Olver, F. W. J. 1956. The asymptotic solution of linear differential equations of the second order in a domain containing one transition point, Phil. Trans. Roy. Soc. London, A249, 65-97.

Olver, F. W. J. 1976. Asymptotics and Special Functions, Academic Press, Inc., New York.

Rial, J. A. 1978. On the focusing of seismic body waves at the epicenter's antipode, Geophys. J. Roy. astr. Soc., in press.

Richards, P. G. 1973. Calculation of body waves for caustics and tunneling in core waves, Geophys. J. Roy. astr. Soc., 35, 243-264.

Richards, P. G. 1976. On the adequacy of plane-wave reflection-transmission coefficients in the analysis of seismic body waves, Bull. Seism. Soc. Am., 66, 701-718.

Scholte, J. 1956. On seismic waves in a spherical earth, Meded. Verh. K. ned. met. Inst., 65, 1-55.

Szego, Von G. 1934. Uber einege asymptotische entwickungen der Legendreschen funktionen, Proc. Lond. Math. Soc., Series 2, 36, 427-450.

Wait, J. R. 1960. Terrestrial propagation of very low frequency radio waves, J. Res. Nat. Bur. Standards, 640, 153-204.

III. Time Domain Studies of Frequency Dependant Anelasticity in the Earth's Upper Mantle: The Mantle Impulse Response - Gary Lundquist

The generation of an Earth mantle impulse response must be accomplished by numerical modelling. Q, τ_1, τ_2 (the relaxation times for an absorption band) and v (the frequency dependent effective wave velocity)all vary as functions of depth, with discontinuous behavior likely at several depths. Thus the impulse response is a path property resulting from the average of widely varying medium properties.

The method used in this work is a uniformly asymptotic full wave theory (Richards, 1976). This theory was developed to solve problems beyond the scope of ray theory, such as are met with at caustics and in diffraction. In particular, the reflection and transmission coefficients of rays at near grazing incidence are frequency dependent. A full wave theory thus inherently includes the ability to model frequency dependent Earth properties, such as the complex modulus needed in this work.

The derivation of complex modulus for the specific rheology in which absorption and dispersion are determined by a distribution of independent relaxation mechanisms in a standard anelastic solid is given by Liu et al. (1976), and can be written:

$$\varepsilon(t) = \sigma(t)\left\{ \frac{1}{M_R}\left[1 - \frac{C}{2} \ln \frac{1+\omega^2\tau_1^2}{1+\omega^2\tau_2^2} + iC \tan^{-1} \frac{\omega(\tau_1 - \tau_2)}{1+\omega^2\tau_1\tau_2} \right]\right\} \qquad (1)$$

where M_R is the relaxed modulus.

This may be written in terms of medium parameters, in particular; v_e, the relaxed phase velocity; and Q_m^{-1}, corresponding to the maximum level of absorption band, by using:

$$v_e = \sqrt{\frac{M_R}{\rho}} \tag{2}$$

$$C = \frac{2}{\pi Q_m}$$

Note that this formulation is referenced to a low frequency, or relaxed modulus rather than to a high frequency, or unrelaxed modulus. In that τ_2 determines the high frequency "roll-off" point, it is the critical absorption band parameter, and it seems best to reference dispersion to a low frequency limit. In the numerical computations, dispersion will be normalized to be independent of the choice of velocity models. For the purpose of this discussion, both Q_m and v_e may be considered to be referenced to the same low frequency (i.e., free oscillation models).

The complex velocity for an absorption band material is obtained by substituting (2) in (1) and using $v_c(\omega) = \sqrt{M(\omega)/\rho}$ where $M(\omega)$ is the complex modulus, so that:

$$v_c(\omega,r) = \left\{ \frac{1}{v_e^2(r)} \left[1 - \frac{1}{\pi Q_m} \ln \frac{1+\omega^2\tau_1^2}{1+\omega^2\tau_2^2} + i \frac{2}{\pi Q_m} \tan^{-1} \frac{\omega(\tau_1-\tau_2)}{1+\omega^2\tau_1\tau_2} \right] \right\}^{-1/2} \tag{3}$$

Note that in the Earth v_e, Q_m, τ_1 and τ_2 may all be functions of radius.

Other Q laws may be obtained from equation (3). For instance, a constant Q is obtained from an absorption band by letting τ_1 approach infinity and τ_2 approach zero. In the limit as $\tau_1^{-1} << \omega << \tau_2^{-1}$, the inverse tangent function approaches a value of $\pi/2$, and the logarithm become

$$\frac{1}{\pi} \ln \omega^2 \tau_1^2 = \frac{2}{\pi} \ln \omega\tau_1$$

Thus v_c reduces to

$$v_c = v_e \left[1 - \frac{1}{Q_m} \left(\frac{2}{\pi} \ln \omega\tau_1 - i \right) \right]^{-\frac{1}{2}} \tag{4}$$

If Q_m is large, that is, if attenuation is small, then application of the binomial theorem reduces (4) to

$$v_c = v_e \left[1 + \frac{1}{\pi Q_m} \ln \omega\tau_1 - \frac{i}{2Q_m} \right] \tag{5}$$

If dispersion is ignored, as it often has been in the past,

$$v_c = v_e \left[1 - \frac{i}{2Q_m} \right] \tag{6}$$

and the case of an elastic Earth is given by

$$v_c = v_e = \sqrt{\frac{M_R}{\rho}} \tag{7}$$

Note that "elastic Earth" as it is used here implies an Earth with no attenuation and no dispersion. The choice of a low frequency velocity model to represent an elastic Earth may otherwise seem contradictory.

The complex velocity is, of course, a pointwise property. With the specification of the depth dependencies of v_e, Q_m, τ_1 and τ_2, the pointwise structure may be used in an integration over ray path to get the mantle impulse response. For the purpose of an example, the velocity model PEMC (Dziewonski et al., 1977) and the Q model SL8 (Anderson and Hart, 1977) were adopted. τ_1 was assumed constant at 1000 sec, using Minster's (1977) study as justification. A τ_2 structure with variable τ_2 in the asthenosphere was taken from combined microphysics and frequency domain studies (Lundquist, 1978). The Q and τ_2 structures are shown in Figure 1.

A representative sample of the frequency dependent Earth properties is shown in Figure 2, with constant-Q and equivalent-elastic-Earth models noted. The upper curve is normalized modulus, which is a direct measure of dispersion. The increase in phase velocity with frequency is normalized in this case to 0.005 Hz because the PEM velocity models are appropriately referenced to 200 sec (Dziewonski, personal communication). Note that S waves will be much more dispersed than P waves, simply because Q_α is smaller than Q_β.

Note that variation in τ_2 is much more critical to absorption than to dispersion. The absorption band begins to decay from a constant Q_m^{-1} more than a decade in frequency before $\omega = 1/\tau_2$. The dispersion, on the other hand, decays from a constant slope; so that a 1 Hz wave has nearly the same dispersion relative to, say, the .001 Hz component of a wave, whether Q is constant or frequency dependent, at least for the case shown. The predicted

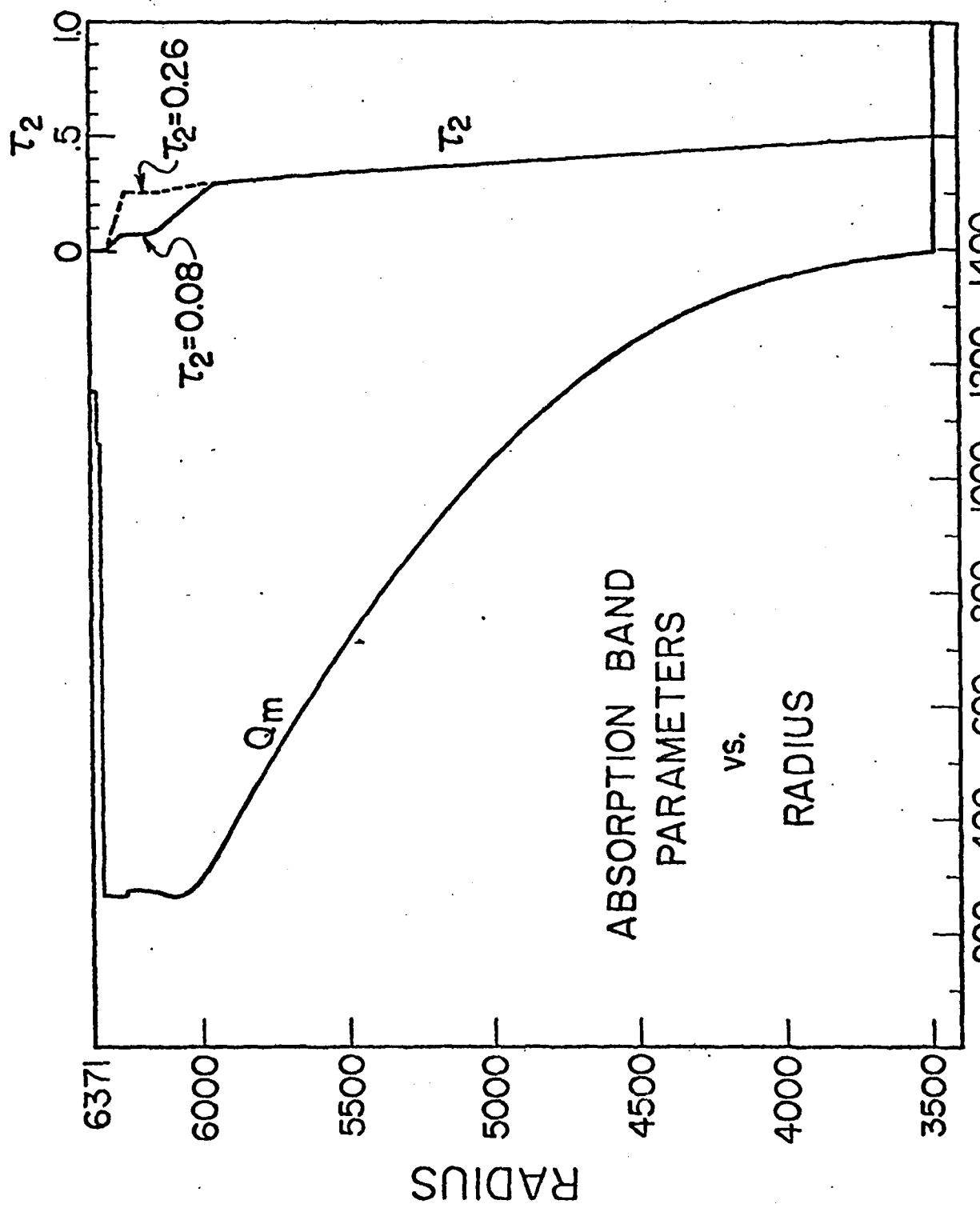

Figure 1: Q and τ_2-vs-Depth: The Q model is that of Anderson and Hart (1977), and corresponds to free oscillation frequencies. The τ_2 structures are taken from Lundquist (1978).

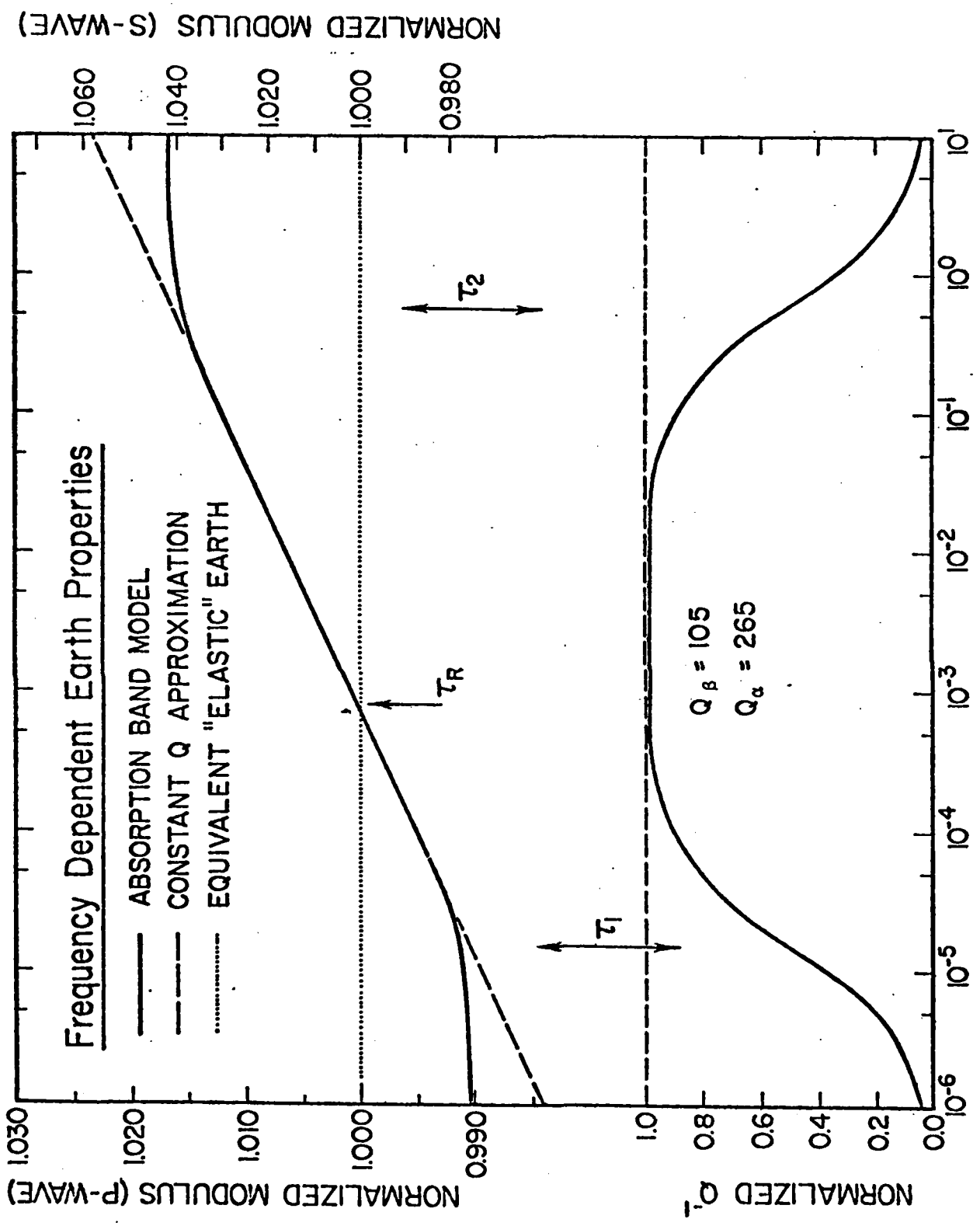

Figure 2. Q^{-1} and normalized modulus-vs-Frequency: Note the differences between constant Q, absorption band and equivalent "elastic" Earth models.

impulse response behavior, then, is that the arrival times of waves propagated through constant Q or absorption band models should be nearly the same, but the frequency content should be markedly different.

This result, by the way, means that a base line shift between travel times computed from free-oscillation and body-wave inversions is not diagnostic of the existence of a corner τ_2, in the absorption. Such a comparison means only that $2\pi\tau_2$ is less than or near the period or the peak of the instrument response. For instance, the τ_2 structures shown in Figure 1 both give base line shifts similar to those reported by Anderson and Hart (1977).

The impulse response is calculated in the frequency domain by performing critical parts of the propagation separately for each frequency. The resulting amplitude and phase responses for a distance of 50° are shown in Figures 3 and 4. Clearly, the "elastic"-Earth and constant-Q models represent limits, with all intermediate possibilities generated by a variation in τ_2. It must be emphasized that the absorption band models used differ only in the value of τ_2 between the base of the crust and the base of the asthenosphere.

Note that the constant Q model gives an amplitude response which decays at the maximum possible rate for a causal function. The Paley-Wiener criterion requires that the amplitude spectrum of a causal function cannot be zero over a finite frequency band; and thus that the spectrum cannot decay faster than a function of exponential order (Lathi, 1968). The Q filter is an exponential defined by

$$A = A_o e^{-\omega T/2Q_E} \qquad (8)$$

where T is travel time and Q_E is averaged or effective Q over the travel path. Thus, if Q is frequency independent, (8) describes a maximum decay rate.

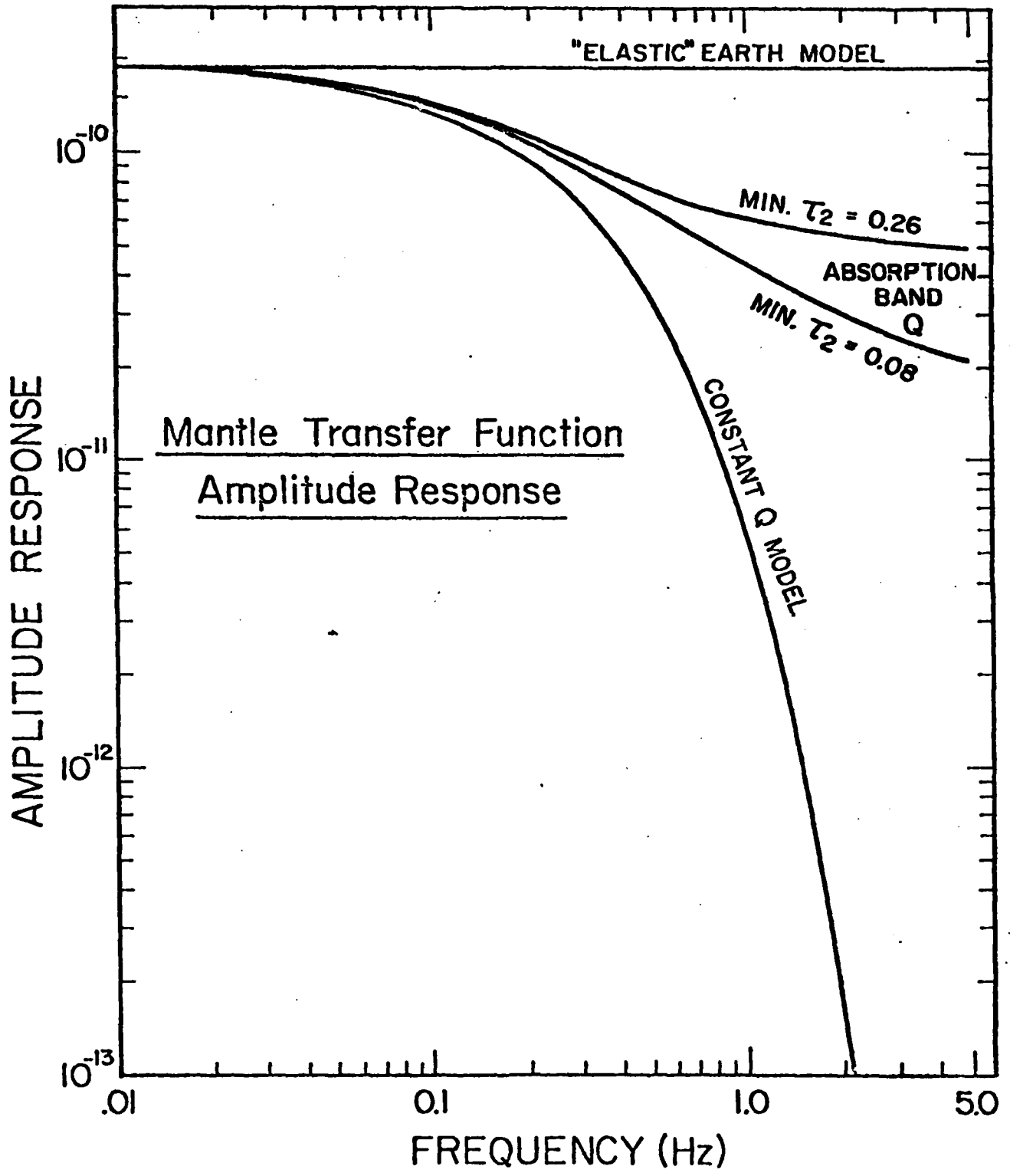

Figure 3. Mantle amplitude response-vs-frequency.

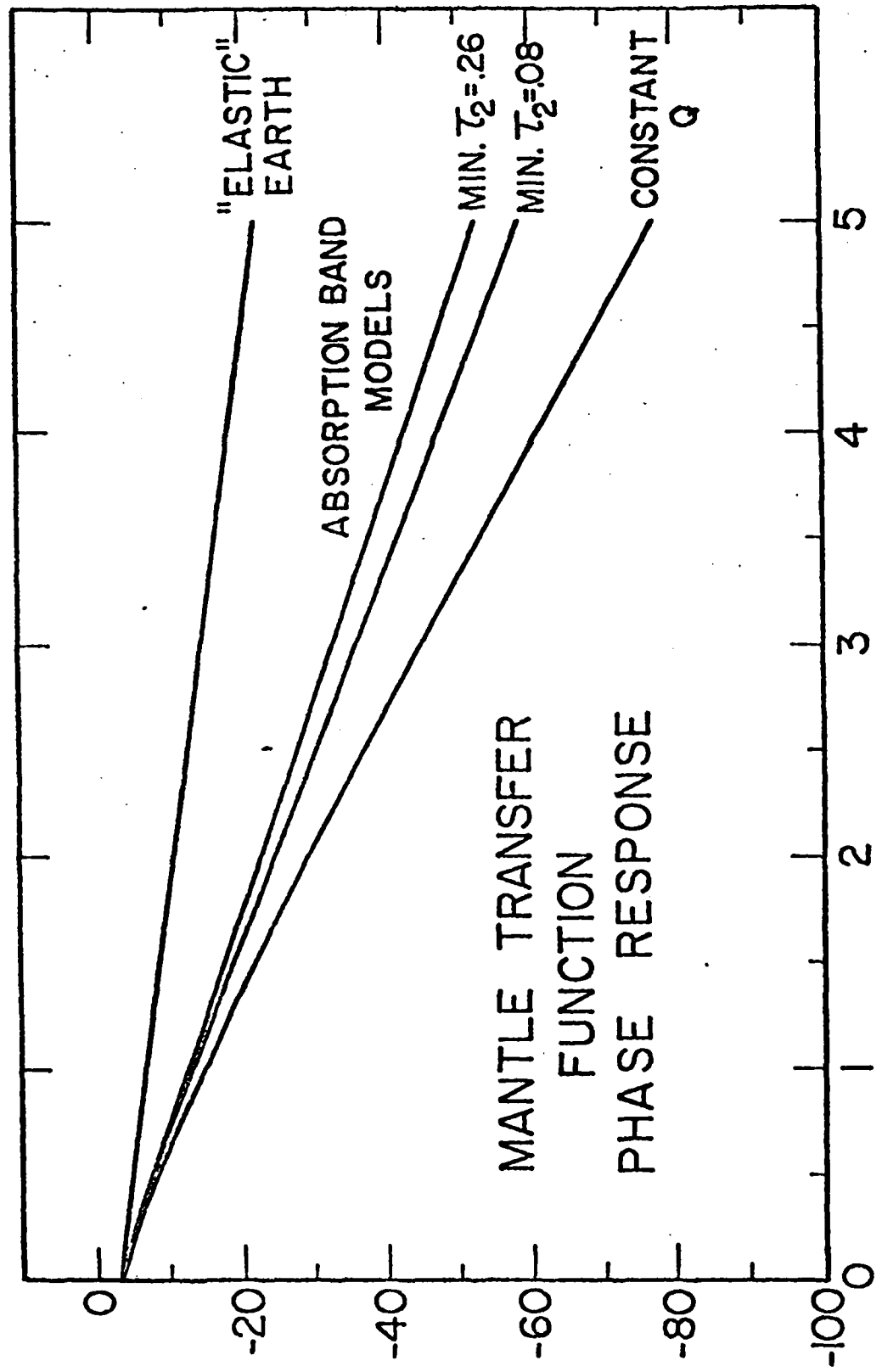

Figure 4. Mantle phase response-vs-frequency.

As a corollary, if Q has a frequency dependence, it must increase with frequency as ω becomes very large.

The impulse response functions for different Q models, at 50°, are shown in Figure 5 as a function of reduced time. Here the "elastic" response is a delta function defining reduced time t = 0. The other impulse response functions shown arrive earlier because the equivalent "elastic" earth is representative of a low frequency velocity model, and because the arrival time is determined by the high frequency waves. (i.e., The relaxed, low frequency, moduli are less than the unrelaxed moduli.) Note that the introduction and shifts in the value of τ_2 change the arrival times only slightly. However, the difference in arrival time between a purely elastic case and any of the anelastic cases is quite large.

Variation of τ_2 does significantly change the frequency content, however. Simply put, peak amplitude is a rapidly increasing function of τ_2, just as demonstrated by Minster. Again, a continuous variation in pulse shape may be obtained, between the delta function and the constant-Q case, by changes in τ_2 alone.

Observations of this type of behavior must be considered in terms of the other frequency dependent processes in the system, including the source and the instrument. Examination of Figure 3 shows that long-period instruments will not be sensitive to the frequency dependence of a typical mantle transfer function. Only short-period observations will be able to determine the existence and relative position of τ_2.

Figure 6 shows source spectrum approximations which may be crudely related to ω^{-2} and ω^{-3} models of the seismic source, corresponding to the source-time functions:

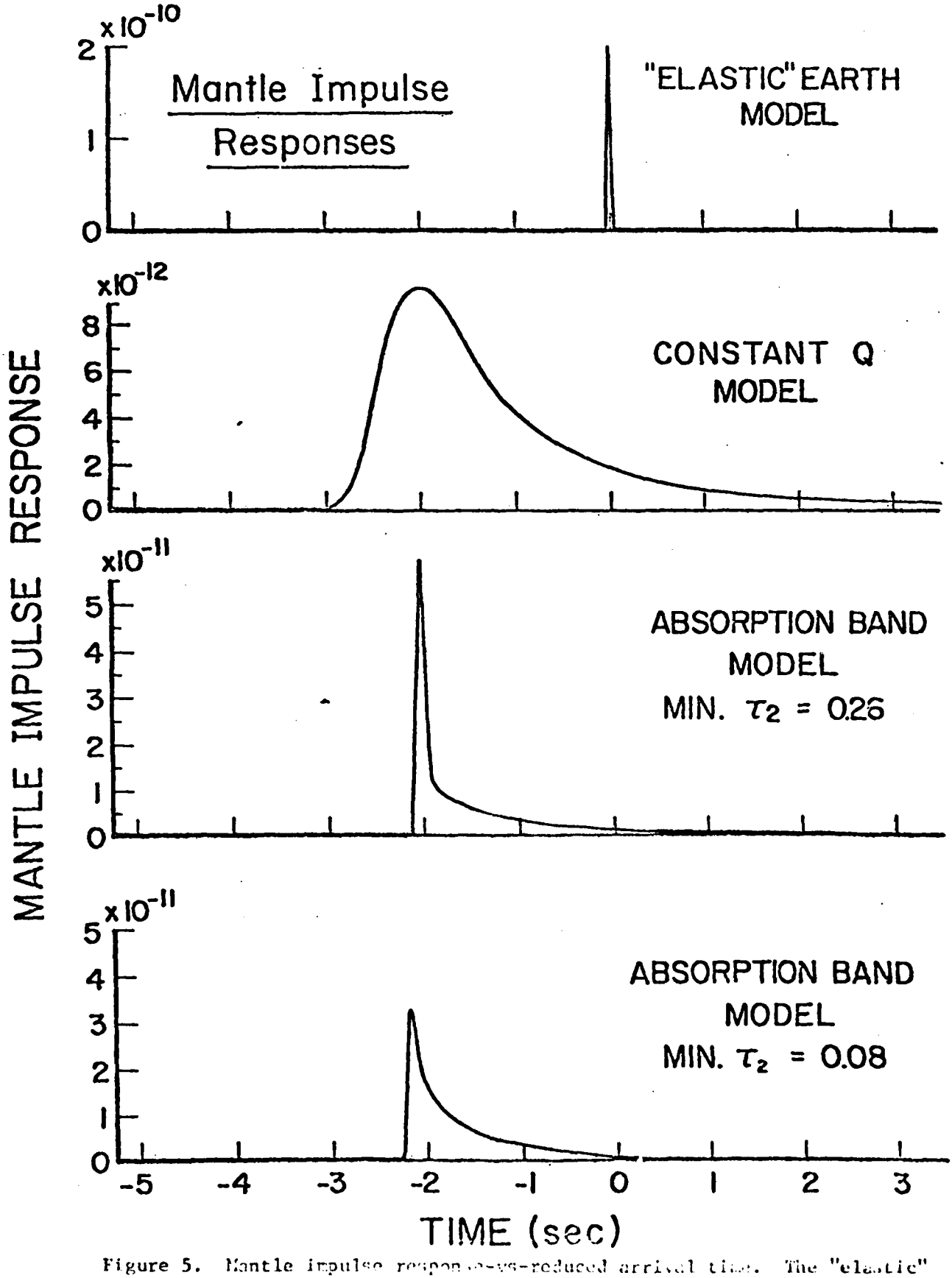

Figure 5. Mantle impulse responses-reduced arrival time. The "elastic" Earth model is defined by a low frequency velocity model and no absorption. Because of dispersion, the high frequencies arrive earlier than the equivalent elastic response.

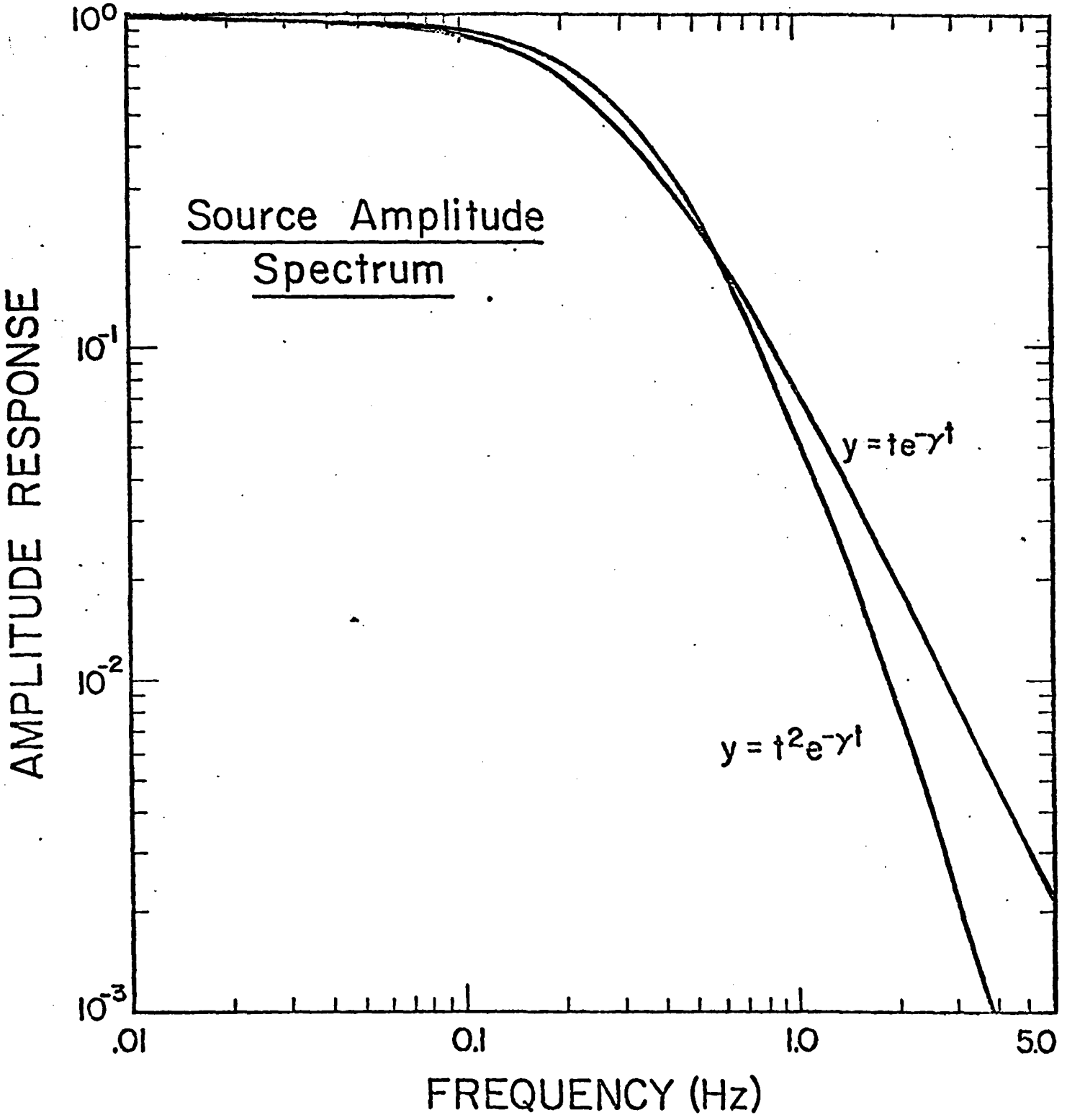

Figure 6. Source amplitude spectrum-vs-frequency. These curves approximately represent the ω^{-2} and ω^{-3} models of seismic source theory. The corner is a function of γ. In this case, the sources have been scaled to roughly magnitude 5 or 6.

$$y = t\, e^{-\gamma t}, \quad (\omega^{-2} \text{ dependence})$$

$$y = t^2 e^{-\gamma t}, \quad (\omega^{-3} \text{ dependence})$$

The curves shown are scaled, very crudely, to surface wave magnitude 5 or 6 (Aki, 1967). It is apparent that the Q filter and the source function have corners in the same frequency range. Thus the apparent frequency content difference between constant Q and absorption-band Q responses should be reduced in the real world, simply because the high frequencies are already reduced in the source spectrum, for the commonly observed magnitude 5 to 6 events.

Figures 7 and 8 show simple synthetic P-wave seismograms for ω^{-2} and ω^{-3} source models, respectively. The instrument response used was the LRSM short period response which peaks at about 3 Hz. The small a causal portions of the signals result from truncation of the insturment response at 5.4 Hz, the highest frequency used in the synthesis.

Figures 7 and 8 demonstrate both the effects of anelasticity and the well known problem of tradeoff. It is not possible, just from the seismogram, to determine whether the frequency content is a result of the source function character or the Q filter. Clearly, reduction of seismic data to Q and τ_2-vs-depth "structures" requires knowledge of and/or elimination of the source filter from the problem. This critical activity is currently being intensely pursued using explosion sources with well constrained ("known") source functions and through the use of spectral ratios between appropriate points of observation.

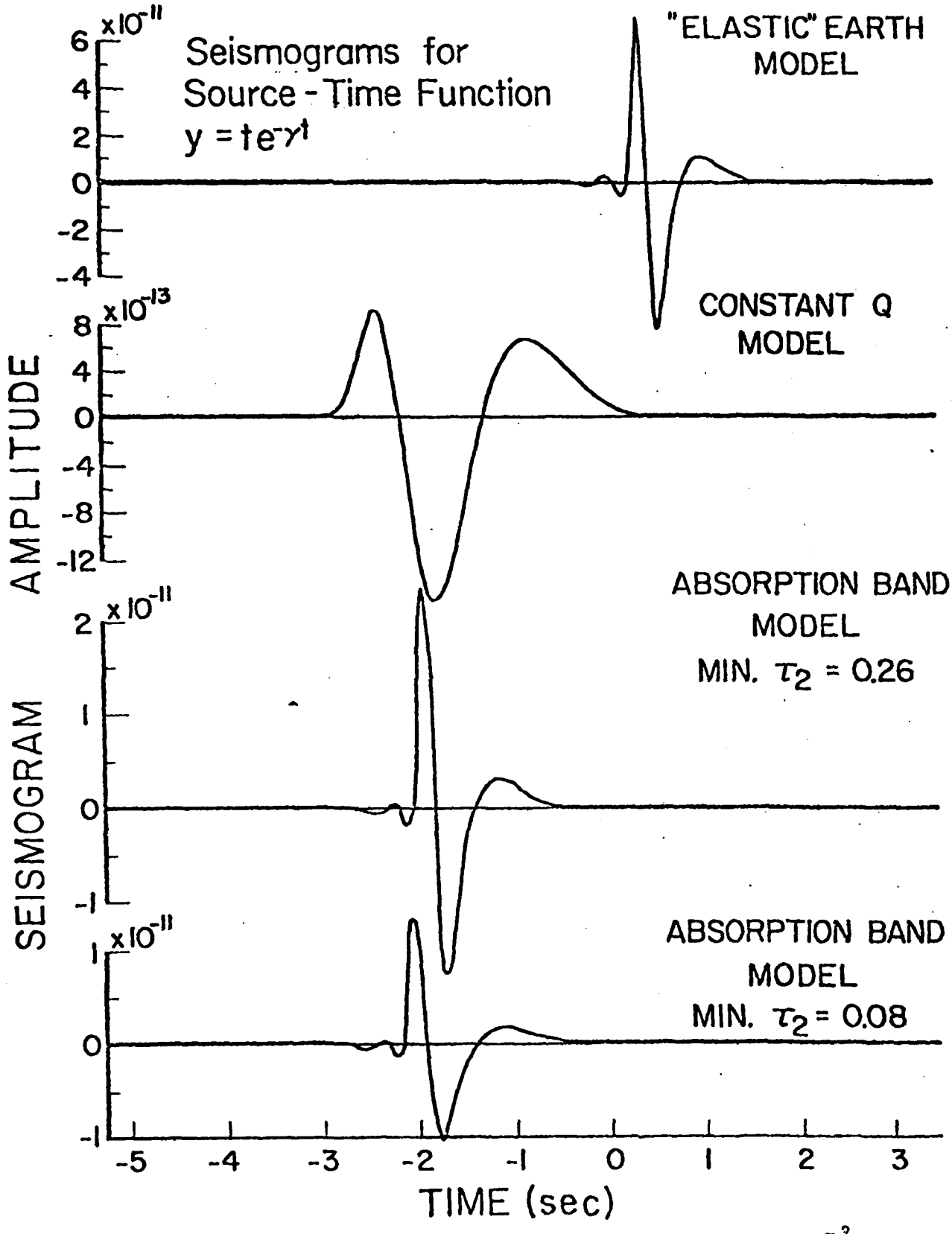

Figure 7. Synthetic seismograms-vs-reduced arrival time: ω^{-2} model.

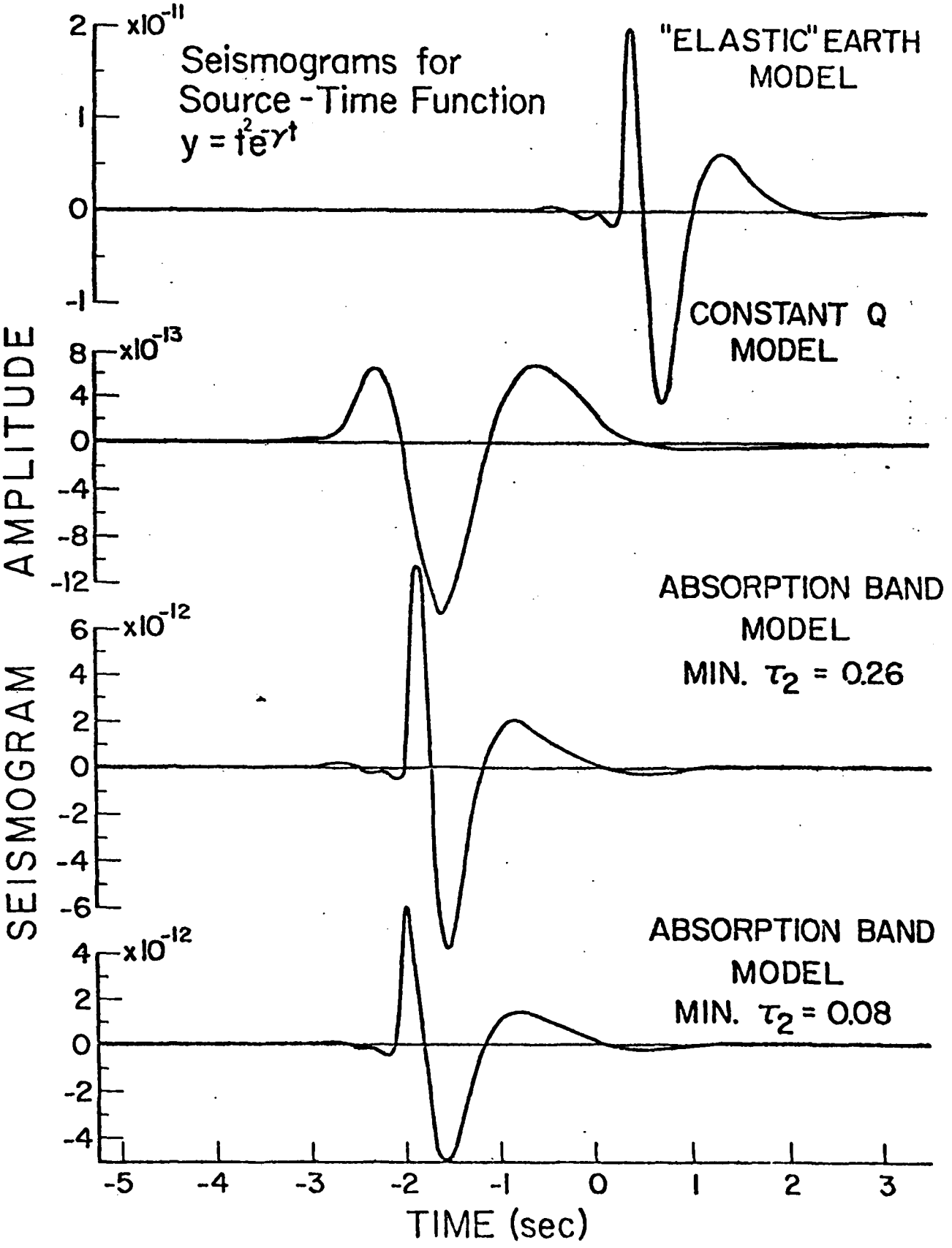

Figure 8. Synthetic seismograms-vs-reduced arrival time: ω^{-3} model.

References

Aki, K., Scaling law of seismic spectrum, J. Geophys. Res., 72, 4, 1217-1231, 1967.

Anderson, D.L., and R. S. Hart, The Q of the Earth, Submitted to J. Geophys. Res., 1977.

Lathi, B.P., Communication Systems, John Wiley and Sons, New York, 1968.

Liu, H.P., D.L. Anderson, and H. Kanamori, Velocity dispersion due to anelasticity; implications for seismology and mantle composition, Geophys. J. R. Astr. Soc., 47, 41-58, 1976.

Lundquist, G. M., Evidence for the frequency dependence of Q, in Earthquake Characteristics and Earthquake Explosion Discrimination, Semi Annual Report #7, AFOSR-75-2175, ed Charles Archambeau, 1978.

Minster, J.B., Transient and impulse responses of a one dimensional linearly attenuating medium: I. Analytical results; II. A parametric study, Geophys. J., 52; 3, 503-530, 1978.

Richards, P.G., On the adequacy of plane-wave reflection/transmission coefficients in the analysis of seismic body waves, Bull. Seis. Soc. Amer., 64, 4, 701-717, 1976.

IV. Seismogram Synthesis Using Normal Mode Superposition: The Locked Mode Approximation Method - D. Harvey

A mode superposition approach, aside from its great accuracy and "completeness", has a number of distinct advantages compared to the asymptotic wave methods such as the time domain Cagnaird method, or the frequency domain Full Wave Theory. In particular: (1) Depth and frequency dependent intrinsic anelastic effects can easily be incorporated, since the procedure is a frequency domain method. (This is true of the Full Wave Theory also.) Anelasticity can, in fact, be incroporated either directly, using complex material moduli in Haskell matrices, or indirectly using a perturbation of the results for the ideal elastic case. Both of these methods will be used to include anelastic and scattering effects. (2) Once the modes are computed for a given earth model, they can be used to generate seismograms for any source type, configuration or depth, at any distance and azimuth. That is, the modes need only be computed once and, since they are independent of source, distance and azimuth, they can be used with a wide variety of source models to generate synthetic seismograms for inversion purposes. (In fact the cost of generating seismograms is so low as to allow simple trial and error procedures to be used for source property inversion.) This is in contrast to the asymptotic methods that utilize "take-off" angle data to compute seismograms and so are source dependent, and thus a different source model requires a complete recomputation from the beginning. This complete recomputation also is required to obtain results at different distances from the source. This makes the ray theoretical approaches extremely awkward and costly for prediction of radiation from different sources and for source inversion work.

The mode superposition approach is extremely well suited to systematic, quantitative inversion procedures and the theoretical framework of this inverse theory has been worked out. On the other hand, no systematic approach has been given for the asymptotic wave theory results - other than trial and error with visual matching to observations in the time or frequency domains

Since a mode superposition method has many advantages in source inversion studies, and in addition, can be used to generate the entire seismogram, with frequency dependent anelastic and scattering effects included as well, we have devised a computational method that enables us to obtain model eigenfunctions at essentially any frequency and to any mode number of interest (Harvey, 1978). That is, we can compute the eigenfuncitons for P - SV or SH modes associated with mode dispersion curves throughout the wave number - frequency plane from zero to, for example, 10 km/sec phase velocity and from zero frequency to 30 Hz, for example. (This range is probably the extent to which it is necessary to obtain eigenfunction results for regional distance ranges.) The procedure involves:

(a) Introduction of a "cap" layer as the half space layer at the bottom of a layered half space earth model. This special half space region is required to have very high compressional and shear wave velocities (non-physical). The inclusion of the high velocity half space is to be made at a depth sufficient that reflections/refractions from the boundary appear well outside the time window of interest. The effect of the half space "cap" is to move the branch point in the k plane, which is introducted by the half space, close to the origin at k = 0 and therefore to minimize the contributions from the branch line integral, which runs

from the origin at k = 0 to the branch point. The movement of the branch point toward the origin leaves in its "wake" a line of poles corresponding to trapped higher modes, which were formerly on the lower Riemann sheet and represented leaking modes. In less mathematical terms then, introduction of the high impedance half space acts to trap the energy in "locked" modes (as opposed to leaking modes) and these modes will represent both P and S body phases. The only energy not represented will be that which has horizontal wave number close to zero, that is propagating waves with nearly vertical incidence. This contribution can, however, be made as small as desired, with the exception of the reflection/refraction from the half space boundary itself, which will be spurious but can always be made to be well separated in time from arrivals of interest.

(b) Computation of the dispersion relation using the matrix partitioning described by Abo-Zena (1978), or equivalently by, for example, Schwab and Knopoff (1970) among others. (Abo-Zena's particular formulation was followed most closely.) This approach, with some refinements, gives a dispersion relation which is accurate to essentially arbitrarily high frequency and phase velocity and can incorporate arbitrary anelastic behavior for the medium.

(c) Compute the eigenfunctions using the regular Thomson-Haskell propagator matrices, but supplemented by a "constraining relation" between the displacements and stresses which states that the eigenfunctions decay exponentially to zero in the half space. This supplemental relation insures that small round-off errors, inherent in the computations using the propagators alone, are not propagated in an additive fashion to depth. (Commonly the eigenfunctions diverge at depth at high frequency

and for high mode number because of the round-off error propagation. The constraining relation described eliminates this problem completely and all eigenfunction computations are stable to arbitrary frequency and mode number.)

Figure 5 shows modal dispersion curves computed by Harvey (1978), using this "locked mode" approach for the layered model SC-1, shown in Figure 4. For the locaked mode approximation, a high velocity (V_p = 20 km/sec) half space was introduced at 350 km. All the modes with phase velocities from 0 to 8.5 km/sec in the frequency range from 0 to 1 cps were computed. At one Hertz this amounted to some one hundred and fifty modes. For synthesis of regional and near field seismograms the computations will be extended to around 15 Hz. In the figure only the first 10 modes are actually shown and the plot is truncated at somewhat over 5.5 km/sec, since the modes are so closely spaced they are difficult to plot. However, the essential features are shown in this partial plot, in particular, the flattening of the modes at phase velocities corresponding to refracted body wave arrivals, such as at 4.3 km/sec and 4.7 km/sec. On these flat portions of the mode curves, the phase and group velocities are equal and constant. Hence all the flat sections on the mode curves when taken together (i.e., superposed) define a wave with nearly constant group and phase velocity (minimally dispersed) as a function of frequency - this, by definition being a body wave.

The eigenfunctions associated with the high mode numbers at high frequencies have been, up to now, essentially impossible to obtain. Figure 6, however, shows higher mode eigenfunction variations with depth at 10 Hz. The mode eigenfunctions are, in fact, the important results, since convolution with a source function and summing produces the synthetic seismograms.

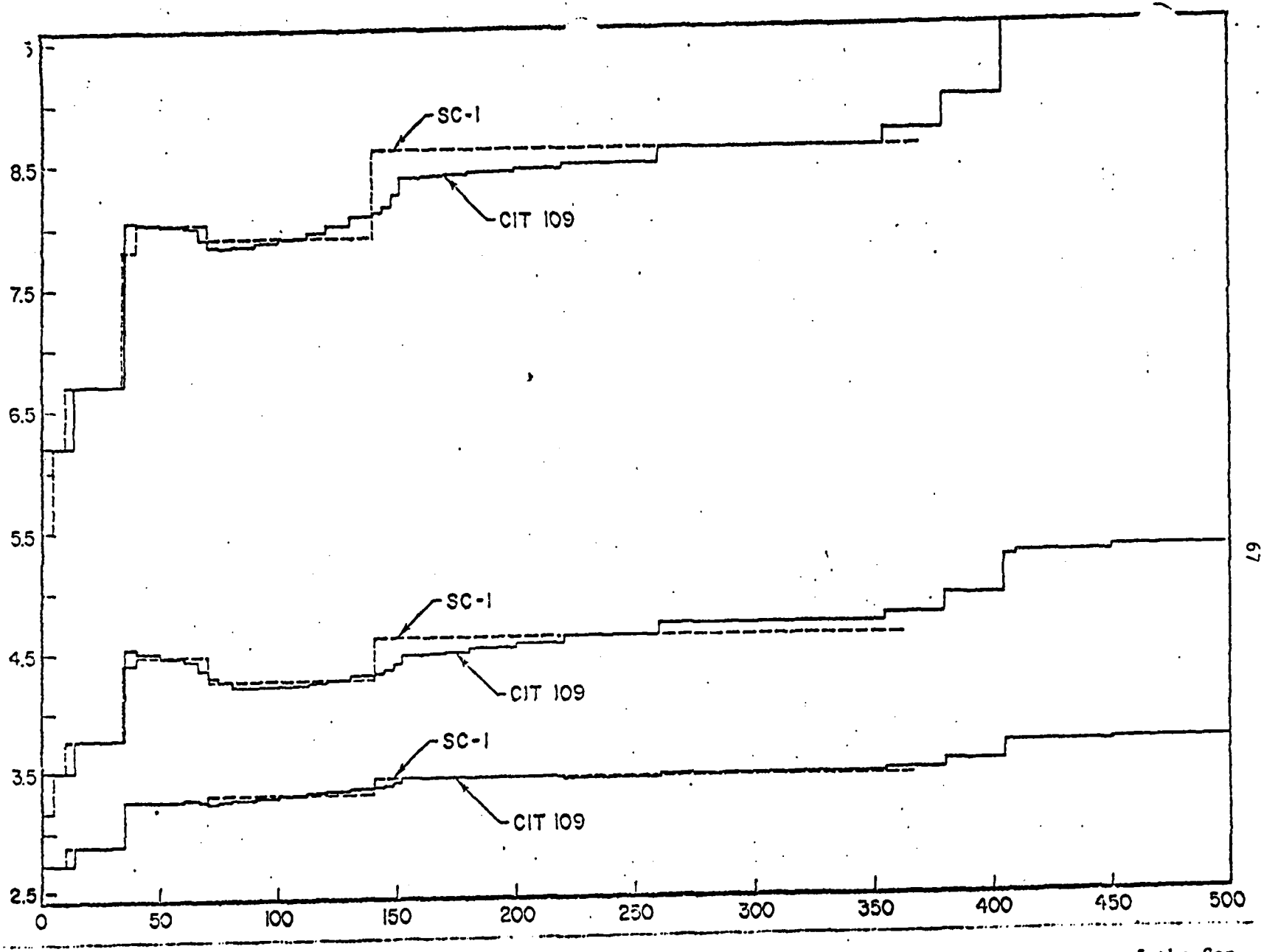

Figure 4. Crust and upper mantle velocity-density structure SC1 for the southern California region west of the San Andreas fault. The compressional velocity crust structure used is based on the velocity models of Hadley and Kanamori (1977) and the upper mantle structure is obtained from the western U.S. upper mantle model CIT 109 (Archambeau, Flinn and Lambert, 1969). The complete CIT 109 model is shown for comparison. The shear velocity and density structure is obtained from the compressional velocity model by assumption of a Poisson's ratio of .25 and an empirical compressional velocity-density relation. The curves from bottom to top are density, shear velocity and compressional velocity.

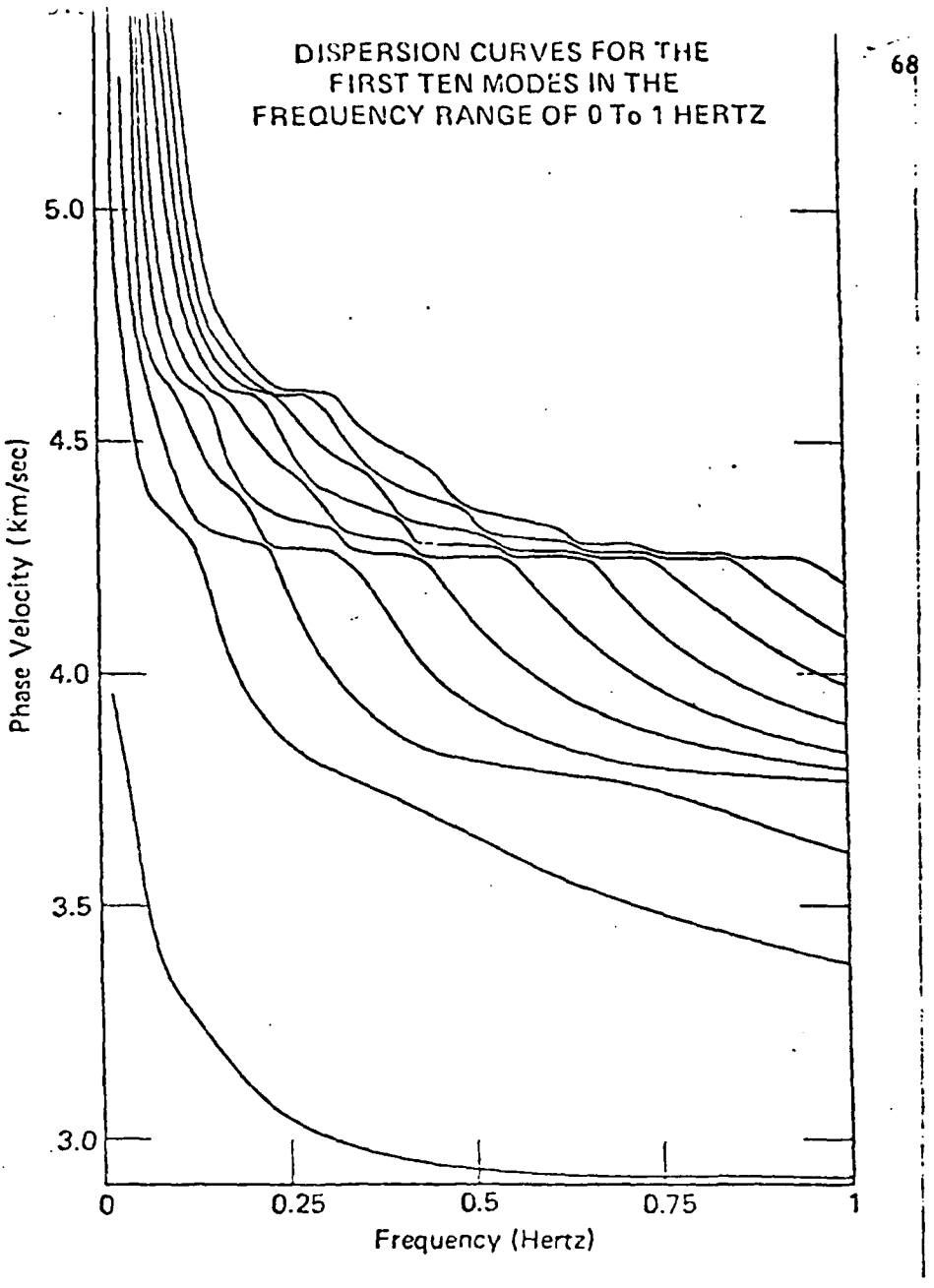

Figure 5. Fundamental and higher mode dispersion curves over the zero to one Hertz range. Sixty-four frequency samples were computed in this range. All the modes "filling" the entire phase velocity-frequency region from 0 to 8.5 km/sec in phase velocity and 0-1 Hz in frequency were obtained for mode superposition. Only the first ten modes are shown here. At 1 Hz approximately 150 modes were obtained in the phase velocity range from 0-85 km/sec. The "flattening" of all the higher mode dispersion curves, near 4.3 km/sec for example, represents an S wave refraction whic when the modes are summed, will have a nearly constant group velocity (of about 4.3 km/sec) corresponding to the composite sum of all the flat portions of the higher mode dispersion curves at this phase velocity. This is an expected characteristic of the dispersion curves which shows how they add to give body wave arrivals. Compressional waves arise similarly but at the higher phase velocity values in this plot.

The eigenfunction computations have proved to be very stable, and we have computed some out to 25 Hz by way of testing this stability, with good results. The structure of the higher modes (that is their variation with depth) often is of the form shown in Figure 6. That is they appear as "leaking plate modes", with the "plate" in this case being one of the earth model layers. In Figure 6, this layer is in the zone from 5 to 10 km, and the higher modes look like plate modes that appear to "leak" from the layer in an oscillatory fashion to the free surface. (However, while oscillatory between the layer and the free surface, the mode is, of course, trapped due to the free suface itself.) The "leaking" to greater depth does not occur, or rather the leaking is exponentially damped with depth. Thus the large amplitude portions of these modes are confined to a single layer, with "leakage" primarily to the free surface. This is, in fact, how the individual mode eigenfunctions look for one of the modes composing a refracted body wave. Of course not all the higher mode eigenfunctions behave in this rather simple manner, but the most important of them, in terms of body wave representations at least, do have this sort of variation with depth.

Inclusion of a source at some depth is accomplished by a simple inner product of the source function with the eigenfunctions for the medium. (In terms of a Green's function representation, the Green's function corresponds to a particular, known, sum of the eigenfunctions and a representation of the radiation field from an arbitrary source is then given by the convolution of the Green's function with the source

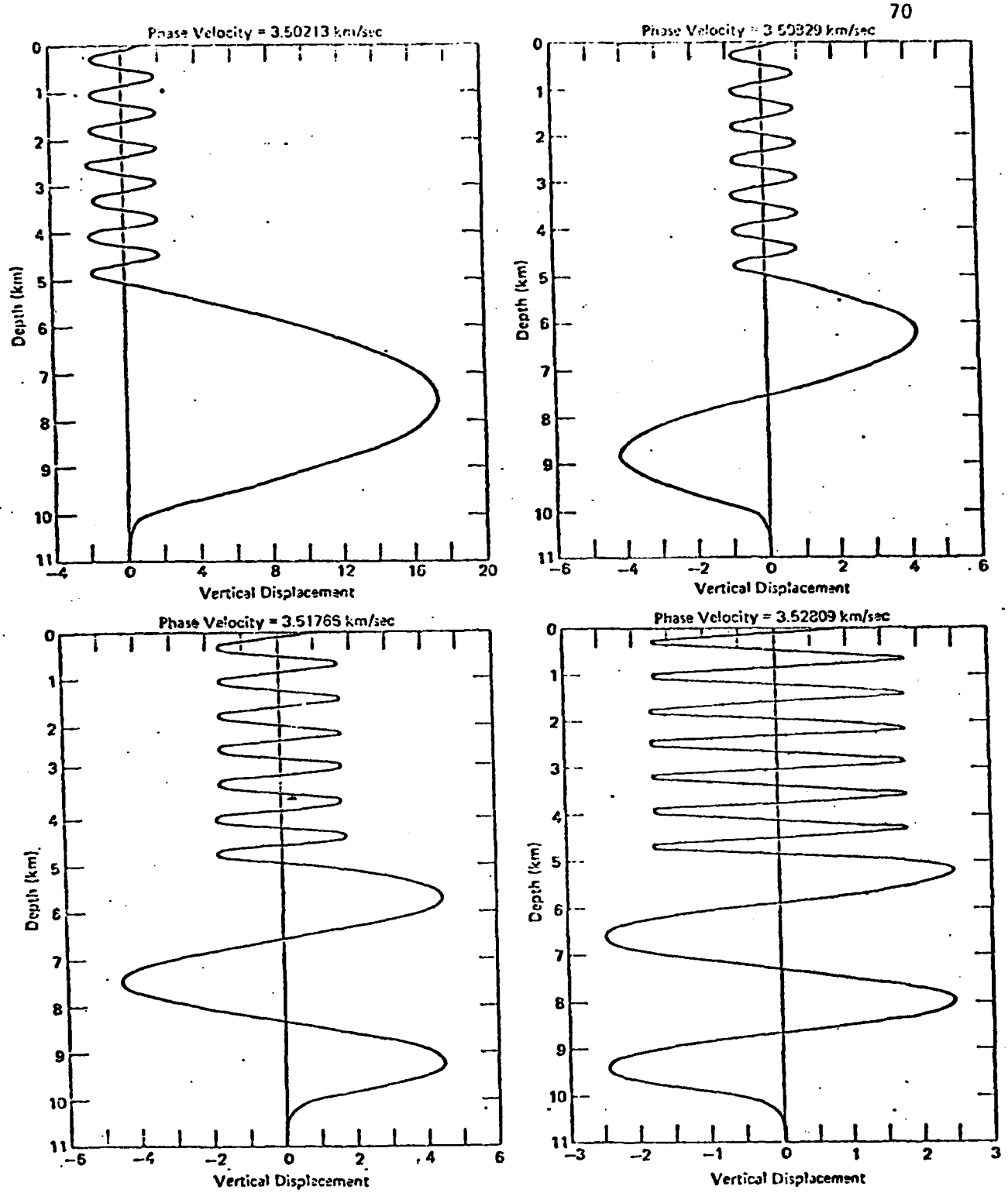

Figure 6. Characteristics of higher mode eigenfunctions at high frequency. The eigenfunctions illustrated correspond to the 14, 15, 16 and 17th higher modes at 10 Hz, all with phase velocities near 3.5 km/sec. The striking feature of the displacement variati with depth is the concentration of the mode displacements in the layer zone from 5 to 1(with the displacement variation in this layer having characteristics of fundamental and higher order plate modes. This series of modes, when added will represent a body wave refracted by this layer.

function in space and time. That is, the "inner product" referred to is an integral convolution, or a Hilbert space inner product.) Thus, with summation over the modes, this yields a theoretical seismogram, at any desired distance and azimuth from the source.

Figure 7 is a theoretical seismogram synthesized in this manner, where a simple explosion source at 1 km depth was used. The result is a complete seismogram with all body wave phases and lower order surface waves included. The "ripple", proceding the P wave arrival time indicated, is the noise level due to truncation of the mode sum over wave number and frequency. Numerous other seismograms, using different phase velocity and frequency windows and filtering have been generated. Figure 8 and Figure 9 are two examples. Comparison of the results leads to the conclusion that the theoretically generated seismograms are not highly sensitive to the truncation of the wave number (or phase velocity) range, so long as the cut-off value for k is small (or high for the phase velocity). The truncation noise, preceding the seismogram in time, can however be reduced by proper tapering by the wave number or phase velocity filter. Moving the cut-off value of the filter to higher phase velocity values, however, moves the truncation noise to earlier times - so time separation of truncation noise and the actual seismic arrivals can be controlled. Thus both the level and the time position of the noise due to wave number truncation can be predicted and controlled, and presents no serious problem.

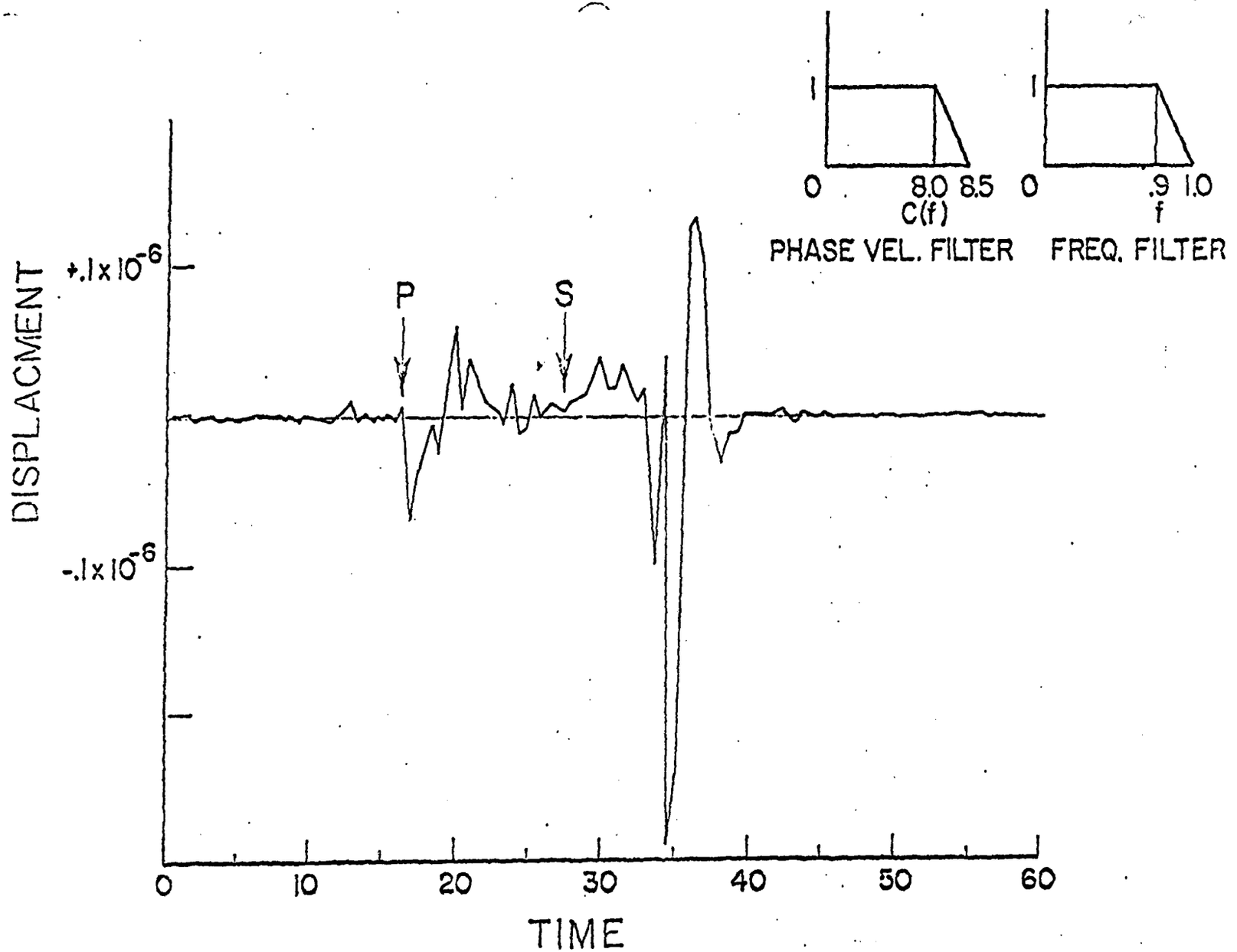

Figure 7. Theoretical seismogram at 100 km distance from the source, produced by mode superposition of all modes in the phase velocity range from 0 to 8.5 km/sec, and over the frequency range from 0 to 1 Hz. The elastic earth structure used is SC-1, without anelastic effects (infinite Q). The source was an explosion model at 1 km depth. The ray theory compressional (P) and shear wave (S) first arrivals times are indicated. The phase velocity and frequency filters used are shown in the insets and correspond to the weighting functions applied in the mode summation in order to minimize truncation effects (Gibbs phenomena). The variations in the time series prior to the first arrival P phase is "noise"

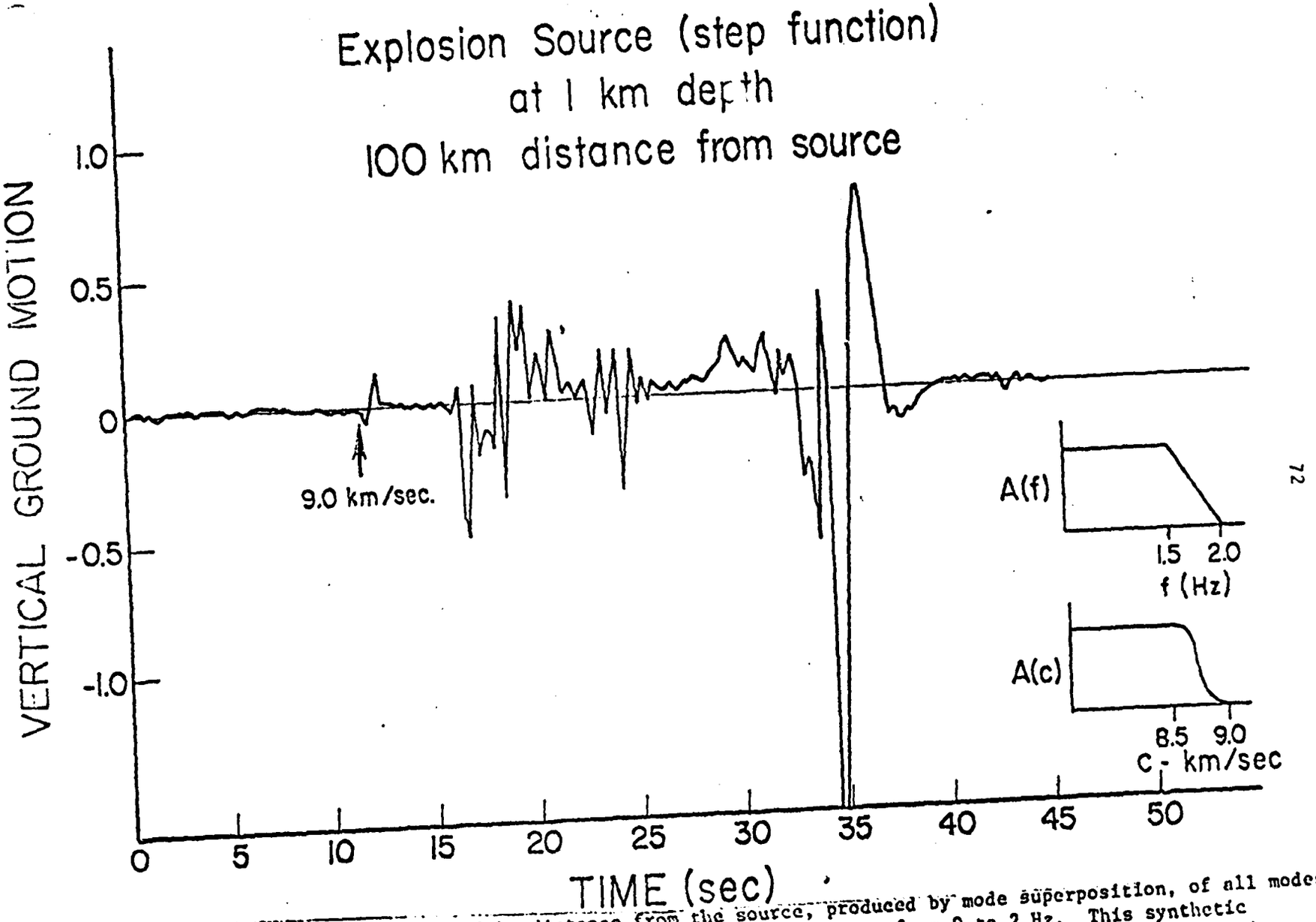

Figure 8. Theoretical seismogram at 100 km distance from the source, produced by mode superposition, of all modes in the phase velocity range from 0 to 9 km/sec and over the frequency range from 0 to 2 Hz. This synthetic was produced using the frequency and phase velocity windows shown in the insets. In all other respects it is comparable to the seismograms in Figures 7 and 9. Comparison of these synthetics shows that only the non-causal truncation noise is affected significantly by the change in the phase velocity window, while the predicted seismogram remains essentially invariant.

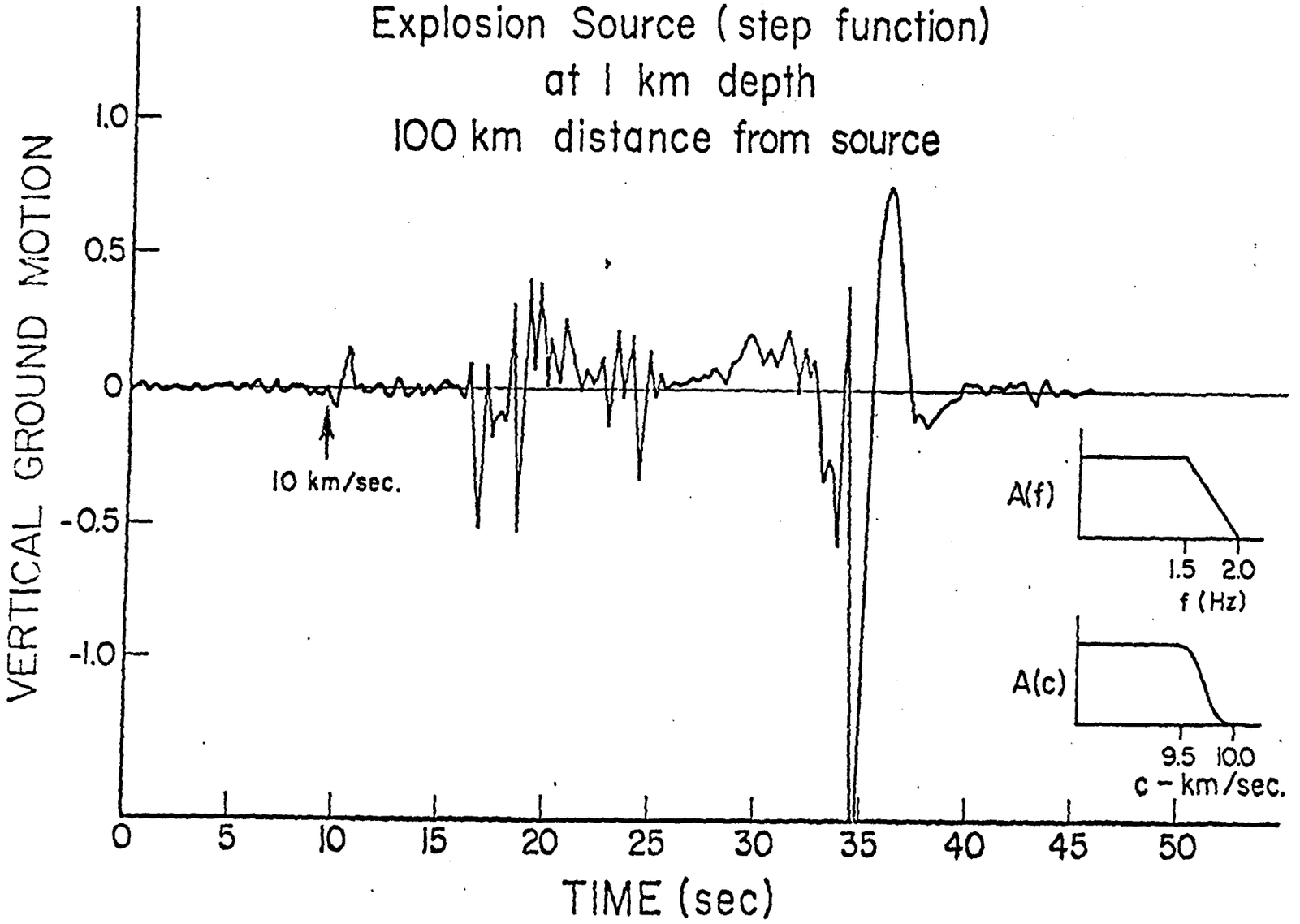

Figure 9. Theoretical seismogram at 100 km distance from the source, produced by mode superposition, of all modes in the phase velocity range from 0 to 10 km/sec and over the frequency range from 0 to 2 Hz. This synthetic was produced using the frequency and phase velocity windows shown in the insets. In all other respects it is comparable to the seismograms in Figures 7 and 8.

Once the modes are computed for a given structure then theoretical seismograms can be rapidly computed at any distance range for which reflections from the half-space "cap layer" are not within the time window of interest (e.g., in the direct S to P time window). For the structure used in the previous computations, where the cap layer is at 350 km, essentially exact, complete seismograms can be obtained to several hundred kilometers from the source, without contamination from the "spurious" cap-layer reflection. In addition, different sources may be used, with the same mode set, to obtain a variety of source generated synthetics.

Figure 18 illustrates a series of theoretical seismograms over the distance range from 75 km to 200 km, from a (vertical) vector point force. In this case the S wave is better developed than in the previous examples, where a pure explosion source was used. The theoretical seismograms shown are only part of the synthetics generated, the surface wave portion being omitted because of the large amplitudes. Various theoretical (ray theory) body wave arrivals are indicated by travel time curves in the figure and the synthetics clearly indicate theoretical pulses at these times. The pulse "arriving" along the time line denoted by the "T", is due to truncation of the modes in the ω-k plane (or frequency - phase velocity plane) and is of course spurious. It is clear that the truncation effect becomes much less important with distance form the source. In any case it can be filtered out of the results by simple time windowing since it does not overlap the earliest arriving P phase. At closer distances (less than 75 km from the source), a larger value of the "cut-off" phase velocity must be used to avoid contamination by this truncation noise.

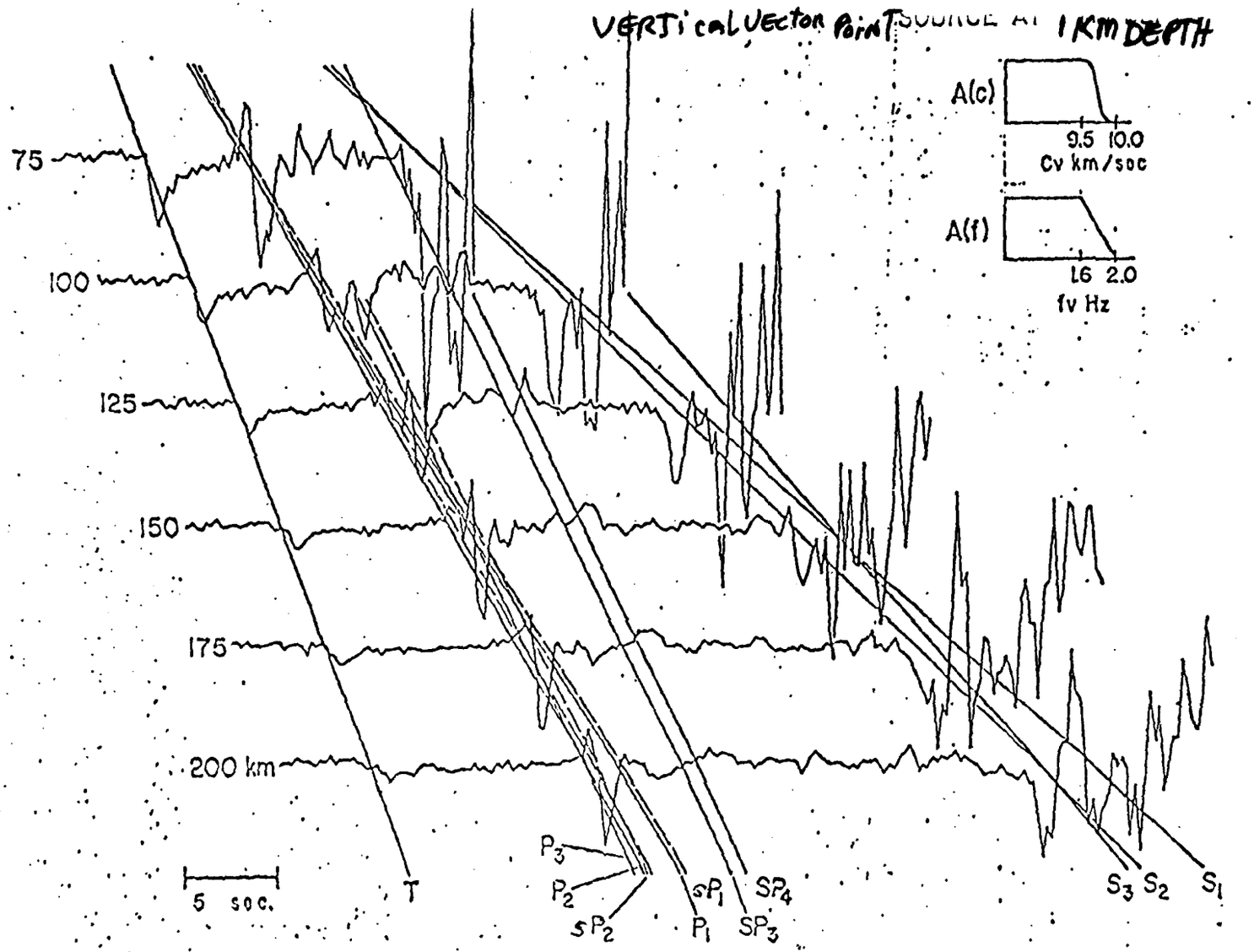

Figure 10. Theoretical record section in the regional distance range from 75 to 200 km. from a simple vector point source at 1 km depth in a eight layered crust - upper mantle earth model. The ray theoret arrival times for various refracted and reflected P and S phases in the crust are indicated. The P-wave refracted from the first crustal layer interface is denoted P_1 and so on. Converted phases due to surf reflections are denoted by sP_1 and so on. The arrival denoted by T is the spurious pulse due to truncat in the $\omega - k$ plane. The filtering applied in the $\omega - k$ plane is indicated by the insets, with the "T pulse" corresponding to the 10. km/s. cut-off value.

V. Seismic Source Theory

A. Seismic Radiation from the Sudden Creation of a Spherical Cavity in an Arbitrarily Prestressed Elastic Medium - J.L. Stevens.+

An earthquake can be considered to result from the creation of an external boundary in a prestressed elastic medium. Similarly, the anomalous radiation from an explosion can be considered to result from the creation of a shatter zone in a prestressed medium. We examine in general the problem of the sudden creation of a stress free surface in an arbitrarily prestressed medium. This problem contains most of the essential characteristics of the earthquake and explosion induced tectonic release problems. This problem may be treated as an initial value problem or, equivalently, as a stress pulse problem.

We solve this problem exactly for the case of a spherical cavity using vector spherical harmonics in the elastic Green's tensor integral equation in the frequency domain. The result is a relatively simple solution for the radiation field involving nothing more than the inverse of a number of two by two matrices and an inverse Fourier transform. The solution is valid for any arbitrary homogeneous or inhomogeneous prestress. The case of inhomogeneous prestress is particularly interesting since almost all previous source models have used the boundary condition of homogeneous shear or its equivalent. Actual stress fields in the earth are likely to be highly inhomogeneous. The main effect of the inhomogeneous prestress is the appearance of considerable seismic energy at frequencies slightly greater than the usual quadrupole corner frequency resulting in a low frequency spectral peak especially at locations near the quadrupole nodes.

+ Stevens, J.L., Seismic Radiation from the Creation of a Spherical Cavity in an Arbitrarily Prestressed Medium, Submitted to Geophys. J. Roy. Astron. Soc., 1979

Basic Relations

The Green's tensor integral equation for the general case of growing phase boundaries is given by Archambeau and Minster (1978). For the case of the sudden creation of a cavity it reduces to:

$$\underset{\sim}{u}(\underset{\sim}{x},t) = \int_o^t dt_o \int_\Sigma [\underset{\sim}{G}\cdot\underset{\sim}{T}(\underset{\sim}{u}) - \underset{\sim}{u}\cdot\underset{\sim}{T}(\underset{\sim}{G})]\cdot\hat{n}\ dA_o + \int_V \rho\left(\underset{\sim}{u}\cdot\frac{\partial \underset{\sim}{G}}{\partial t_o}\right)\Bigg|_{t_o=0} dV_o \qquad (1)$$

T(u) represents the stress operation $C_{ijk\ell}\ \partial_k u_\ell$

The transformed equation is given by:

$$\tilde{\underset{\sim}{u}}(\underset{\sim}{r},w) = -\int_\Sigma [\underset{\sim}{u}\cdot\underset{\sim}{T}(\tilde{\underset{\sim}{G}}) - \tilde{\underset{\sim}{G}}\cdot\underset{\sim}{T}(\underset{\sim}{u})]\cdot\hat{n}\ dA_o - \omega^2\int_V \rho\tilde{\underset{\sim}{u}}^*\cdot\underset{\sim}{G}\ dV_o \qquad (2)$$

where u^* is the initial displacement from equilibrium caused by the creation of the cavity.

The entire displacement from equilibrium is a step function at t=0 since the cavity is created "instantaneously", so that the transform is given by:

$$\tilde{\underset{\sim}{u}}^*(\underset{\sim}{r},\omega) = \frac{1}{i\omega}\ \tilde{\underset{\sim}{u}}^*(\underset{\sim}{r}) \qquad (3)$$

If the newly created surface is stress free, the above equation reduces to:

$$\tilde{\underset{\sim}{u}}(\underset{\sim}{r},\omega) = -\int_{\Sigma} \tilde{\underset{\sim}{u}}\cdot\underset{\sim}{\underset{\sim}{T}}(\underset{\sim}{\underset{\sim}{G}})\cdot\hat{n}\, dA - \omega^2\int_{V}\rho\tilde{\underset{\sim}{u}}^*\cdot\underset{\sim}{\underset{\sim}{G}}\, dV_o \tag{4}$$

The difficulty with this formulation is that $\underset{\sim}{u}^*$ must first be evaluated and then the volume integral must be evaluated over all space. This can be transformed to a boundary value problem in the following way.

$$\underset{\sim}{\underset{\sim}{L}}\underset{\sim}{u}^* = 0 \tag{5}$$

The dynamic Green's tensor satisfies

$$\underset{\sim}{\underset{\sim}{L}}\underset{\sim}{\underset{\sim}{G}} + \rho\omega^2\,\underset{\sim}{\underset{\sim}{G}} = -\underset{\sim}{\underset{\sim}{I}}\,\delta(\underset{\sim}{x}-\underset{\sim}{x}_o) \tag{6}$$

Multiplying (5) by $\underset{\sim}{\underset{\sim}{G}}$ and (6) by $\underset{\sim}{u}^*$, subtracting and integrating over V we have:

$$\underset{\sim}{u}^*(\underset{\sim}{x}) = -\omega^2\int_V \rho\,\underset{\sim}{u}^*(\underset{\sim}{x}_o)\cdot\underset{\sim}{\underset{\sim}{G}}(\underset{\sim}{x},\underset{\sim}{x}_o)\, dV$$

$$+\int_V [\underset{\sim}{\underset{\sim}{G}}\cdot\underset{\sim}{\underset{\sim}{L}}\underset{\sim}{u}^* - \underset{\sim}{u}^*\cdot\underset{\sim}{\underset{\sim}{L}}\underset{\sim}{\underset{\sim}{G}}]\, dV \tag{7}$$

We observe that

$$\underset{\sim}{G}\cdot\underset{\sim}{\underset{\sim}{L}}\,\underset{\sim}{u}^* - \underset{\sim}{u}^*\cdot\underset{\sim}{\underset{\sim}{L}}\underset{\sim}{G} = \underset{\sim}{\nabla}\cdot\left(\underset{\sim}{G}\cdot\underset{\sim}{\underset{\sim}{T}}(\underset{\sim}{u}^*) - \underset{\sim}{u}^*\cdot\underset{\sim}{\underset{\sim}{T}}(\underset{\sim}{G})\right) \tag{8}$$

and use Gauss' theorem. Then

$$-\omega^2\int_V \rho\underset{\sim}{u}^*\cdot\underset{\sim}{G}\,dV = \underset{\sim}{u}^* + \int_\Sigma \left[\underset{\sim}{u}^*\cdot\underset{\sim}{\underset{\sim}{T}}(\underset{\sim}{G}) - \underset{\sim}{G}\cdot\underset{\sim}{\underset{\sim}{T}}(\underset{\sim}{u}^*)\right]\cdot\hat{n}\,dA \tag{9}$$

This is the initial value term in equation (4). Substituting and rearranging terms, we have for the case of a traction-free cavity of arbitrary shape:

$$(\underset{\sim}{u}-\underset{\sim}{u}^*) = -\int_\Sigma (\underset{\sim}{u}-\underset{\sim}{u}^*)\cdot\underset{\sim}{\underset{\sim}{T}}(\underset{\sim}{G})\cdot\hat{n}\,dA - \int_\Sigma \underset{\sim}{G}\cdot\underset{\sim}{\underset{\sim}{T}}(\underset{\sim}{u}^*)\cdot\hat{n}\,dA \tag{10}$$

This relation is also valid for an arbitrary initial stress field.

The initial value term is now reduced to a surface integral. This means that to solve for the relative displacement field $\underset{\sim}{u}-\underset{\sim}{u}^*$ we need to know only the initial normal tractions on the surface of the cavity rather than the initial value field $\underset{\sim}{u}^*$ over all space.

Solution for Arbitrary pre-stress

We can extend the results of the previous section to the solution of the radiation field for the sudden creation of a spherical cavity in an arbitrarily prestressed medium. To do this we use expansions in vector spherical harmonics. We need to solve the equation

$$\underset{\sim}{u} = \int_{\partial V} \underset{\sim}{u}\cdot\underset{\sim}{\underset{\sim}{T}}(\underset{\sim}{G})\cdot\hat{n}\, dA + \underset{\sim}{u}^{I} \tag{11}$$

Here $\hat{n}$ is the outward normal $\hat{e}_r$ at the spherical surface.
$\underset{\sim}{u}^{I}$ may be either the initial value term:

$$\underset{\sim}{u}^{I} \text{ initial value} = -\rho\omega^2 \int_{V} \underset{\sim}{u}^{*}\cdot\underset{\sim}{G}\, dV \tag{12}$$

where V is the volume external to the sphere, or the stress pulse term:

$$\underset{\sim}{u}^{I} \text{ stress pulse} = \int_{\partial V} \underset{\sim}{G}\cdot\underset{\sim}{\underset{\sim}{T}}(\underset{\sim}{u}^{*})\cdot\hat{n}\, dA \tag{13}$$

In general the stress pulse term will be easier to evaluate. It is only necessary to evaluate the initial value term if $\underset{\sim}{u}^{*}$ is not really the difference between two equilibrium states. This would be the case, for example, if $\underset{\sim}{u}^{*}$ was caused in part by body forces which varied with time.

Any vector function can be expanded in the following way:

$$\underset{\sim}{u}(r,\theta,\phi) = \sum_{\ell=0}^{\infty} \sum_{m=-\ell}^{\ell} a_{\ell m}^{(1)}(r)\, \underset{\sim}{P}_{\ell m}(\theta,\phi) + a_{\ell m}^{(2)}(r)\, \underset{\sim}{B}_{\ell m}(\theta,\phi) + a_{\ell m}^{(3)}(r)\, \underset{\sim}{C}_{\ell m}(\theta,\phi) \tag{14}$$

$\underset{\sim}{P}_{\ell m}$, $\underset{\sim}{B}_{\ell m}$, $\underset{\sim}{C}_{\ell m}$ are vectors defined by (see Morse and Feshbach (1953) or Ben-Menahem and Singh (1968)):

$$\underset{\sim}{P}_{\ell m} = \hat{e}_r \, Y_{\ell m}(\theta,\phi)$$

$$\sqrt{\ell(\ell+1)}\, \underset{\sim}{B}_{\ell m} = \left[\hat{e}_\theta \frac{\partial}{\partial\theta} + \hat{e}_\phi \frac{1}{\sin\theta}\frac{\partial}{\partial\phi}\right] Y_{\ell m}(\theta,\phi) \qquad (15)$$

$$\sqrt{\ell(\ell+1)}\, \underset{\sim}{C}_{\ell m} = \left[\hat{e}_\theta \frac{1}{\sin\theta}\frac{\partial}{\partial\phi} - \hat{e}_\phi \frac{\partial}{\partial\theta}\right] Y_{\ell m}(\theta,\phi)$$

$$Y_{\ell m}(\theta,\phi) = P_{\ell m}(\cos\theta)\, e^{im\phi}$$

where $P_{\ell m}(x)$ is the associated Legendre function. These vectors have the following orthogonality relations:

$$\int \overline{\underset{\sim}{P}}_{\ell m} \cdot \underset{\sim}{B}_{\ell' m'}\, d\Omega = \int \overline{\underset{\sim}{P}}_{\ell m} \cdot \underset{\sim}{C}_{\ell' m'}\, d\Omega = \int \overline{\underset{\sim}{B}}_{\ell m} \cdot \underset{\sim}{C}_{\ell' m'}\, d\Omega = 0 \qquad (16)$$

and

$$\int \overline{\underset{\sim}{P}}_{\ell m} \cdot \underset{\sim}{P}_{\ell' m'}\, d\Omega = \int \overline{\underset{\sim}{B}}_{\ell m} \cdot \underset{\sim}{B}_{\ell' m'}\, d\Omega = \int \overline{\underset{\sim}{C}}_{\ell m} \underset{\sim}{C}_{\ell' m'}\, d\Omega = \delta_{\ell\ell'}\delta_{mm'}\Omega_{\ell m}$$

$$\Omega_{\ell m} = \frac{4\pi}{2\ell+1}\frac{(\ell+m)!}{(\ell-m)!}$$

Either by inspection or by using the orthogonality relations we can expand $\underset{\sim}{u}^I$ in the form:

$$\underset{\sim}{u}^{I}(\omega r,\theta,\phi) = \sum_{\ell=0}^{\infty} \sum_{m=-\ell}^{\ell} d^{1}_{\ell m}(r,\omega)\, \underset{\sim}{P}_{\ell m}(\theta,\phi)$$

$$+ d^{2}_{\ell m}(r,\omega)\, \underset{\sim}{B}_{\ell m}(\theta,\phi) + d^{3}_{\ell m}(r,\omega)\, \underset{\sim}{C}_{\ell m}(\theta,\phi) \qquad (17)$$

We can also expand the unknown displacement field $\underset{\sim}{u}$ in the form

$$\underset{\sim}{u}(\omega,r,\theta,\phi) = \sum_{\ell=0}^{\infty} \sum_{m=-\ell}^{\ell} b^{1}_{\ell m}(r,\omega)\, \underset{\sim}{P}_{\ell m}(\theta,\phi)$$

$$+ b^{2}_{\ell m}(r,\omega)\, \underset{\sim}{B}_{\ell m}(\theta,\phi) + b^{3}_{\ell m}(r,\omega)\, \underset{\sim}{C}_{\ell m}(\theta,\phi) \qquad (18)$$

The Green's tensor for this problem is given by:

$$\underset{\sim}{G}(\underset{\sim}{r},\underset{\sim}{r}_{o}) = -\frac{ik_{\beta}}{4\pi\mu} \sum_{\ell=1,1,0}^{\infty} \frac{2\ell+1}{\ell(\ell+1)} \sum_{m=-\ell}^{\ell} \frac{(\ell-m)!}{(\ell+m)!} \left[\overset{*\varepsilon}{\underset{\sim}{M}}_{\ell m}(r_{o})\, \underset{\sim}{M}^{-\varepsilon}_{\ell m}(r) \right.$$

$$\left. + \overset{*\varepsilon}{\underset{\sim}{N}}_{\ell m}(r_{o})\, \underset{\sim}{N}^{-\varepsilon}_{\ell m}(r) + \ell(\ell+1) \left(\frac{\beta}{\alpha}\right)^{3} \overset{*\varepsilon}{\underset{\sim}{L}}_{\ell m}(r_{o})\, \underset{\sim}{L}^{-\varepsilon}_{\ell m}(r) \right] \qquad (19)$$

In terms of the vectors $\underset{\sim}{P}$, $\underset{\sim}{B}$, $\underset{\sim}{C}$ we can write (Ben-Menahem and Singh (1968))

$$\underset{\sim}{M}^{\pm}_{\ell m} = \sqrt{\ell(\ell+1)}\ \underset{\sim}{C}_{\ell m}\, f^{\pm}_{\ell}(y)$$

$$\underset{\sim}{N}^{\pm}_{\ell m} = \ell(\ell+1)\, \underset{\sim}{P}_{\ell m} \frac{f^{\pm}_{\ell}(y)}{y} + \sqrt{\ell(\ell+1)}\ \underset{\sim}{B}_{\ell m} \left(f^{\pm\prime}_{\ell}(y) + \frac{f^{\pm}_{\ell}(y)}{y} \right) \qquad (20)$$

$$\underset{\sim}{L}^{\pm}_{\ell m} = \underset{\sim}{P}_{\ell m} f^{\pm\prime}_{\ell}(x) + \sqrt{\ell(\ell+1)}\, \underset{\sim}{B}_{\ell m} \frac{f^{\pm}_{\ell}(x)}{x}$$

where $y = k_\beta r$, $x = k_\alpha r$

and f_ℓ^+ are spherical Bessel (+) and outgoing Hankel (-), function.

The orthogonality relations (16) can now be used to reduce the integral equation (11) to a set of algebraic equations. In fact, since the integrals for each value of ℓ uncouple, there are only two simultaneous equations to solve for each order of ℓ . The solution is therefore inexpensive to compute. Figure 1 shows the spectrum for a homogeneous shear field. The sharp peaks correspond to free oscillations at the cavity. Figure 2 shows the far field pulses computed using the equivalent stress pulse (equaiton 13) alone and the exact solution. The effect of the exact solution is to stretch out and increase in magnitude the stress pulse solution.

We want to consider the radiation from a stress free sphere spontaneously created in a prestressed elastic medium. This should be a good model for predicting the tectonic release from explosions. It should also be a good model for spontaneous rupture in an inhomogeneous stress field since the material inside the failure zone has little effect on the motion of the cavity surface. The geometry is not very good for an earthquake, of course, but the general features of failure in an inhomogeneous stress field are not likely to be highly dependent on the failure geometry.

The first question to be answered is the nature of different kinds of prestress which are physically acceptable. We regard the initial and final stress fields as due to some complicated distribution of body force due primarily to dislocations in the medium. The initial field satisfies

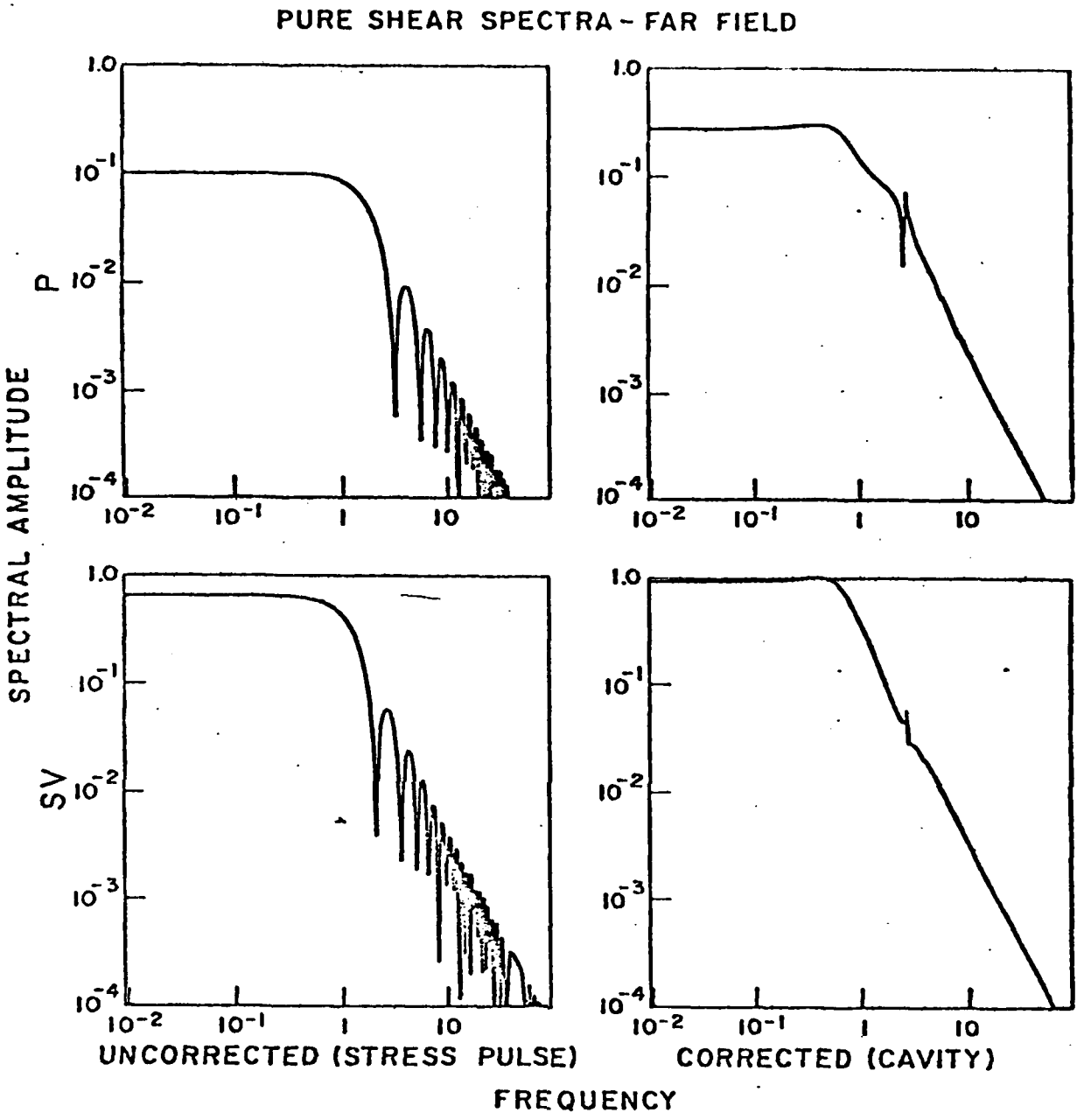

Fig. 1. P and S wave spectra for pure shear. In the exact solution the dips in the spectrum are removed, but peaks corresponding to free oscillations appear. All examples in this paper use α = 8 km/sec and β = 5 km/sec with a cavity radius of 10 km.

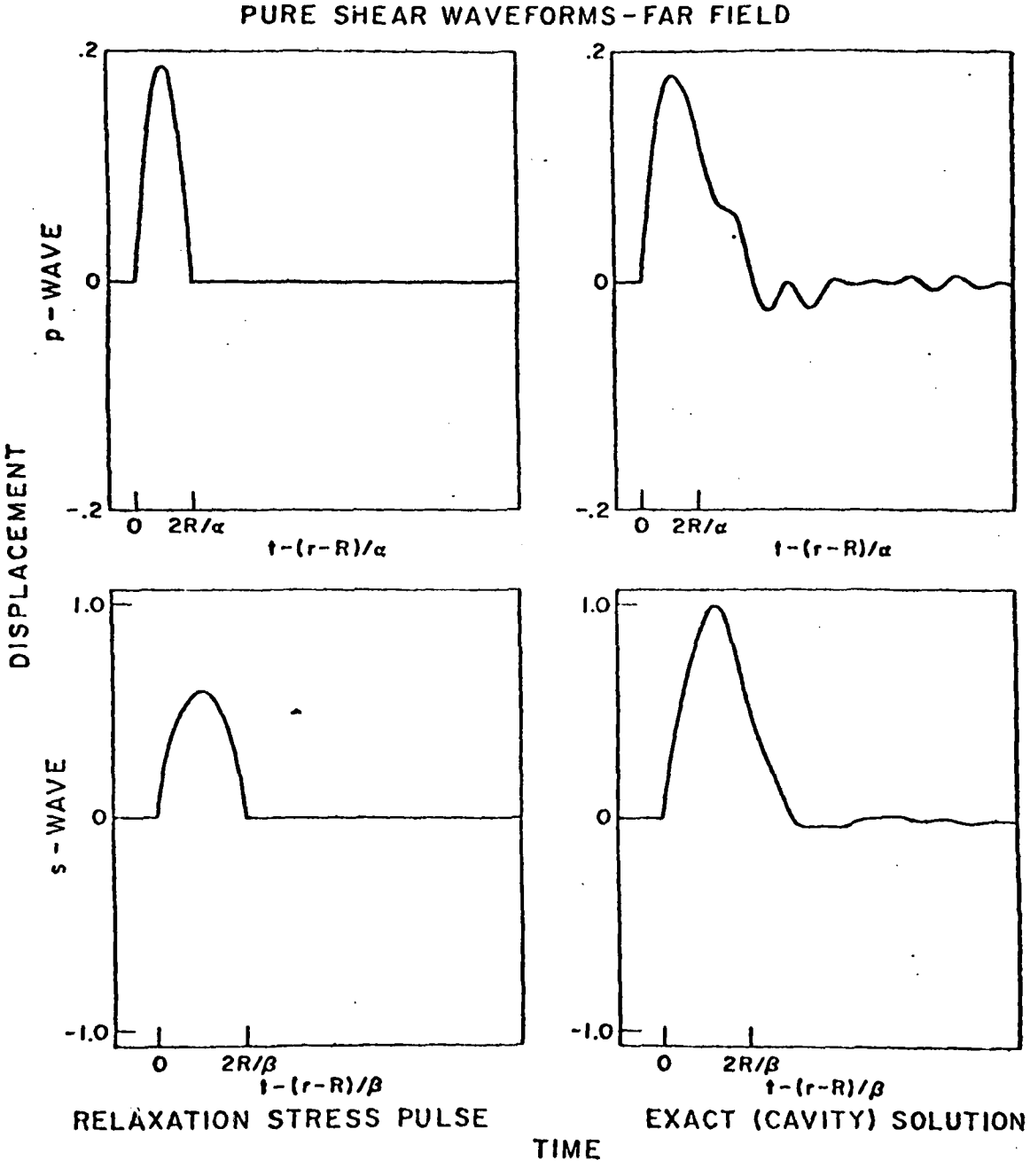

Fig. 2. Far field pulses due to the creation of a stress free sphere in a pure shear field.

$\mathcal{L}\underset{\sim}{u}^f = \underset{\sim}{f}$ and the final field satisfies $\mathcal{L}\underset{\sim}{u}^1 = \underset{\sim}{f}$ so the difference field satisfies $\mathcal{L}u^* = 0$ the static elastic equation with no body forces acting. This difference field must be finite at infinity. Since we are interested in the region outside $r = R$, the solution need not be finite at $r = 0$. The most general displacement field at this form can be written (Ben-Menahem and Singh, 1968):

$$\underset{\sim}{u}^*(\underset{\sim}{r}) = \sum_{\ell m} [-a_{\ell m}(\ell+1)\, r^{-\ell-2} + c_{\ell m}\ell\, \frac{\gamma+\ell-1}{\gamma}\, r^{-\ell}]\, \underset{\sim}{P}_{\ell m}$$

$$+ [a_{\ell m}\sqrt{\ell(\ell+1)}\, r^{-\ell-2} + c_{\ell m}\sqrt{\ell(\ell+1)}\, \frac{\gamma-\ell}{\gamma}\, r^{-\ell}]\, \underset{\sim}{B}_{\ell m}$$

$$+ f_{\ell m}\, r^{-\ell-1}\, \underset{\sim}{C}_{\ell m} \qquad (21)$$

where

$$\gamma = 4(1-\hat{\sigma}) = \frac{2(\lambda+2\mu)}{\lambda+\mu} = \frac{2\alpha^2}{\alpha^2 - \beta^2}$$

where σ is Poisson's ratio.

The $\ell = 1$ terms are forbidden by conservation of energy and angular momentum.

We are now in a position to compute the radiation field. The easiest way to do this to use the stress pulse solution

$$\underset{\sim}{u} = \int_{\partial V} \underset{\sim}{u} \cdot \underset{\sim}{T}(\underset{\sim}{G}) \cdot \hat{n} dA + \underset{\sim}{u}^I \qquad (22)$$

where

$$\underset{\sim}{u}^{I} = \frac{1}{i\omega} \int_{\partial V} \underset{\sim}{G} \cdot \underset{\sim}{T}(\underset{\sim}{u}^{*}) \cdot \hat{n} dA \qquad (23)$$

It is not difficult to compute the tractions $\underset{\sim}{T}(\underset{\sim}{u}^{*}) \cdot \hat{n}$. They again are a sum of vector harmonics $\underset{\sim}{P}$, $\underset{\sim}{B}$, $\underset{\sim}{C}$. We can now compute the radiation from the most general possible stress field. Each value of ℓ has three waves associated with it - two coupled P-SV (spheroidal) waves and one uncoupled SH (toroidal) wave. All of the higher modes are oscillatory.

The waveforms for higher ℓ values have more and more oscillations. An example is given in Figure 3 for the $\ell = 4$ waveforms. The result of this is that the spectra become more and more peaked for higher order ℓ values and the maximum frequency increases slightly for each increment in ℓ. Figure 4 shows the individual P1 spectra for $\ell = 3, 4, 5$ and 6 . The magnitude of these peaks will vary with angle as the corresponding vector spherical harmonic. It will therefore vary more rapidly with angle than pure shear.

These results shed some light on the old argument about low frequency spectral peaks in relaxation problems. Archambeau (1968) solved the problem for the radiation from a spherical cavity in pure shear, but he made an approximation for a more localized stress field by truncating the volume integral (see equation 2) at a radius R_s. This always leads to a low frequency spectral peak in the far field. Minster (1973) discussed this problem in some detail. Snoke (1976) showed that this approximation leads

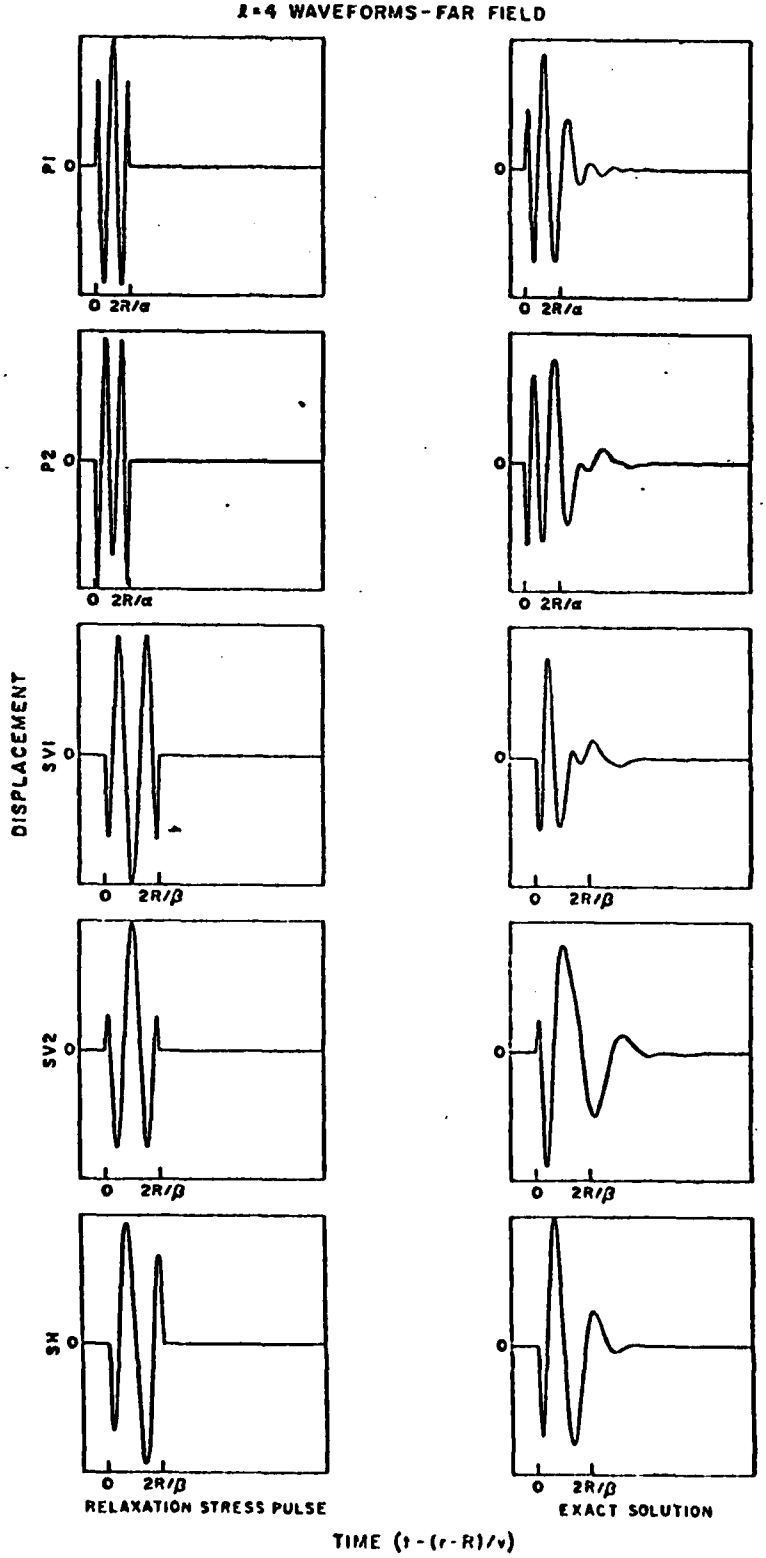

Fig. 3. Waveforms for $\ell = 4$. All higher ℓ modes are oscillatory. The number of oscillations increases with ℓ.

to acausal results in the time domain and concluded that the approximation was incorrect and that the spectral peaks were therefore spurious. Our results are somewhat different from those of Archambeau's R_s spectral peak. That approximation removed energy from the low frequency part of the spectrum at wavelengths greater than R_s. Our results show that a spectral peak can in fact exist, but the effect is to add in additional energy at frequencies slightly above the "corner frequency" defined by the pure shear spectrum. Also, the magnitude of the spectral peak will vary with angle. If the radiation is predominantly pure shear, then a spectral peak will be observed only near the quadrupole nodes. If the stress were more inhomogeneous then the peak might be observed at all or nearly all angles of observation. It should be possible to use data from explosions to invert for the local tectonic stress field if there are a sufficient number of observation points.

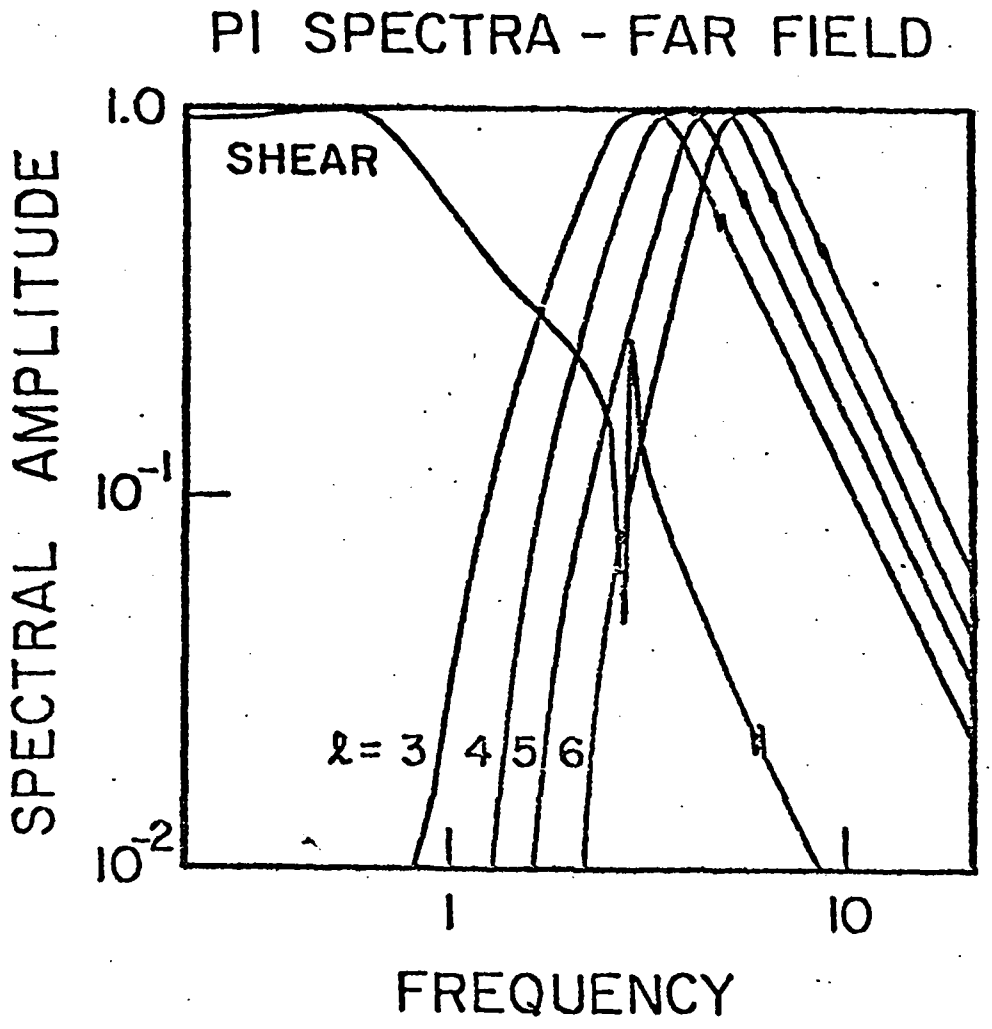

Fig. 4. The effect of an inhomogeneous prestress is to add in energy at frequencies higher than the usual corner frequency corresponding to uniform shear. Shown here are the spectra of the far-field first P-wave for $\ell = 3$ to $\ell = 6$ and the pure shear spectrum for comparison. A sufficiently inhomogeneous prestress can result in a low frequency spectral peak which varies in magnitude according to the variation of the vector spherical harmonics.

Conclusions.

We have developed a simple general method for computing the radiation due to the instantaneous creation of a spherical cavity in an arbitrarily prestressed medium. Vector spherical harmonics are found to be convenient for solving the Green's tensor integral equation in the frequency domain. Previous solutions to this problem which have been used as earthquake source models were examined and found to contain either dangerous approximations or contained the implicit assumption that the elastic space is infinite and uniform even within the sphere. Solving the elastic equations with the use of vector harmonics simplifies the interpretation of the solution, since potentials are never introduced and only the physical quantities of displacement and stress are used. Although the spherical geometry used here is not the ideal geometry to use for an earthquake source, it should be an improvement over previous spherical sources, and should be a good model to estimate the radiation due to tectonic strain release by explosions.

Almost all earthquake source models in the past have assumed the unphysical condition of uniform shear. The method given here can be used to investigate the radiation from more complicated initial stress fields. We have shown that the radiation field due to more complicated stress fields tends to be oscillatory rather than one-sided in nature. Failure in a sufficiently inhomogeneous stress field can therefore result in a complicated angular distribution of radiation and may produce a low frequency far-field spectral peak. The magnitude of the peak will vary with angle and may exist at all angles or only at the quadupole nodes depending on the amount of inhomogeneity in the stress field.

B. Normal Mode Excitation from Relaxation Sources with Applications to Source Parameters Inversion Studies - C.B. Archambeau, J.L. Stevens and K. Wyss.

The integral equation expressing the general elastodynamic displacement field for an inhomogeneous (and possibly anelastic) medium (Archambeau and Minster, 1978) can be written in the compact form:

$$4\pi\tilde{u}_\mu(\underline{x},\omega) = \mathcal{L}_o[\langle \rho f_\beta | \tilde{H}^\mu_\beta \rangle_{V_o} + i\omega \langle \rho \partial_{t_o} u^*_\beta | \tilde{H}^\mu_\beta \rangle_{V_o} - \langle \tau_{\alpha\beta}\eta_\alpha | \tilde{H}^\mu_\beta \rangle_{\partial V_o} + \langle u_\beta | \tilde{H}^\mu_{\alpha\beta}\eta_\alpha \rangle_{\partial V_o}] \quad (1)$$

where $\tilde{u}_\mu(\underline{x},\omega)$ is the Fourier transform with respect to the observers time t of the displacement field at a point of observation at $\underline{x}$. Similarly, $\tilde{H}(\underline{x};\underline{x}_o)$ is the Fourier transform with respect to t of the Greens displacement function for the medium, and $\tilde{H}^\mu_{\alpha\beta}$ is the associated stress tensor, so that with η_α the normal to a surface ∂V_o, then $\tilde{H}^\mu_{\alpha\beta}\eta_\alpha$ is the (transformed) traction+.

Here $\mathcal{L}_o$ is the Fourier transform operator with respect to the time variable t_o (source time variable), so that, for example:

+Repeated indices are summed over, in all tensor relations.

$$\mathcal{L}_o[u_\beta(\underline{x}_o,\ t_o)] = \int_{-\infty}^{+\infty} u_\beta(\underline{x}_o,\ t_o)\ell^{-i\omega t_o}\, dt_o$$

The notation $\langle f|g\rangle_{V_o}$ denotes an inner product in the function space to which f and g belong (a Hilbert space), over the region V_o. Here $V_o \equiv V(t_o)$ is a spatial volume, which may depend parametrically on the source time variable t_o. (This occurs in the case when a moving boundary is present, such as during a spontaneous failure process, so this case is of greatest interest here.) Thus for example:

$$\langle \rho f_\beta | \tilde{H}^\mu_\beta \rangle_{v_o} = \int_{v(t_o)} \rho(\underline{x}_o)\ f_\beta(\underline{x}_o, t_o)\ \tilde{H}^\mu_\beta(\underline{x}; x_o)\ d^3\underline{x}_o$$

The notation ∂v_o represents the external boundary of v_o, that is the bounding surfaces of the linear region. (v_o does not contain a failure zone, since such a zone is a nonlinear region. Hence, a failure surface is an exterior boundary of v_o.) Therefore, terms in (1) of the form $\langle f|g\rangle_{\partial v_o}$ represent surface integrals over the external boundaries of v_o.

Finally, the various "source" terms in (1) are ρf_β the body force associated with external force fields (ρ is the density) and $\rho\, \partial_{t_o} u^*_\beta$, the relaxation source term associated with changes in the equilibrium field u^*_β within the medium. The latter can be dependent parametrically on the source time t_o, for example if a failure surface extends itself with time within an initially stressed medium. The surface integral terms over ∂v_o involve $u_\beta(\underline{x}_o, t_o)$, the dynamic displacement field on the boundaries of v_o and $\tau_{\alpha\beta}(\underline{x}_o, t_o)\eta_\alpha$ the traction on these same boundaries. These may be known functions, for example, at the earth's surface the tractions $\tau_{\alpha\beta}\eta_\alpha$ vanish and the associated terms in (1), on this part of the external boundary of V_o, will therefore vanish. (Further the Green's function traction, $\tilde{H}^\mu_{\alpha\beta}\eta_\alpha$, can be also constructed to vanish at the earth's free surface, as will be seen below, and so the integral term involving the unknown displacement u^*_β in (1) will also vanish on the free surface.) On a failure surface however, the dynamic tractions $\tau_{\alpha\beta}\eta_\beta$ and displacements u_β may be unknown and it is not usually possible to construct $\tilde{H}^\mu_\beta$ or $\tilde{H}^\mu_{\alpha\beta}\eta_\alpha$ to vanish there. Thus both these terms are present on the part of ∂v_o corresponding to the (growing) failure surface. Therefore they are required parts of the solution for the radiation field from an earthquake source. They are generally recognized as boundary scattering terms and usually neglected in what is called the "transparent boundary approximation" (e.g. Archambeau, 1968, 1972). More recently, methods have been suggested for incorporating them in a complete solution of (1), in particular, by

Archambeau and Minster (1978). Stevens (1978), using this approach, has recently obtained a closed form solution of (1) for the "cannonical" problem of instantaneously created tractionless spherical failure zone in a arbitrarily stressed medium. He showed that these terms, at least in this rather extreme special case, can be quite important. Consequently, we retain them in our current work on source radiation representations and inversion studies. (We expect the contributions to be quite small for true earthquake geometries and for finite failure zone growth rates however.)

Thus (1) can be used to provide the complete formal representation of the radiation field from an earthquake, the problem is to solve this rather difficult integral equation. The first difficulty is to obtain an appropriate form for the Green's function $\tilde{H}^{\mu}_{\beta}(\underline{x};\underline{x}_o)$. Indeed, if a proper form for $\tilde{H}^{\mu}_{\beta}$ can be found, the solution of (1) might be quite straightforward. We have, in fact, obtained what appears to be an ideal form for the purposes of formulating the inverse problem, designed to deduce source properties (spatial stress changes, rupture rate, etc.), as well as for solving (1) in the forward direction, to predict the radiation field $\tilde{u}_{\mu}(\underline{x},\omega)$.

Our approach, in this regard, is to observe that a Greens function can, at least in part, always be expanded in terms of the eigenfunctions for the medium corresponding to the modes of free oscillation. Only in an unbounded medium is such a modal expansion incomplete, and even in that case leaking modes can be included, by suitable manipulations,

to provide a complete representation of the Greens function in terms of mode eigenfunctions. In the case of a finite medium, the mode eigenfunctions will, of course, give the complete Greens function and so for a spherical earth model there is no problem with completeness. However, layered half space earth models are clearly useful, if not necessary, for prediction of wave propagation effects at near and regional distance ranges. Therefore we have considered modal eigenfunction expansions for both layered spherical earth models and layered half space models.

From the discussion of the half space mode approximation in Section IV it is apparent that the Greens function for an unbounded half space problem can always be written in the form:

$$\tilde{H}^{\mu}_{\alpha}(\underline{x};\underline{x}_o) = \tilde{G}^{\mu}_{\alpha}(\underline{x};\underline{x}_o) + \tilde{h}^{\mu}_{\alpha}(\underline{x};\underline{x}_o) \qquad (2)$$

where $\tilde{G}^{\mu}_{\alpha}(\underline{x};\underline{x}_o)$ is the response function for the medium corresponding to its resonances or "trapped" modes of oscillation and $\tilde{h}^{\mu}_{\alpha}$ corresponds to free waves propagating to, or from, infinity. The existence of $\tilde{h}^{\mu}_{\alpha}$ is, of course, due to the fact that the model medium is unbounded. In the case of a spherical earth model, $\tilde{h}^{\mu}_{\alpha}$ is identically zero. For a half space model $\tilde{h}^{\mu}_{\alpha}$ can, at least in part, be represented by leaking modes; that is by "resonance modes" that leak energy to infinity, in which case the dispersion relation or functional relation between frequency ω and wave number k is complex, with k itself being a complex

number. In general $\tilde{h}_\alpha^\mu$ is represented by integrals over the wave number k (i.e., branch-line integrals), whereas $\tilde{G}_\alpha^\mu$ corresponds to a residue sum. However, in the context of the previous discussion of the mode theory approximation, it is possible to reduce the contributions of terms in (1) associated with $\tilde{h}_\alpha^\mu$ to an arbitrarily small level relative to those arising from $\tilde{G}_\alpha^\mu$. As was described earlier, this is achieved by inserting a strongly "opaque" boundary at a large, but finite, distance from the source region. In this case the medium is effectively bounded and appears as a quasi-finite model, such that the trapped modes describe all the significant wave propagation in the system. The use of a remote "non-transmitting" boundary insures that contributions to the complete medium response function, H_α^μ, from h_α^μ are small and, in any case, that what contributions do arise are at times that are well removed from those of H_α^μ, and outside the time window of interest. (This time shift is assured by the distant placement of the opaque boundary from the source region. In particular, if $\underline{d}$ represents the boundary coordinates, then the contributions from h_α^μ will be outside the time window when $|\underline{x}-\underline{x}_o| < |\underline{d}-\underline{x}_o|$, where $\underline{x}_o$ is a source coordinate and $\underline{x}$ a receiver coordinate.)

Therefore, for a half space in which an opaque boundary has been inserted at an appropriately remote depth, then $\tilde{H}_\alpha^\mu$ is accurately represented by the modal Green's function $\tilde{G}_\alpha^\mu$. This Green's function for a layered half space, can be expressed in the form (Archambeau

and Stevens, 1978)+:

$$\tilde{G}^{\mu}_{\alpha}(\underline{x},\underline{x}_o;\omega) = \sum_m \left[\mathop{S}_{\omega_R(k)} \frac{{}_R\psi^m_{\mu}(\underline{x};\omega_R(k))\ {}_R\bar{\psi}^m_{\alpha}(\underline{x}_o;\omega_R(k))}{\omega^2 - \omega_R^2(k)} \right. \tag{3}$$

$$\left. + \mathop{S}_{\omega_L(k)} \frac{{}_L\psi^m_{\mu}(\underline{x};\omega_L(k))\ {}_L\bar{\psi}^m_{\mu}(\underline{x}_o;\omega_L(k))}{\omega^2 - \omega_L^2(k)} \right]$$

where $\omega_R(k)$ and $\omega_L(k)$ are the Rayleigh and Love mode eigenfrequencies, which are known function of the wave number k, and ${}_R\psi^m_{\mu}$ and ${}_L\psi^m_{\mu}$ the corresponding eigenfunctions. The notation ${}_R\bar{\psi}^m_{\alpha}$ means the complex conjugate of ${}_R\psi^m_{\alpha}$. As was illustrated in the previous section (A), the eigenfrequencies and eigenfunctions can be computed at all frequencies.

The symbol $\mathop{S}$ is used to represent a generalized sum (e.g. an integral or discrete sum, or both). Here, if $F(\omega;\omega_o,k_o)$ is a function of frequency ω (associated with the reciever time t), the mode frequency ω' and mode wave number k'; then when k' is considered the independent variable in the dispersion relation $\omega' = \omega_R(k')$:

$$\mathop{S}_{\omega_R(k')} F(\omega;\omega',k') \equiv \int_o^{\infty} dk' \sum_n F(\omega;{}_n\omega_R(k'),k')$$

$$= \sum_n \int_{{}_n\omega_R(k')} dk'\ F(\omega,{}_n\omega_R(k'),k') \tag{4a}$$

+Here only Greek indices refer to tensor components while all latin indices will be used for all other kinds of indices - such as mode numbers, etc. Therefore the summation convention applies only to Greek indices.

When ω' is considered the independent variable in the mode dispersion relation $k' = k_R(\omega') = \omega'/{}_n c_R(\omega')$, then

$$\sum_{\omega_R(k')} F(\omega;\omega',k') \equiv \int_0^\infty d\omega' \sum_n F(\omega;\omega',{}_n c_R(\omega'))/{}_n U_R(\omega')$$

$$= \sum_n \int_{{}_n c_R(\omega')} \frac{d\omega'}{{}_n U_R(\omega')} F(\omega;\omega',{}_n c_R(\omega')) \qquad (4b)$$

with similar representations for the Love modes with eigenfrequencies $\omega_L(k')$. All the forms in (4a) and (4b) are equivalent since either ω' or k' can be considered as the independent variable, and the other as dependent. Here $U(\omega')$ is the group velocity:

$$U(\omega') = \frac{d\omega'}{dk'}$$

The integers $\{n\}$ are the mode number indices and the discrete sums in (4a) and (4b) are over the modes. This, of course, arises from the fact that for a particular value of the wave number k', the dispersion relation $\omega_R(k')$ has a whole set of allowed values. The integrals $\int_{{}_n\omega_R} dk'$ where k' is considered the independent variable, denote integration along the dispersion curve defined by $\omega' = {}_n\omega_R(k')$ in the ω' vs k' plane, appropriate to the nth mode. Similarly, $\int_{{}_n c_R(\omega')} d\omega'$ means a frequency integration along the curve $c' = {}_n c_R(\omega')$ in the phase velocity versus frequency plane.

The expressions on the right side in (4a) (or (4b)) simply say: add up the modes and then integrate over wave number (or frequency), or equivalently, integrate over wave number (or frequency) along the allowed mode curve and then add up the modes. The only difference in (4a) and (4b) is the presence of the group velocity as a weight function in (4b).

The expression of the Green's function in a layered spherical earth model is given exactly by the mode expansion, as opposed to the approximation of (2) by the half space expansion in (3), and is formally of the identical form as (3). That is, for the sphere:

$$\tilde{H}^{\mu}_{\alpha}(\underline{x},\underline{x}_o;\omega) = \tilde{G}^{\mu}_{\alpha}(\underline{x},\underline{x}_o;\omega) = \sum_{m}\left[\sum_{{}_n\omega_\ell^s} \frac{{}_s\psi^m_\mu(\underline{x};{}_n\omega_\ell^s)\ {}_s\bar{\psi}^m_\alpha(\underline{x}_o;{}_n\omega_\ell^s)}{\omega^2 - ({}_n\omega_\ell^s)^2} \right.$$

$$\left. + \sum_{{}_n\omega_\ell^T} \frac{{}_T\psi^m_\mu(\underline{x};{}_n\omega_\ell^T)\ {}_T\bar{\psi}^m_\alpha(\underline{x}_o;{}_n\omega_\ell^T)}{\omega^2 - ({}_n\omega_\ell^T)^2} \right] \qquad (5)$$

where ${}_n\omega_\ell^s$ and ${}_n\omega_\ell^T$ are the spheroidal and toroidal oscillation frequencies. Here the integer ℓ (the "mode number") is analogous to the wave number k in the infinite half space, while n (the "overtone number") is the same as the mode index n for the half space. For this case, the mode sum represented by $\sum_{{}_n\omega_\ell}$ corresponds to a discrete summation over the ℓ and n indices. In particular

$$\sum_{{}_n\omega_\ell} F(\omega;{}_n\omega_\ell) \equiv \sum_{\ell}\sum_{n} F(\omega;{}_n\omega_\ell) \qquad (6)$$

The eigenfunctions ${}_s\psi_\alpha^m$ and ${}_T\psi_\alpha^m$ are, of course, expressed in spherical coordinates, rather than in cylindrical coordinates as are ${}_R\psi_\alpha^m$ and ${}_L\psi_\alpha^m$. In particular, ${}_s\psi_\alpha^m$ and ${}_T\psi_\alpha$ may be expressed in closed form in terms of vector spherical harmonics for a layered sphere, while ${}_R\psi_\alpha$ and ${}_T\psi_\alpha$ may similarly be expressed in terms of vector cylindrical harmonics for the layered half space (Archambeau and Stevens, 1978). In both cases the normalizations of the eigenfunctions (such that their inner products are delta functions with unit coefficient) contain factors representing frequency derivatives of the characteristic equation, which are regular (analytic) functions of the eigenfrequencies $\omega(k)$ or ${}_n\omega_\ell$.

For both (3) and (5), it is clearly reasonable to suppress the mode name designations (i.e., Rayleigh and Love, spheroidal and toroidal) and simply write ω_n for the set $\{{}_n\omega_R(k),\ {}_n\omega_L(k)\}$ and ψ_α^m for $\{{}_R\psi_\alpha^m,\ {}_L\psi_\alpha^m\}$, with similar notation for the layered spherical model. Here the index n on ω_n will serve to remind us that ω_n is a prescribed function of k in the half space model, and a prescribed function of ℓ in the spherical model.

With these conventions the Green's function for layered spherical or half space models may be expressed compactly as:

$$\tilde{H}_\alpha^\mu(\underline{x},\underline{x}_o;\omega) = \sum_{m,\omega_n} \frac{\psi_\mu^m(\underline{x};\omega_n)\ \overline{\psi}_\alpha^m(\underline{x}_o;\omega_n)}{\omega^2 - \omega_n^2} \qquad (7)$$

where $\sum_{m,\omega_n}$ is the generalized sum over both m and ω_n, i.e., $\sum_{m,\omega_n} \equiv \sum_m \sum_{\omega_n}$. This representation is exact for the layered sphere

and an approximation, in the sense previously described, for the layered half space.

It is worth noting that it is the separability of this Green's function representation, in $\underline{x}$ and $\underline{x}_o$, that makes this expansion form so powerful, as will be demonstrated below. Further, the eigenfunctions themselves are easily shown to be separable in the coordinate components (e.g Archambeau and Stevens, 1978) and to be such that, with x^1, x^2, x^3 representing components of the general coordinate variable $\underline{x}$ (i.e., either spherical or cylindrical coordinates),

$$\underline{\psi}^m(\underline{x};\omega_n) = D(x^1;\omega_n)\ \underline{P}_m(x^2,x^3;\omega_n)$$

$$+ E(x^1;\omega_n)\ \underline{B}_m(x^2,x^3;\omega_n) + F(x^1;\omega_n)\underline{C}_m(x^2,x^3;\omega_n) \qquad (8)$$

The $\underline{P}_m$, $\underline{B}_m$ and $\underline{C}_m$ are the vector harmonics (spherical or cylindrical) and are themselves separable in x^2 and x^3, while the functions D, E and F are <u>independent</u> of m, and are functions of the coordinate x^1, along which the medium properties vary. (For the sphere, x^1 corresponds to the radial coordinate r, and for the half space x^1 is the vertical coordinate z.) Here the Rayleigh (spheroidal) eigenfunctions are represented by $\underline{P}_m$ and $\underline{B}_m$ terms, while the Love (toroidal) modes are represented by the $\underline{C}_m$ term.

Thus in general we have[+]

$$\tilde{H}^{\mu}_{\alpha}(\underline{x},\underline{x}_o;\omega) = \sum_{m,\omega_n} \frac{1}{\omega^2 - \omega_n^2}$$

$$\Big[\Big(D(x^1;\omega_n)\ P^{\mu}_m(x^2,x^3;\omega_n)$$

$$+ E(x^1;\omega_n)\ B^{\mu}_m(x^2,x^3;\omega_n)$$

$$+ F(x^1;\omega_n)\ C^{\mu}_m(x^2,x^3;\omega_n)\Big)$$

$$\Big(D(x^1_o;\omega_n)\ P^{\alpha}_m(x^2_o,x^3_o;\omega_n)$$

$$+ E(x^1_o;\omega_n)\ B^{\alpha}_m(x^2_o,x^3_o;\omega_n)$$

$$+ F(x^1_o;\omega_n)\ C^{\alpha}_m(x^2_o,x^3_o;\omega_n)\Big)\Big]$$

The wave field $\tilde{u}_{\mu}$ in (1) can now be represented as:

$$4\pi\ \tilde{u}_{\mu}(\underline{x};\omega) = \sum_{m,\omega_n} \frac{A_m(\omega,\omega_n)}{\omega^2 - \omega_n^2}\ \psi^m_{\mu}(\underline{x};\omega_n) \qquad (9a)$$

with

$$A_m(\omega,\omega_n) \equiv E_m(\omega,\omega_n) + S_m(\omega,\omega_n) \qquad (9b)$$

where E_m can be termed the mode excitation function; due to body forces and initial value excitation, and S_m the scattering function, due to the internal boundary of ν_o. These functions are, from (1) and (2):

[+]Note that, for example, in P^{μ}_m and P^{α}_m, only the greek indices represent vector components.

$$E_m(\omega,\omega_n) = \delta_o\left[\langle \rho f_\beta | \bar{\psi}^m_\beta \rangle_{v_o} + i\omega \langle \rho \partial_{t_o} u^*_\beta | \bar{\psi}^m_\beta \rangle_{v_o}\right] \tag{9c}$$

$$S_m(\omega,\omega_n) = \delta_o\left[\langle u_\beta | T^{(\bar{\psi}^m)}_\beta \rangle_{\partial v_o} - \langle T^{(u)}_\beta | \bar{\psi}^m_\beta \rangle_{\partial v_o}\right] \tag{9d}$$

where we have introduced tractions $T^{(u)}_\beta$ and $T^{(\psi^m)}_\beta$ defined by:

$$\left.\begin{aligned} T^{(u)}_\beta &\equiv \tau_{\alpha\beta}\eta_\alpha = C_{\gamma\delta\alpha\beta}\left(\frac{\partial u_\gamma}{\partial x_\delta}\right)\eta_\alpha \\ T^{(\psi^m)}_\beta &= C_{\gamma\delta\alpha\beta}\left(\frac{\partial \psi^m_\gamma}{\partial x_\delta}\right)\eta_\alpha \end{aligned}\right\} \tag{10}$$

Here $C_{\gamma\delta\alpha\beta}$ is the elastic tensor, which is a function of the coordinates. In the case of the layered half space or sphere, then $C_{\gamma\delta\alpha\beta}$ is a function of x^1 only; however (9) holds in general, that is for any medium in which eigenfunctions can be found+.

Now we have, in fact, shown that $\tilde{u}_\mu$ has a simple form when expressed in terms of the eigenfunctions ψ^m_μ; that is, it has the form given in (9a) where A_m is just some unknown coefficient. We may use this fact to advantage in reducing the integral equation for $\tilde{u}_\mu$ to a solution. Specifically, recognizing that the eigenfunction expansion for $\tilde{u}_\mu$ applies to the integral terms in (9c), then after transforming $\tilde{u}_\mu$ to the time domain we may use it in the scattering integral S_m. We have therefore, for $u_\mu(\underline{x},t)$:

+It is quite important to note, for all the eigenfunctions expansions introduced in this development, that we define them to be the eigenfunctions for an earth model with an inclusion zone, such as a failure zone, included in the model. These eigenfunctions are defined by a perturbation series of the regular "simpl layered earth eigenfunctions without the inclusion zone. The eigenfunctions used here therefore depend on the effective elastic properties of the inclusion zone material, among other material properties.

$$4\pi\, u_\mu(\underline{x},t) = \int_{-\infty}^{+\infty} e^{i\omega t}\, d\omega \sum_{m',\omega_n'} \left[\frac{A_{m'}(\omega,\omega_n')}{\omega^2 - \omega_n'^2}\, \psi^{m'}(\underline{x},\omega_n') \right]$$

or, using the fact that $A_{m'}$ is an analytic function of ω (i.e., neglecting inclusion zone resonances and forced oscillations due to externally applied forces) and applying the residue theorem to evaluate the integral over ω, we have:

$$u_\mu(\underline{x},t) = \sum_{m',\omega_n'} \left[\frac{A_{m'}(\omega_n')}{\omega_n'} \sin \omega_n' t \right] \psi_\mu^{m'}(\underline{x};\omega_n')$$

Now inserting this in S_m, using the expansion for $\tilde{u}_\mu$ on the left side of (9) as well; then rearranging terms allows equation (9) to be expressed as:

$$\sum_{m,\omega_n} \left[\hat{A}_m(\omega;\omega_n) - E_m(\omega;\omega_n) \sum_{m',\omega_n'} \frac{A_{m'}(\omega_n')}{\omega_n'}\, \delta_o \left\{ \left(\langle T_\beta^{(\psi^{m'})} | \bar{\psi}_\beta^m \rangle_{\partial v_o} \right.\right.\right.$$

$$\left.\left.\left. - \langle T_\beta^{(\bar{\psi}^m)} | \psi_\beta^{m'} \rangle_{\partial v_o} \right) \sin \omega_n' t_o \right\} \right] \frac{\psi_\mu^m(\underline{x};\omega_n)}{\omega^2 - \omega_n^2} = 0 \qquad (12)$$

In this expression

$$\langle T_\beta^{(\psi^{m'})} | \bar{\psi}_\beta^m \rangle_{\partial v_o} - \langle T_\beta^{(\bar{\psi}^m)} | \psi_\beta^{m'} \rangle_{\partial v_o} \equiv \langle J^{mm'} \eta_\beta \rangle_{\partial v_o}$$

where J_β is the bilinear concomitant of ψ_β^m and $\psi_\beta^{m'}$ and η_β is the surface normal to ∂v_o. (That is, the combination: $T_\beta^{(\psi^{m'})}\overline{\psi}^m - T_\beta^{(\overline{\psi}^m)}\psi^{m'} = J_\beta^{mm'}\eta_\beta$, by definition of $J_\beta^{mm'}$ for the elastic operator. See, for example Archambeau and Minster, 1978.)

Now, when transformed to the time domain this result takes the form, again using the analyticity of the functions of ω in (12):

$$\sum_{m,\omega_n}\left[A_m(\omega_n) - E_m(\omega_n) - \sum_{m',\omega'_n}\frac{A_{m'}(\omega'_n)}{\omega'_n}\,\mathcal{L}_o\left\{\langle J_\beta^{mm'}\eta_\beta\rangle_{\partial v_o}\cdot\right.\right.$$

$$\left.\left.\cdot\,\sin\omega'_n t_o\right\}_{\omega_n}\right]\psi_\mu^m(\underline{x};\omega_n)\,\sin\omega_n t = 0$$

Here the notation $\mathcal{L}_o\{\ \}_{\omega_n}$ means the Fourier transform with respect to t_o with the transform variable ω evaluated at $\omega = \omega_n$.

Since the $\psi_\mu^m(\underline{x};\omega_n)\sin\omega_n t$ form a complete orthonormal basis, then this expression can vanish only if each coefficient of the sum over m and ω_n vanishes separately. Thus we have that:

$$A_m(\omega_n) = E_m(\omega_n) + \sum_{m',\omega'_n}\frac{A_{m'}(\omega'_n)}{\omega'_n}\,\mathcal{L}_o\left\{\langle J_\beta^{mm'}\eta_\beta\rangle_{\partial v_o}\,\sin\omega'_n t_o\right\}_{\omega_n}$$

If we write out the "summation" operator over m' and ω_n', we have:

$$A_m(\omega_n) = E_m(\omega_n) + \sum_{m'}\sum_{n'} \left[\int_{c_{n'}} \frac{A_{m'}(\omega', c_{n'}(\omega'))}{\omega' U_{n'}(\omega')} \cdot \delta_o \left\{ \langle J_\beta^{mm'} \eta_\beta \rangle_{\partial v_o} \sin \omega' t_o \right\}_{\omega_n} d\omega' \right] \tag{13}$$

Here we again note that the integral over frequency ω' is along a particular mode curve, with mode number n', the curve being characterized by its phase velocity $c_{n'}$ as a function of ω'. We have taken explicit account of the fact that the coefficients $A_{m'}$ depend on ω' and the phase velocity function $c_{n'}(\omega')$ as well, in writing out the summation operation.

The critical factor in this expression is the surface integral term over $J_\beta^{mm'} \eta_\beta$. This term accounts for the exchange or scattering of energy from the eigenfunctions $\psi_\beta^m(\underline{x};\omega_n,c_n)$ into the eigenfunctions $\psi_\beta^{m'}(\underline{x},\omega',c_{n'})$, due to the interaction of the elastic wave field, characterized by the $\psi_\beta^m(\underline{x};\omega_n,c_n)$, with the surface $\partial v(t_o)$. However, we know that this "scattering" process is linear, so that the frequency of the scattered field due to $\psi_\beta^m(\underline{x};\omega_n,c_n)$ must be ω_n. That is, by any linear process, we obtain coupling between modes ψ_β^m and $\psi_\beta^{m'}$ only when $\omega' = \omega_n$. However, this is the only general restriction and coupling can occur for all m' and between all modes n' at the frequency ω_n. This means then, that the

surface integral term has the form[+]:

$$\delta_o \left\{ \langle J_\beta^{mm'} \eta_\beta \rangle_{\partial v_o} \sin \omega' t_o \right\}_{\omega_n} = J_m^{m'}(\omega_n, c_n; \omega', c_{n'}) \cdot \delta(\omega' - \omega_n) \qquad (14)$$

Use of this result in (13) therefore reduces the frequency integral over ω' to a single contribution at $\omega' = \omega_n$, and we have:

$$A_m(\omega_n, c_n) = E_m(\omega_n, c_n) + \sum_{m'} \sum_{n'} A_{m'}(\omega_n, c_{n'}(\omega_n)) \cdot \frac{J_m^{m'}(\omega_n, c_n; \omega_n, c_{n'})}{\omega_n U_{n'}(\omega_n)} \qquad (15)$$

This can be written more usefully in a compact matrix form obtained by writing, $A_m(\omega_n) \equiv A_{mn}$, etc. That is, we have in matrix notation:

$$(A_{mn}) = (E_{m'n'}) + (\Lambda_{m'n'})\,(S_{mn}^{m'n'}) \qquad (16)$$

where the product sum is over (the repeated indices) m' and n'. Here:

$$S_{mn}^{m'n'} \equiv \frac{J_m^{m'}(\omega_n, c_n; \omega_n, c_{n'})}{\omega_n U_{n'}(\omega_n)}$$

with $J_m^{m'}$ given by (14) and $U_{n'}(\omega_n)$ the group velocity of the n'th mode at the frequency ω_n.

[+]This is ordinarily shown by direct computation.

The matrices E_{mn} and S_{mn} can be termed the excitation and scattering matrices. It is assumed that E_{mn} involves <u>all</u> known integral terms in the original Green's function integral equation for $\tilde{u}_\mu$, including known surface integral terms. This can change the definitions of E_{mn} and S_{mn} given here slightly, but obviously the same analysis applies.

To solve the problem completely for $\tilde{u}_\mu$, we need to obtain the A_{mn} functions from (16). Formally the solution is:

$$A_{m'n'} = (I_{mn}^{m'n'} - S_{mn}^{m'n'})^{-1} \cdot E_{mn} \tag{17}$$

with

$$I_{mn}^{m'n'} = \delta_m^{m'} \delta_n^{n'}$$

A more useful form is obtained by iteration, which can give both exact closed form and series solutions, as well as approximate solutions. In particular, take (i) to be an iteration index and, in (16), take

$$(A_{mn}^{(0)}) = (E_{mn})$$

as the zeroth order solution. Then the first order solution is:

$$(A_{mn}^{(1)}) = (E_{mn}) + (A_{m'n'}^{(0)})(S_{mn}^{m'n'})$$

or:

$$(A^{(1)}_{mn}) = (E_{mn}) + (E_{m'n'})(S^{m'n'}_{mn})$$

Here it is important to remember that $S^{m'n'}_{mn}$ is independent of A_{mn}. Likewise for $A^{(2)}_{mn}$, we have:

$$(A^{(2)}_{mn}) = (E_{mn}) + (A^{(1)}_{m'n'})(S^{m'n'}_{mn})$$

or, substituting for $A^{(1)}_{m'n'}$:

$$(A^{(2)}_{mn}) = (E_{mn}) + (E_{m''n''})(S^{m''n''}_{mn}) + (E_{m''n''})(S^{m''n''}_{m'n'})(S^{m'n'}_{mn})$$

Continuing this process, we get:

$$(A_{mn}) = E_{m_1n_1} \sum_{i=0}^{\infty} \left(S^{m_{i+1}n_{i+1}}_{m_in_i} \right)^i \qquad (18)$$

where we assume convergence in the limit, so that:

$$\lim_{i\to\infty} (A^{(i)}_{mn}) \to (A_{mn}).$$

Here:

$$\left(S^{m_1n_i}_{m_on_o} \right)^o \equiv I^{m_1n_1}_{m_on_o}$$

$$\left(S^{m_{p+1}n_{p+1}}_{m_1n_1} \right)^p \equiv \left(S^{m_{p+1}n_{p+1}}_{m_pn_p} \right) \left(S^{m_pn_p}_{m_{p-1}n_{p-1}} \right) \cdots \left(S^{m_2n_2}_{m_1n_1} \right)$$

and we use the convetion $m_o \equiv m$ and $n_o \equiv n$.

The results (18) or (17) provide complete solutions, in that, using (17) or (18), then u_μ can be prescribed in the form (9-a). Here we need to compute the E_{mn} and $S_{mn}^{m'n'}$ matrices using the definitions (9-b) and (14). For prescribed material properties and initial stress conditions, then the integrals in E_{mn} and $S_{mn}^{m'n'}$ can always (in principle) be evaluated.

Special applications of these results have been considered; in particular the case of the instantaneous creation of a spherical cavity in an arbitrarily prestressed medium (Stevens, 1978). In this important special case a series result equivalent to (18) was found to be summable, so that an exact closed form result was obtained for the radiated displacement field u_μ. The solution showed that the spectrum of u_μ, in the far field, was in general peaked when the initial stress field was not homogeneous, the peak becoming more pronounced when the initial stress was more strongly inhomogeneous spatially. However, the spectral peaking was azimuth and "take-off" angle dependent, so that the degree of peaking would be variable. This result clearly suggests, however, that earthquake radiation fields will, in general, also be peaked spectrally when failure occurs in an inhomogeneously stressed medium. This of course would be the expected initial stress state, so that the effect should ordinarily prevail, although with angular variations.

The results obtained also can be used directly for source inversion studies. In particular, we need only note that the various coefficient matrices, A_{mn}, E_{mn} and $S_{mn}^{m'n'}$, will depend on the fundamental source parameters, such as the initial stress magnitude and orientation and a variety of material parameters, including those describing failure. If we let these parameters be denoted by the set $\{p_k\}$, then we can write

$$\delta_p u_\mu = \sum_{m,\omega_n} \frac{\delta_p A_{mn}}{\omega_n} \psi_\mu^m(\underline{x};\omega_n) \sin \omega_n t \qquad (19)$$

for the variation in the displacement field u_μ due to a variation in "source" parameters p_k. Hence "P-variations" in u_μ are described in terms of variations in the coefficient matrix A_{mn} alone. For inverse studies, we can consider a starting solution $u_\mu^{(0)}$, obtained by some initial "guess" for the source parameters $p_k^{(0)}$, and associate $\delta_p u_\mu$ with the difference between this starting solution $u_\mu^{(0)}$ and the observed field u_μ. Thus we have:

$$u_\mu - u_\mu^{(0)} = \delta_p u_\mu = \sum_{m,\omega_n} \frac{\delta_p A_{mn}}{\omega_n} \psi_\mu^m(\underline{x};\omega_n) \sin \omega_n t$$

Now, given $\delta_p u_\mu$ as an observed difference, we want to solve for $\delta p_k = p_k - p_k^{(0)}$, the change in the source parameters implied by the difference $\delta_p u_\mu$. However, this is equivalent to solving for δp_k from;

$$A_{mn} - A_{mn}^{(0)} = A_{mn}(p_k^{(0)} + \delta p_k) - A_{mn}(p_k^{(0)})$$

where, by A_{mn} on the left, we mean that coefficient matrix associated with the observed displacement u and by $A_{mn}^{(0)}$ we mean that matrix computed using the starting values $p_k^{(0)}$. Here we can define $\delta_p A_{mn} = A_{mn} - A_{mn}^{(0)}$.

There are a number of ways to proceed with this inversion for the δp_k. In the linearized approach one expands $A_{mn}(p_k^{(0)} + \delta p_k)$ around $p_k^{(0)}$, keeping only the first two terms in the expansion. This gives:

$$\delta_p A_{mn} = A_{mn} - A_{mn}^{(0)} \cong \sum_k \left(\frac{\partial A_{mn}}{\partial p_k} \right)_{p_{j \neq k}} \delta p_k \tag{20}$$

where $(\partial A_{mn}/\partial p_k)_{p_{j \neq k}}$ is the partial derivative with respect to the kth parameter p_k holding all others constant.

Observations of $\delta_p A_{mn}$ for a range of m and n values provides a set of equations of the form (20), which can be written as the matrix equation:

$$\delta_p A = A \delta p \tag{21}$$

with

$$A \equiv \left[\left(\frac{\partial A_{mn}}{\partial p_k} \right)_{p_{j \neq k}} \right] \equiv \left[A_{\ell k} \right]$$

where the indices m and n are treated as a composite column index, ℓ, in A.

The explicit values of the derivatives appearing as elements in A are obtained from (18) by differentiation. Thus

$$\left(\frac{\partial A_{mn}}{\partial p_k} \right)_{p_{j \neq k}} = \left(\frac{\partial E_{m_1 n_1}}{\partial p_k} \right)_{p_{j \neq k}} \sum_{i=o}^{\infty} \left(S_{m_i n_i}^{m_{i+1} n_{i+1}} \right)^i$$

$$+ E_{mn} \frac{\partial}{\partial p_k} \left[\sum_{i=0}^{\infty} \left(S_{m_i n_i}^{m_{i+1} n_{i+1}} \right)^i \right]_{p_{i \neq k}}$$

Both E_{mn} and $S_{mn}^{m'n'}$ can be expressed analytically in terms of the parameters p_k. Further, the scattering series can sometimes be summed and in most cases truncated after, at most, a few terms. Therefore the derivatives in (22) can be expressed analytically, so that the matrix $\underline{A}$ is known.

The solution for the required parameters is therefore given by:

$$p = p^{(0)} + \delta p = p^{(0)} + \underset{\sim}{A}^{-1} \delta_p A \qquad (23)$$

where $\underset{\sim}{A}^{-1}$ is an appropriate generalized inverse (e.g. Bjerhammer, 1973). Of course, once these new values of p_k are obtained from (23), then a new prediction $u_\mu^{(1)}$ can be obtained using them, and the process can be repeated until δA_{mn} is sufficiently small to justify the conclusion that a good fit has been achieved with some final set of source parameters. It is clear that a wide variety of procedures are available to solve for the "appropriate" source parameters by minimizing the "difference" in the observed and computed values of A_{mn}. The choice of generalized inverse $\underset{\sim}{A}^{-1}$ prescribes in what sense this difference is "small", and hence the accuracy with which the source parameters are obtained.

Our present approach in this respect is to "filter" the observations u_μ yielding limited observational data which depends strongly on only a few of the source parameters. This data would then be used in an inversion to obtain reliable estimates of some of the source parameters. (An example of a "first-cut" filter would be one that just yielded arrival times of major energy pulses contained within u_μ. Then, of course, the inversion of this data alone would yield source hypocentral location parameters.) With these

later parameters fixed, then a second filter operation would give additional limited observations, dependent on these plus additional parameters and the new parameters could then be obtained by formal inversion. (eg. Hypocentral stress field and/or failure plane orientation using first motion data, with the hypocentral location fixed.) This process can be continued until a good "starting" model for the source is obtained. The procedure can also be formalized in terms of specified matrix operations.) At this stage the full formal joint inversion, for all the source parameters together, could be performed, using (22) -(23) and the entire observed data set represented by A_{mn}.

This approach is basically that used in classical seismology. In the current study we include stress magnitude and fault plane dimension estimates using the $m_b(f)$ data obtained by time domain filtering of u_μ, as well as location and "fault plane solutions". At this stage, after obtaining estimates of location, fault plane orientation, stress magnitude and orientation plus fault plane dimensions by this procedure, we intend to apply the formal joint inverse method just described to selected events in order to obtain more precise estimates as well as quantitative estimates of resolution and trade-offs among the parameters.

VI. Signal Detection and Analysis by Quasi-Harmonic Decomposition (QHD) Methods - C.B. Archambeau

Analysis of the seismic data from numerous small events at regional distance ranges poses some special problems, in addition to those ususally encountered. In particular, in view of the shear numbers and diversity of seismic recordings to be analyzed, it is necessary to apply largely automated analysis methods to the data that are: precisely defined, fast and that, of course, yield data that is both simply interpreted and highly discriminatory with respect to event type.

In this regard we have devised a signal analysis method that is very fast computationally and that, most importantly, decomposes the observed seismic time series into a form that allows (automated) selection of spectral data (amplitude and phase) that is associated, one to one, with particular seismic phases, the phases being defined by their group arrival dispersion curves. This decomposition, in both frequency content and time, allows us to select particular seismic phases along with their associated spectra, and to use this seismic phase related spectra for source identification.

The analysis approach is similar to the usual time varying spectral estimation methods that simply employ a moving time window over which the Fourier spectrum is computed, but the approach we use avoids time window truncation effects and is not dependent on an arbitrary choice of a time window length. Further, the approach we use gives much better time resolution, more accurate spectral estimates and, perhaps most important, can be analytically formulated in a manner allowing noise and interfering signal pulse corrections to be made (Archambeau, 1978; Savino and Archambeau, 1976).

The method we employ is simply to use a large set of ultra-narrow band filters whose output is a modulated sinusoid, with peaks in the modulation function that occur at the energy arrival time (group time) for a signal "pulse", or coherent wave train, with amplitude equal to the spectral amplitude at the filter center frequency. Thus, both the group time and the spectral amplitude are obtained from the modulation or envelope function of a particular filter output and both these quantities can be associated with the center frequency of the filter. Use of a large set of such filters at different center frequencies therefore defines the dispersion of the seismic signals, their time of arrival (smallest group arrival time over the recorded frequency range), and their amplitude spectrum. In addition, the phase of the modulated "carrier" sinusoid can be measured (relative to some reference point) at the group arrival time, and in fact at all times as well, to provide an "instantaneous phase" determination as a function of time, and in particular at the time of the seismic phase group arrival time. Thus we obtain both a spectral amplitude and phase as a function of frequency, that is the complete spectral definition, at the group arrival time. Further, if two (or three) spatial components of the seismic vector wave field are available, then by computing the instantaneous phase on two or more components we can determine the polarization of a signal. Finally, since the instantaneous phase is obtained as a function of time for the duration of the time series, we can compute the instantaneous frequency by taking its time derivative; this also, then, being obtained as a function of time.

This processing of the seismic event reciever data, which we call quasi-harmonic decomposition (QHD), produces a large amount of information about the recorded signals that can be used both to isolate the individual signals

making up a given reocrded time series and to describe them in terms suitable for source identification. The procedure, in fact, produces a great deal of redundant data about the source, and we have only made use of the first arrival compression wave (P) data. However, in later studies we intend to use much more of the available results.

Some results of an application of this automated signal processing to actual data is illustrated in Figure 1. The Figure 1-a is the computer generated envelope (or modulation function) of the filter output at 15 Hz, where the peaks at P_1, P_2 and P_3 are signed arrivals in the narrow band of frequency around the center frequency of the filter.

The filter Q value (where $Q^{-1} = \Delta f / f_c$, with Δf the half band width at the half power point) is selected as optimal in the sense that both time and frequency resolution are adequate, and with such a Q value at this frequency, the filter output gives an amplitude at a peak in its envelope that is very close to the true spectral amplitude at 15 HZ. The lower trace

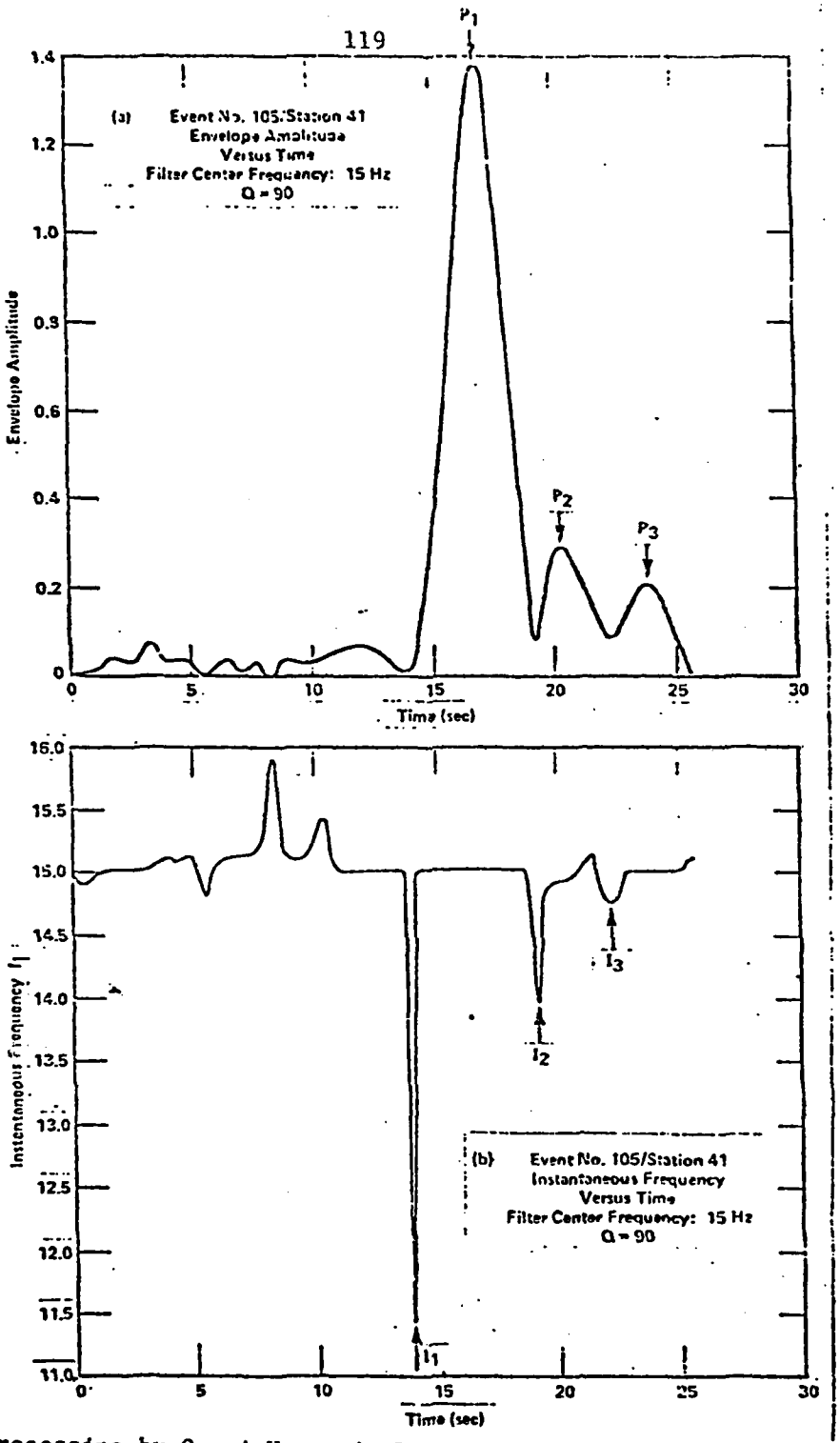

Figure 1. Signal processing by Quasi-Harmonic Decomposition of time series, designed to provide noise and interferring signal corrected spectral data that can be associated with a particular signal pulse. Figure 1-a shows the envelope function of the narrow band Gaussian filter output. The center frequency of the filter (f_c) is at 15 Hz, and the filter has a Q of 90. The peaks of the envelope function, at P_1, P_2 and P_3 in particular, can be shown to occur at the group arrival time (energy arrival time) of the signal at the center frequency of the filter. The amplitude of the peak can also be shown to be equal to the regular Fourier spectral amplitude of the signal arriving at this time. Figure 1-b shows the instantaneous frequency versus time. For a well defined phase variation with time, the instantaneous frequency should be very close to the filter center frequency f_c. At points where two signals interfer with each other however, then the phase variation with time may be "poorly defined" (i.e., discontinuous or have discontinuous deviative) and wide variations from f_c may occur. These can be seen to occur in this example at the time I_1, I_2, and I_3. These times therefore mark the onset of new, pulse-like "signal" arrivals.

shown, in (b), is the instantaneous frequency, ω_I . It is apparent that the sharp peaks or spikes in ω_I serve to delineate time intervals within which coherent signals arrive, and that spikes at I_1, I_2, I_3 alternate with the peaks in the envelope function. Thus the instantaneous frequency trace provides information regarding the onset time of a (new) coherent signal pulse, in a background of noise, while the envelope function gives the group or energy arrival time and spectral amplitude of the signal.

The seismic time series is processed through a set of filters, each giving results such as those in Figure 1, and these are then combined in order to obtain a complete definition of signals making up a wave train. Figure 2 illustrates how this is currently accomplished. This figure shows the computer plot of the group arrival time, t_g, obtained versus filter center frequency, f, with the amplitudes at the peaks in the envelope functions, which occur at the times t_g, providing a basis for contouring the amplitude variations with time and frequency. It should be understood, however, that the amplitudes along the contours are the spectral amplitudes of signals only at the points of intersection of the signal dispersion curve and the amplitude contours. Hence in the example shown in Figure 2 the computer is coded to search for body waves are minimally dispersed signal pulses in this t_g vs f plane. (This is accomplished by a pattern recognition procedure.) The straight line denoted t_g in the figure is the (first order) dispersion curve selected by the computer as a body phase dispersion curve. The spectral amplitude of this identified seismic signal (and similarly for the spectral phase) is obtained by measuring the amplitude values defined by the contours, along this dispersion line. This is also done automatically by the computer.

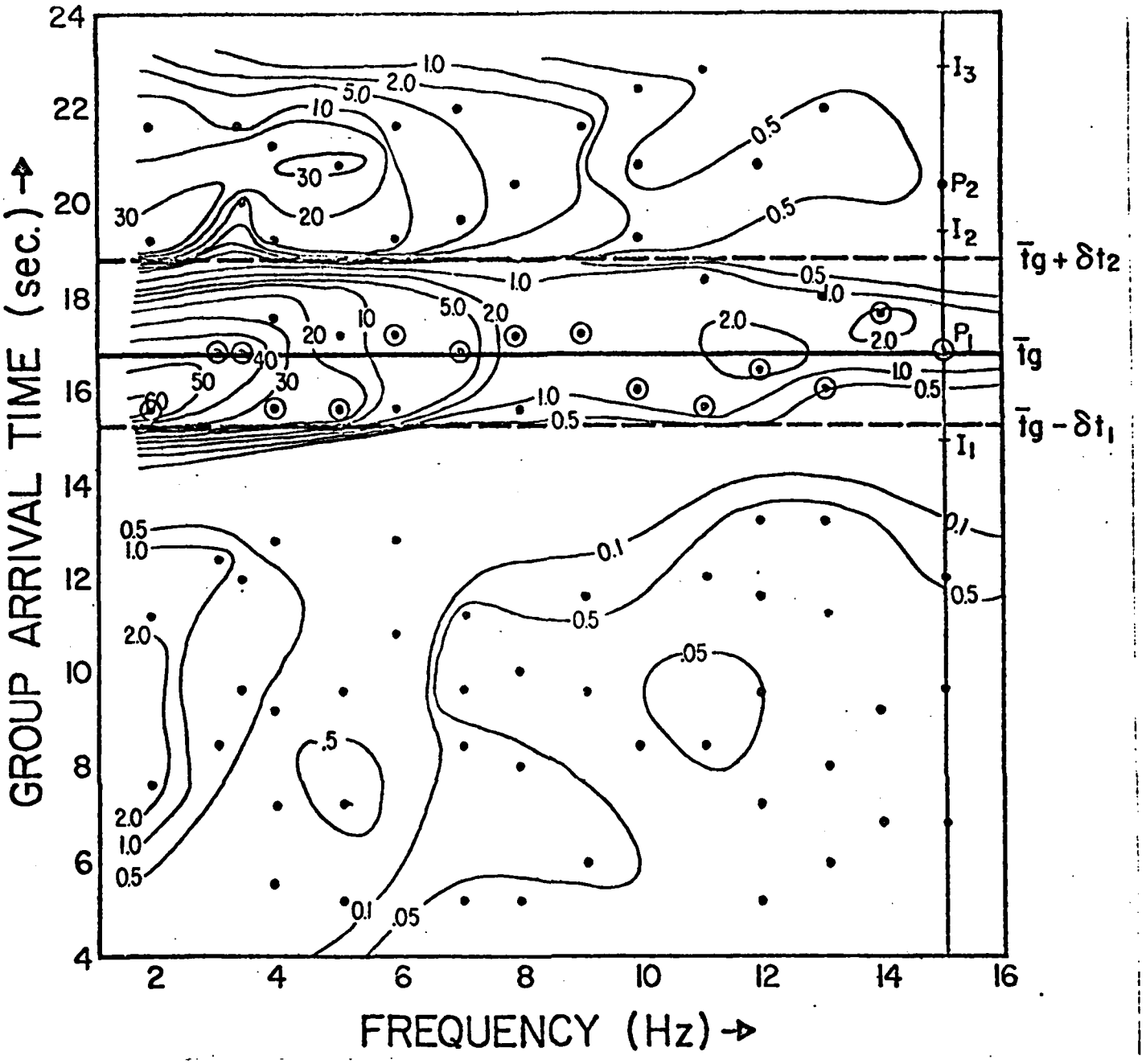

Figure 2. Computer generated group arrival (t_g) versus frequency (f) plane data with spectral amplitude contoured for event 105, as recorded at the southern California array station no. 41. The solid points indicated in this plane correspond to narrow band filter envelope maxima, and represent pulse group arrival times for signal and noise. The contours are based on the envelope amplitudes at these maxima, which can be shown to be equal to the Fourier spectral amplitudes. Two discrete body phases are obtained, with the first arrival average group arrival time, $\bar{t}_g$, indicated by the solid line. The signal window, as determined by the computer, is indicated by the dashed lines at $\bar{t}_g - \delta t_1$ and $\bar{t}_g + \delta t_2$. The times indicated on the right by I_1, I_2 and I_3 are the "interference times" at which large deviations of the instantaneous frequency from the center frequency of the narrow band filter at $f_c = 15$ Hz are observed. (See Figure 1-b). The times indicated by P_1 and P_2 are times at which envelope peaks occur for the filter at $f_c = 15$ Hz (Figure 2-a). Each filter output provides such data, which is then used to automatically isolate, time and spectrally analyze individual signal pulses. Note that individual signal pulses are separated by the interference times, which along with the envelope peak times, provide the basis for signal pulse separation and "signal velocity" timing (i.e., signal arrival times and group arrival times).

Thus, for each identified seismic phase, the computer obtains a spectrum as well as timing information by this process. In addition, noise corrections based on the background amplitude levels, as well as corrections for interferring signal contamination are made automatically.

The spectral results generated by this processing have been used successfully in the discrimination of earthquakes and explosions at teleseismic distances. In this case we have used the spectral amplitude associated with the first arriving teleseismic compressional wave to compute frequency dependent body wave magnitudes, $m_b(f)$. Figure 3 shows variable frequency magnitude data for a small California earthquake as generated by the QHD analysis.

The discrimination approach is to make use of the theoretically predicted differences in the amplitude spectra between explosions and earthquakes; specifically the prediction that explosions having the same low frequency or maximum spectral level as a comparison earthquake , will have a higher corner frequency and a less negative high frequency slope (Archambeau, 1974). Thus for a comparable explosion-earthquake pair, the explosion will be "richer" in high frequencies. This prediction can be exploited (and tested) by considering explosion and earthquake populations in "$m_b(f)$ planes", these defined by a low frequency $m_b(f)$ plotted against a high frequency $m_b(f)$ value for the first arrival compressional wave from the individual events.

As an example of the use of the $m_b(f)$ discrimination approach, Figure 4 and Figure 5 show the map location of a number of Eurasian events and the population distribution of these events in the $m_b(f)$ plane, where m_b values at .45 and 2.25 Hz were used. These $m_b(f)$ values were not corrected for

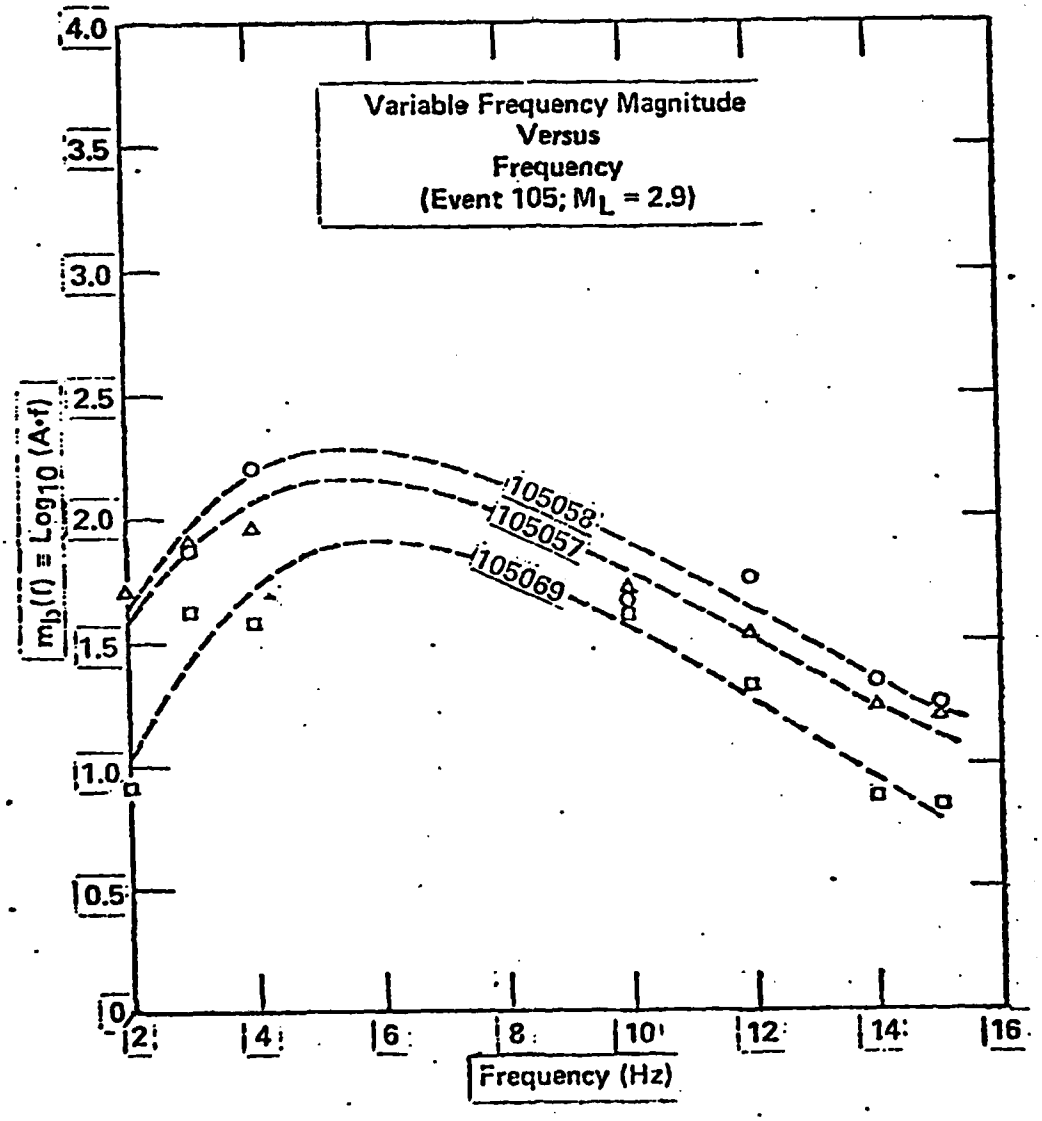

Figure 3. Variable frequency magnitude versus frequency for event no. 105 at three stations. The inferred variation of $m_b(f)$ (dashed curves) is a smooth function of frequency and is consistant from station to station. Scatter in the observed $m_b(f)$ values from the curves averages less than .1 magnitude unit.

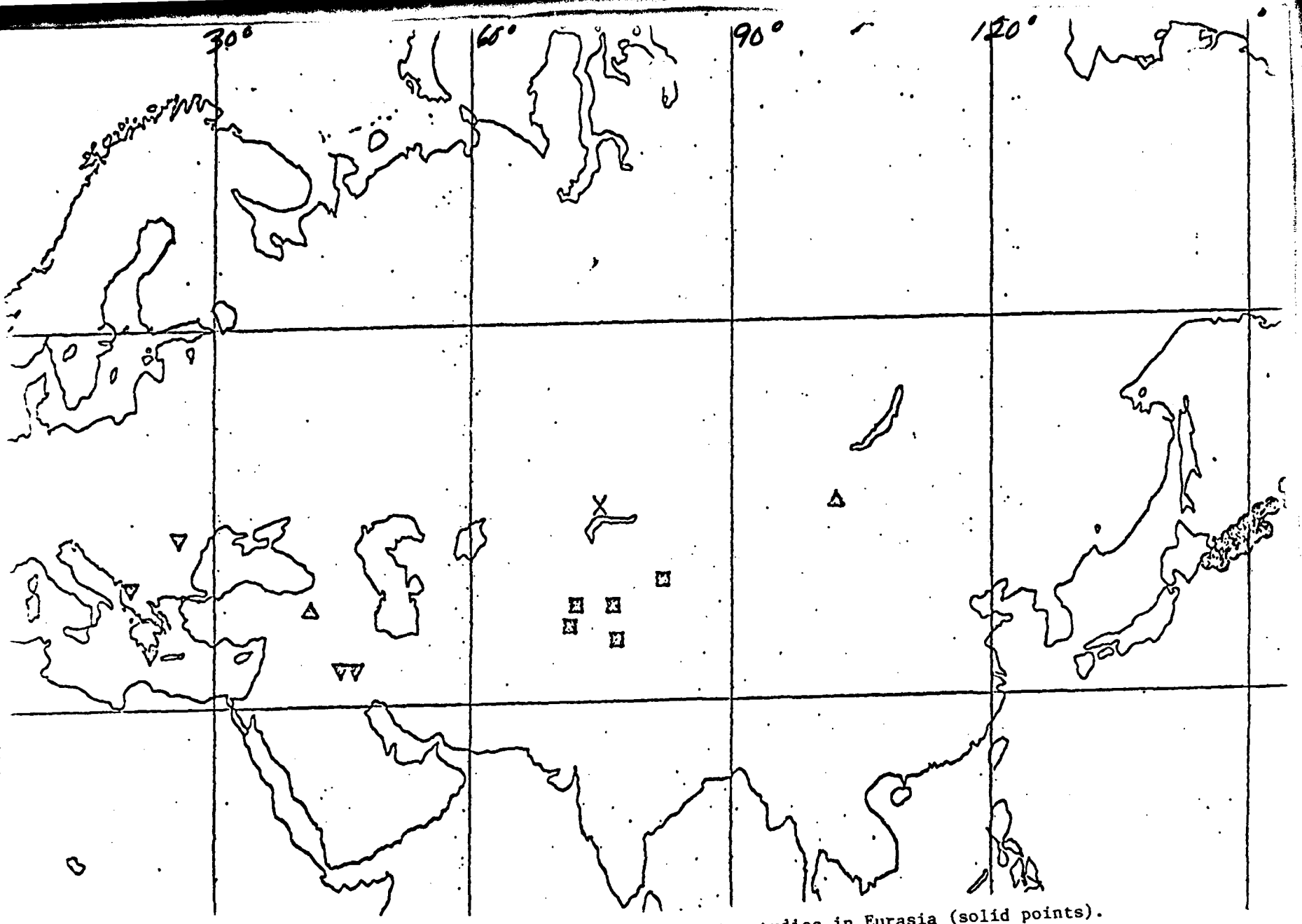

Figure 4. Earthquake locations for some of the events studies in Eurasia (solid points). The X denotes the location of the explosions studied.

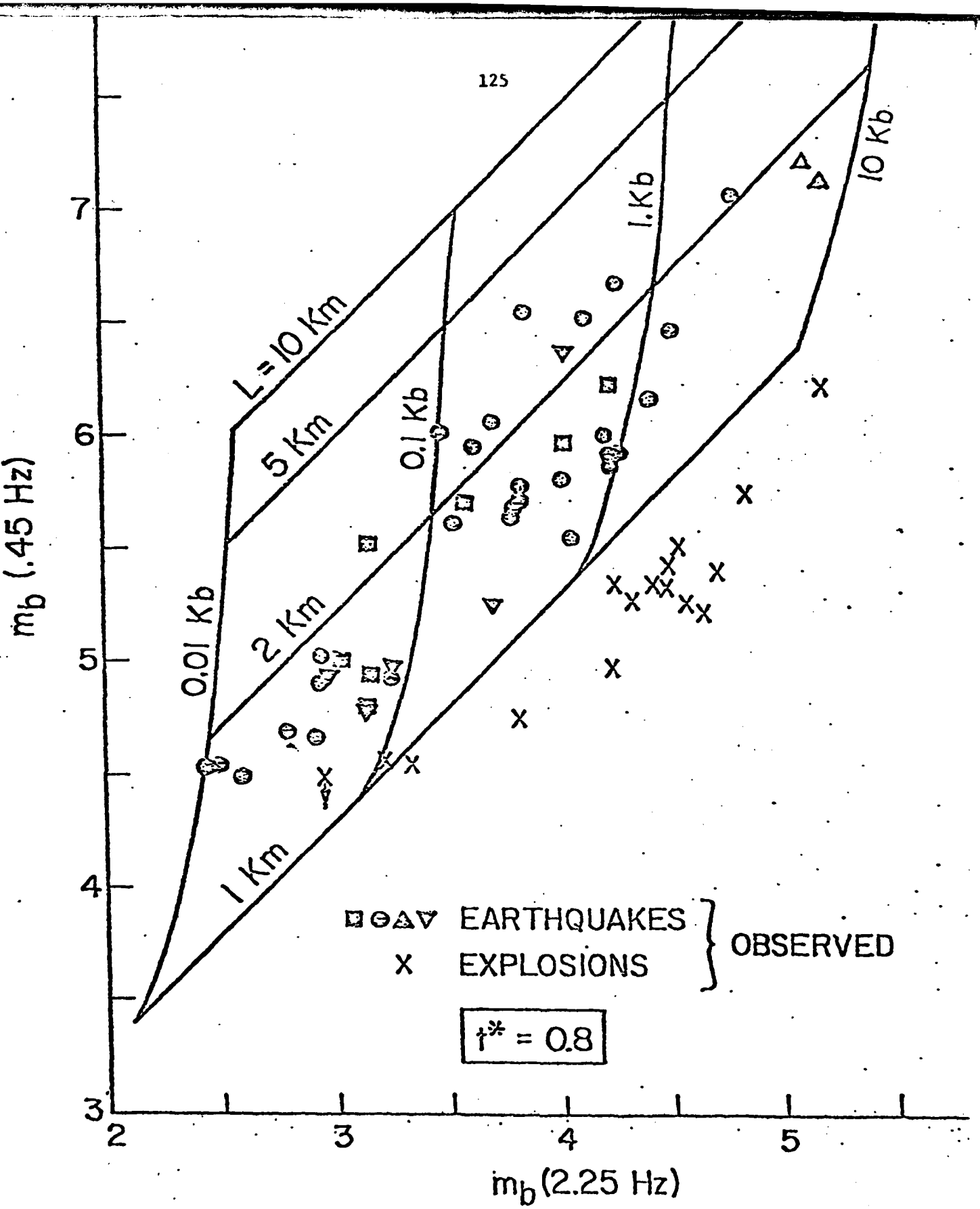

Figure 5. Eurasian event data in the $m_b(f)$ plane. The events are located in the areas shown in Figure 13. The theoretical curves are based on relaxation source theory models and provide a basis for the estimation of hypocentral stress drop, that is the average stress change near the hypocenter averaged over a region of dimension given by the location of the observed point in the $m_b(f)$ plane

noise, but in any case the explosion and earthquake populations separate quite well down to low magnitude levels. (These low magnitude events are around the ordinarily defined m_b of about 4.0). With noise corrections applied however, we find that the two populations are better separated, with no convergence at the very low magnitudes.

References

Abo-Zena, A., Dispersion Function Computations for Unlimited Frequency Values, Gulf Science and Technology Co., Pittsburgh, PA 15230, Technical Report, 1978; submitted to Geophysical Journal Roy. Astron. Soc., 1978.

Archambeau, C.B. and J. B. Minster, Dynamics in Prestressed Media with Moving Phase Boundaries: A Continuum Theory of Failure in Solids, Geophys. J., Roy. Astron. Soc., 52, 65-96, 1978.

Archambeau, C. B., Applications of Variable Frequency Magnitude Data to the Estimation of Seismic Source Properties, EOS, vol. 59, no. 12, p. 1139, 1978.

Archambeau, C.B., E.A. Flinn and D. G. Lambert, Fine Structure of the Upper Mantle, J. Geophys. Res., 75, 5825-5865, 1969.

Archambeau, C.B., The Theory of Stress Wave Radiation from Explosions in Prestressed Media, Geophys. J. Roy. Astron. Soc., 29, 329-366, 1972.

Archambeau, C.B., Studies of Multiple Seismic Events, report prepared for U.S. Arms Control and Disarmament Agency, ACDA/ST-220, 1974.

Bjerhammer, A., Theory of Errors and Generalized Matrix Inverses, Elsevier Scientific Publ. Co., Amsterdam, 1973.

Cormier, V.F., and P.G. Richards, 1977. Full Wave Theory Applied to a Discontinuous Velocity Increase: The Inner Core Boundary, J. Geophys., 43, 3-31, 1977.

Harvey, D., Seismogram Synthesis Using Normal Mode Superposition: The Locked Mode Approximation Method, in preparation, to be submitted to Geophys. J. Roy. Astron. Soc., 1979.

Helmberger, D.V., Generalized Ray Theory for Shear Dislocations, Bull. Seism. Soc. Am., 64, 45-64, 1974

Kanamori, H., and D. Hadley, Crustal Structure and Temporal Velocity Change in Southern California, Pageoph., vol. 113, 258-280, 1975.

Savino, J. M. and C. B. Archambeau, Discrimination of Earthquakes from Single and Multiple Explosions Using Spectrally Defined Event Magnitudes; EOS, 56, 1148, 1974.

Schwab, F., and L. Knopoff, Surface Waves: Dispersion Computations, Bull. Seism. Soc. Am., 50, 321-344, 1970.

Stevens, J., Seismic Radiation from the Sudden Creation of a Spherical Cavity in an Arbitrarily Prestressed Elastic Medium, EOS, vol. 59, No. 12, p. 1139, 1978.

UNCLASSIFIED

SECURITY CLASSIFICATION OF THIS PAGE (When Data Entered)

REPORT DOCUMENTATION PAGE	READ INSTRUCTIONS BEFORE COMPLETING FORM
1. REPORT NUMBER: AFOSR-TR-79-0451 — 2. GOVT ACCESSION NO.: AD-A089 683	3. RECIPIENT'S CATALOG NUMBER
4. TITLE (and Subtitle): Earthquake Characteristics and Earthquake-Explosion Discrimination	5. TYPE OF REPORT & PERIOD COVERED: May 1-October 31, 1978 Final
	6. PERFORMING ORG. REPORT NUMBER
7. AUTHOR(s): C.B. Archambeau, V. Cormier, G. Lundquist, J. Stevens	8. CONTRACT OR GRANT NUMBER(s): AFOSR-75-2775
9. PERFORMING ORGANIZATION NAME AND ADDRESS: CIRES, University of Colorado, Boulder, Colorado 80309	10. PROGRAM ELEMENT, PROJECT, TASK AREA & WORK UNIT NUMBERS: ARPA Order 3291, Program Code 7F10, Program Element 62701E
11. CONTROLLING OFFICE NAME AND ADDRESS: Advanced Research Projects Agency /NMR, 1400 Wilson Boulevard, Arlington, Virginia 22209	12. REPORT DATE: 1979
	13. NUMBER OF PAGES: 130
14. MONITORING AGENCY NAME & ADDRESS(if different from Controlling Office): Air Force Office of Scientific Research/NP, Bolling Air Force Base, Bldg. 410, Washington, D. C. 20332	15. SECURITY CLASS. (of this report): UNCLASSIFIED
	15a. DECLASSIFICATION/DOWNGRADING SCHEDULE

16. DISTRIBUTION STATEMENT (of this Report)

Approved for public release; distribution unlimited

17. DISTRIBUTION STATEMENT (of the abstract entered in Block 20, if different from Report)

18. SUPPLEMENTARY NOTES

19. KEY WORDS (Continue on reverse side if necessary and identify by block number)

earthquake sources
Langer approximation
synthetic seismograms
Greens' functions
Signal analysis
Inelastic attenuation
Inversion
Tectonic stress
Mode Theory

20. ABSTRACT (Continue on reverse side if necessary and identify by block number)

SEE ATTACHED SHEETS

DD FORM 1 JAN 73 1473 EDITION OF 1 NOV 65 IS OBSOLETE

SECURITY CLASSIFICATION OF THIS PAGE (When Data Entered)

20. Abstract

During this report period, from May through October, 1978, we concentrated on four areas of study, in particular: (1) The development of asymptotic and modal wave propagation methods for the description of seismic wave propagation effects in the near regional and teleseismic distance ranges; (2) The study of the frequency dependence of earth's anelasticity as a function of depth and geologic province; (3) The development of theoretical relaxation source representations for seismic sources in non-homogeneously prestressed media and inversion procedures for such sources and; (4) The development of advanced methods for seismic (vector field) signal detection and analysis. The major results of this work are: (1) We have developed and applied full-wave asymptotic methods, which employ the Langer approximation in the frequency domain, and in a systematic comparative study with the Cagniard method have demonstrated that there is general agreement in the predictions of both methods when they can be compared. However, in some distance ranges, observable differences occur, notably in the regional distance range from 10°-20°. In these cases convergence of results from the two methods only occur when multiple reflections, within finely layered zones in regions of large velocity gradient, are included in the Cagniard method. Other observable differences occur when anelasticity is included, particularly if a frequency dependent intrinsic Q factor is considered, since the Cagniard approach cannot directly treat anelasticity except in an approximate, incomplete fashion. On the other hand, the frequency domain full-wave theory incorporates anelasticity directly and all the effects of a frequency dependent intrinsic Q parameter can be computed. We have also applied the full wave theory to the synthesis of complete seismograms in the near field distance range and developed the analytical relations required to compute synthetics. This theoretical development has also been extended to provide a basis for the computation of synthetics at the source anti-pole. In both cases we have computed seismograms based on the theoretical results. Comparisons, between mode superposition methods on the one hand and observations on the other, indicate that the method is both accurate and fast computationally. (2) We have developed a mode superposition approach, which has been descriptively termed the "Locked Mode Approximation Method", for the generation of complete synthetic seismograms (P-SV and SH). The method is applicable in both the near and regional distance ranges, using a layered half space as the model, and can easily be extended to a spherical earth for teleseismic studies. The method is approximate in the sense that a high velocity layer at depth is introduced to trap the modes so that P and S waves can be synthesized. The method has been completely formulated, with general source representations included, and has been tested computationally for accuracy (relative to an exact result without the artificial high velocity layer) and speed of computation. Complete P-SV seismograms, for explosion sources for example, over the distance range from 50 to 500 km and the frequency range from 0 to 2 Hz have been generated for a layered crust-upper mantle model, with all the P wave reflected and refracted arrivals obtained conforming in arrival time with ray theory predictions and similarly for the SV body phases. Initial comparisons with asymptotic wave theory results and known analytic solution show good agreement in wave form and amplitude as well. This modal superposition method, in addition to giving complete results in the distance and frequency range of interest, with stable results having been obtained up to 25 Hz, is capable of incorporating complex medium moduli (or complex velocities), so that anelastic effects may be directly treated. In addition, it is ideally suited to source studies since the modes need only be computed once for a particular earth model and these results can be combined with source representations, corresponding to

any source hypocentral depth and source type, to obtain theoretical seismograms at all distances and azimuths, for a variety of source configurations, by means of a very simple and fast mode excitation computation. (3) A frequency dependent "absorption band model" for the intrinsic Q (quality factor or dissipation function) in the earth has been introduced into the theoretical wave propagation methods. Based on comparative studies of predictions using this anelastic model with observations, we have concluded that such a frequency dependence is appropriate for the earth's upper mantle in particular, and that the variation of the intrinsic Q and its frequency dependence is such that the resulting teleseismic mean dissipation function, Q_m (the Q function averaged over the ray path) is such that a high Q_m "window" exists at relatively high frequencies (in the range from 1.5 to about 4.5 Hz, with the peak at about 3 Hz). This result has important implications for source property and magnitude studies (m_b) and event detection work, as well as conquences with respect to the earth's thermal and mechanical properties. (4) The creation of a spherical cavity in a prestressed medium has been used in the past as a model for the tectonic release effects from explosions as the fundamental generating solution for relaxation models of earthquakes. An exact solution is given for the seismic radiation from the sudden creation of a spherical surface in an arbitrarily prestressed medium. The radiation for the case of pure shear is worked out in detail and compared with previous solutions to show how previous solutions approximate the exact solution. The most important results consist of the spectra and waveforms computed for inhomogeneous stress fields. It is found that failure in an inhomogeneous prestress environment results in a radiation pattern which is not pure quadrupole in nature. The inhomogeneous case also can lead to a low frequency far field spectral peak with the magnitude of the peak varying as a function of the angular coordinates. (5) An elastodynamic source of radiation is most generally and compactly expressed in terms of a Green's function integral equation and this representation serves as a convenient analytical form in the generation of an inversion scheme designed to provide estimates of source properties from observed radiation. A principal difficulty with this approach is specification of a sufficiently general Green's function in an appropriate analytical form. In this regard we have derived suitable layered space Green's functions expressed as eigenfunction expansions in the frequency domain. These functions are then used in the integral solutions for a relaxation source representation of the radiation field from an earthquake. The resulting field is shown to have an analytical structure which allows field variations to be expressed in integral relations similar to those for the field itself. These results serve as the basis for the systematic inversion of observed earthquake radiation field data for source properties and, in particular, we show how spatially variable tectonic stress changes due to failure can be estimated. (6) Narrow-band filtering can be used to generate well-defined magnitude data from seismic time series; these magnitudes being measures of energy arriving at particular group arrival times. Sets of variable frequency magnitudes have been computed for both observed and synthetic seismograms, where the latter results have been used to provide a theoretical framework for the interpretation of the observed data. These magnitude data can be associated with particular phases (P, S, or surface waves) and used in a manner similar to the ordinary m_b and M_s data. In particular, the data can be used to discriminate between underground explosions and earthquakes and to provide estimates of the tectonic stress changes produced by earthquakes as well as failure zone dimensions. The use of very high-frequency magnitudes along with relatively low-frequency magnitudes is however, a more powerful and sensitive means of identifying explosions than is the ordinary m_b versus M_s criteria, as is shown by a comparative study of a large group of seismic events. Further, the inference of tectonic stress levels using this approach provides estimates of the stress changes produced near the point of failure initiation, and this information is probably more pertinent to the description and understanding of an earthquake failure process than is the gross average stress drop estimates obtained by most other methods.